UNIVERSITÀ
DEGLI STUDI
DI PADOVA

Head Office: Università degli Studi di Padova

Department of Cardiac, Thoracic, and Vascular Sciences and Public Health

---

Ph.D. COURSE IN: Doctoral Program in Translational Specialist Medicine “G. B. Morgagni”

CURRICULUM: Cardiothoracic and Vascular Sciences

SERIES: XXXI Cycle

Preservation strategies for decellularized cardiovascular scaffolds for off-the-shelf availability

Thesis was funded by the People Programme (Marie Curie Actions) of the European Union's Seventh Framework Programme FP7/2007-2013/ under REA grant agreement n° 317512.

Coordinator: Prof. Prof. Annalisa Angelini

Supervisor: Prof. Gino Gerosa

Co-Supervisor: Ch.mo Prof. (name and surname)

Ph.D. student : Sabra Zouhair

Abstract

The rapid evolution of heart valve tissue engineering is progressively moving from an *in vitro* to *in vivo* setting, pushing human decellularized grafts into preclinical and clinical application. The cost effectiveness and relatively straightforward processing of acellular heart valves would make this concept potentially available for both adult and paediatric patients. This approach relies on the body's endogenous regenerative capacity. The most appealing results to date have been realized using human acellular biological scaffolds. At present, two crucial limitations pose a significant delay to their application in routine clinical practice: the lack of donor tissues and the limited storage stability of biological scaffolds at 4°C in saline solution. Therefore, decellularized xenogeneic scaffolds, such as pericardium, which is abundantly available and ideally devoid from endogenous cell elements and immunogenic epitopes, could potentially be used for manufacturing cardiovascular substitutes. In order to ensure routine use of cardiovascular scaffolds, off-the-shelf availability requires tissue banking.

The objective of this study was to evaluate the suitability of three different preservation methods for preservation of decellularized bovine and porcine pericardial scaffolds: cryopreservation (as the standard preservation method currently in use), vitrification, and freeze-drying. The implementation of novel preservation technologies for tissue banking of such scaffolds requires careful validation to demonstrate the maintenance of their biological and functional integrity.

Bovine and porcine pericardia were decellularized using Triton X-100, sodium cholate and endonucleases. Following decellularization, bovine and porcine samples were subjected to either slow-freezing-rate cryopreservation, vitrification or freeze-drying (n=6 in all cases).

Slow-freezing-rate cryopreservation was conducted at ~1°C/min using 10% DMSO as a cryoprotectant. Vitrification was performed using VS83 (4.65mol/L formamide, 4.65 mol/L DMSO and 3.31 mol/L propylene glycol in EuroCollins solution) and cooling above the vapour phase of liquid nitrogen. Freeze-drying was carried out using a programmable freeze-drier with temperature-controlled shelves, while samples were infiltrated with sucrose for lyoprotection. The impact of these preservation methods on the structural integrity of the scaffolds was assessed using histological staining, scanning electron microscopy (SEM), multiphoton microscopy (TPM) and uniaxial tensile testing. Fourier transform infrared spectroscopy (FTIR) was performed to study the overall protein secondary structure and differential scanning calorimetry (DSC) was used to determine thermal protein denaturation profiles. In addition, cytotoxicity analysis was performed.

Histological staining, SEM and TPM revealed that the extracellular matrix (ECM) integrity was maintained after all preservation treatments compared to the non-preserved control in both species. Inspection of the protein amide-I band (1600–1700 cm^{-1}) in the FTIR spectra showed no statistically significant differences in overall protein secondary structure after preservation and reconstitution. DSC results indicated that the protein denaturation temperature was not significantly affected by any of the preservation protocols. Uniaxial tensile testing demonstrated the preservation of the biomechanical properties of porcine scaffolds, whereas for bovine scaffolds significant differences were observed following cryopreservation treatment.

Furthermore, differently treated scaffolds possess excellent cytocompatibility *in vitro*. This is of major importance since the preservation of ECM components and their bioactive properties may guarantee endogenous tissue regeneration upon implantation.

The most commonly used preservation method for cardiovascular tissue banking is cryopreservation by slow-rate freezing. It is shown, however, that cryopreservation of bovine pericardial tissues using 10% DMSO and slow-rate freezing results in more rigid tissues compared

to vitrified or freeze-dried tissues, whereas the biomechanical behavior of porcine scaffolds was unaffected by any of the preservation methods. This change in mechanical properties seen in DBP might be caused by damage due to ice crystal formation disturbing the ECM histoarchitecture. However, all preservation technologies were suitable for preserving ECM components with no apparent sign of denaturation of collagen or loss of elastin and sGAGs. Similarly, proteins were found to be stable as no changes were introduced to their structure.

In conclusion, freeze-drying and vitrification represent alternative methods to conventional cryopreservation that demonstrate excellent outcomes regarding preservation of ECM structure and its components. Both cryopreserved and vitrified tissues are usually stored in liquid nitrogen or a mechanical freezer, and include the use of highly toxic cryoprotective agents. Freeze-drying is carried out using non-toxic protective agents and the scaffolds can be stored in operating rooms at room temperature, which gives surgeons the opportunity to choose the ideal graft for the benefit of the patient. Freeze-drying reduces infrastructural costs for storage and shipment and preserves ECM integrity as well as vitrification and even better than conventional cryopreservation.

It is therefore suggested that freeze-drying could replace currently used cryopreservation and vitrification approaches for the preservation of xenogeneic decellularized scaffolds.

Table of content

1 Introduction

Cardiovascular disease (CVD) has become the largest cause of morbidity and mortality globally. It is responsible for almost one million deaths each year. CVD includes all the major disorders of the heart and blood vessels, comprising coronary, congenital and valvular heart disease; stroke; hypertension; and vascular dementia [1]. One of the most common diseases affecting the heart is valvular disease, which is manifested by two types of valve deficiencies, stenosis and regurgitation. In both cases, significant morbidity and mortality will affect these patient populations if no suitable therapy is provided. Around 290,000 heart valve replacements are performed each year and this figure is estimated to triple by 2050 [2,3].

Over the past decades, major advancements have been made in the reconstruction and replacement of malfunctioning valvular heart tissues. Valve replacements can be categorized into human heart valves and prosthetic valves. Human heart valves include autografts and allografts, while prosthetic valves consist of either mechanical or xenogeneic valve tissues harvested from animals such as pigs. The first FDA-approved mechanical valve was introduced by Dr. Albert Starr and Lowell Edwards [4]. This revolutionary step considerably improved outcomes for patients with valvular disease. Unfortunately, enthusiasm for mechanical valves was tempered as soon as their related complications to thromboembolic events and the need for lifelong anticoagulation were recognized [5]. Due to these complications, the main goal of subsequent research was to develop bioengineered tissues for use as alternative heart valves to overcome the drawbacks of mechanical prostheses. In 1965, Carpentier successfully introduced the use of xenogeneic porcine bioprosthesis to substitute for the aortic heart valve. Unfortunately, non-treated porcine valves were characterized by limited durability (from 6 months to 1

year), mainly caused by immune response to animal tissues [6]. In order to improve these outcomes, Carpentier employed glutaraldehyde (GA) to stabilize the collagen and reduce antigenicity, increasing the durability of functioning valves from a few months to 6 years [7]. With the application of a low concentration of GA for xenogeneic tissues, a new era of commercialization of bioprosthetic heart valves began. Bovine and porcine pericardia subjected to GA were introduced in this period as biomaterials for the fabrication of heart valves [8,9] as well as patches for repair and reconstruction in the cardiac and vascular surgical field [10]. Despite the absence of regeneration and growth potential and the manifestation of calcification, clinical experience confirmed low thrombogenicity and improved durability *in vivo*, which was becoming interestingly attractive to implantation centers and hospitals around the world. Along the same lines, the use of homograft heart valves in clinical practice was introduced in 1962 by Ross [11] and in 1965 by Boyes [12], and showed excellent hemodynamic performance and resistance to infection [13]. Heart valves can be isolated from multi-organ donors, cadavers or from recipients of heart transplantation.

The growing clinical need for homograft valve substitutes in different sizes in cardiac surgery and the progress made in the cryobiology field encouraged the establishment of allograft valve banks. Cryopreservation is the gold standard method, which has been used for many years for the long-term storage of allograft heart valves in tissue banks. Cryopreserved allografts are usually preferred for right ventricular outflow reconstruction in children with congenital heart disease, young patients, and women of childbearing age. Clinical concerns about cross-infections and bacterial contamination during storage led to application of harsh disinfection and sterilization methods. However, these pretreatments resulted in a decrease in allograft longevity during the early 1970s [14,15]. Another factor associated with the degeneration of cryopreserved heart valves, is cell-mediated calcification and the host's immune response to foreign antigens expressed on allograft implants. In order to overcome these

limitations and to reduce the antigenic response upon transplantation, decellularization methods have been developed to produce biological scaffolds composed of extracellular matrix (ECM), which are free from cell elements including cell membranes, organelles and nucleic acids. Many decellularization protocols applied to human heart valves have proven to be very promising treatments with excellent outcomes in preclinical and clinical studies [16,17]. However, it remains questionable whether standard cryopreservation is suitable for preserving the long-term performance of decellularized grafts. It has been reported that cryopreserved heart valves demonstrated structural matrix damage and deterioration of their components (Collagen and Elastin), probably due to ice damage [18]. Indeed, several preclinical [19] and clinical studies [20] have shown that cryopreservation after decellularization might cause calcification, compromising the positive outcomes of the application of decellularized allografts. Rival candidates for the long-term storage of decellularized scaffolds are ice-free cryopreservation (also called “vitrification” and “freeze-drying”). Both technologies rely on the use of specific protectants that form a glassy state, enabling preservation of the ECM and representing promising alternatives to standard cryopreservation by slow-rate freezing.

The aim of this PhD thesis was to evaluate the impact of freeze-drying, vitrification and standard cryopreservation on xenogeneic decellularized bovine and porcine scaffolds. The impact of the different preservation methods was assessed in terms of histoarchitecture, biochemical composition, protein stability, biomechanical integrity, and cytocompatibility. Combining an effective decellularization method, such as TRICOL, with adequate preservation technology could provide off-the-shelf, functional, durable and self-regenerating scaffolds for cardiovascular surgery.

The thesis is structured into four main chapters. The first chapter provides an introduction to the PhD project. The second chapter describes experimental methods and protocols applied for the

decellularization and preservation of xenogeneic scaffolds and their assessment. The third chapter consists of the main results obtained from characterization of decellularized and differently preserved bovine and porcine scaffolds, and finally, the last chapter concludes with a discussion of the work and the future outlook.

1.1 The Heart

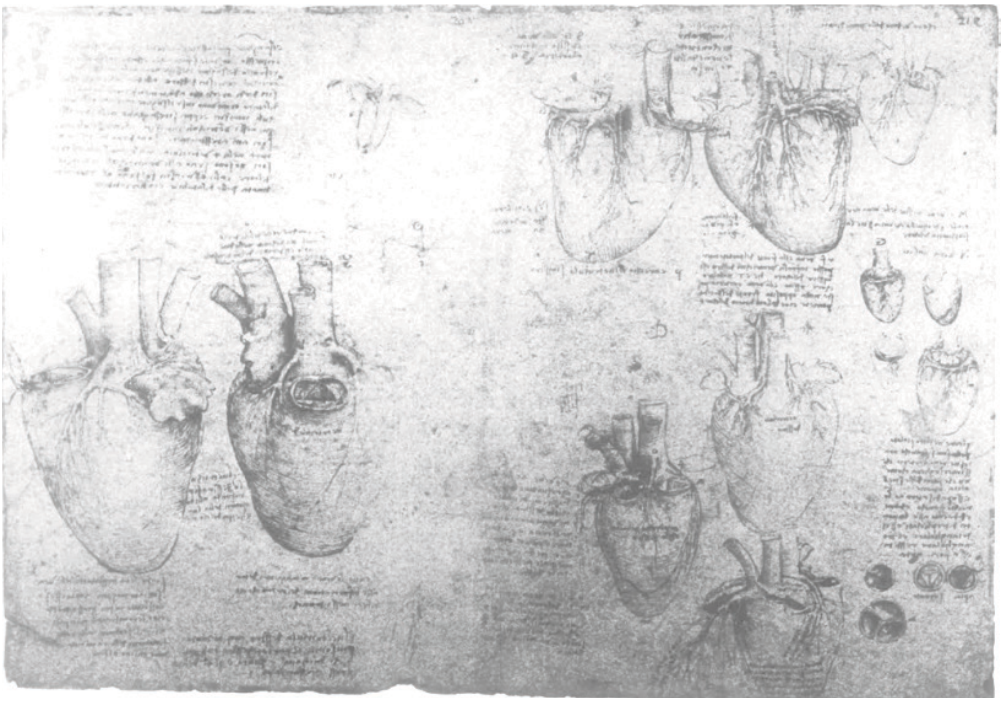

Figure 1-1: *The Heart Coronary, Arteries and Veins by Leonardo Da Vinci. Adapted from [21]*

The heart has always been a center of interest for many physicians and philosophers for understanding the functioning of the body. As far back as the beginning of the eleventh century, Avicenna (980-1037 CE) recognized and described the heart in “Canon of medicine” as one of the body’s vital organs, which controls and guides the others. There was widespread controversy in medieval Europe surrounding Galen's view of the heart as the vital and soul force and the liver as the operating organ supplying the body with nutrients through the venous vein [22]. However, Galen's anatomical work became accepted in Europe through Avicenna's book. In the 1490s, Leonardo da Vinci (1452-1518 CE) challenged the Galenist view by describing the heart as the most powerful muscle in the body [23]. He was the first to recognize that the heart is a muscle and that systole is the active phase of the cardiac cycle, not diastole as hypothesized in the Galenist theory [24]. Furthermore, Da Vinci 's drawings of the

coronary arteries are the earliest known detailed anatomical sketches involving the aorta (Fig.1-1).

Today, it is known that the human heart is a muscular pump which never rests. It beats 100,000 times a day, pumping around 8,000 liters of blood through our body [25] (Fig. 1-2). It is cone-shaped with a mass of between 250 and 350 grams [26]. The heart is part of the circulatory system, along with a network of blood vessels (arteries, veins and capillaries). Their function is to supply the organs and tissues with oxygen and nutrients and to take on carbon dioxide and waste.

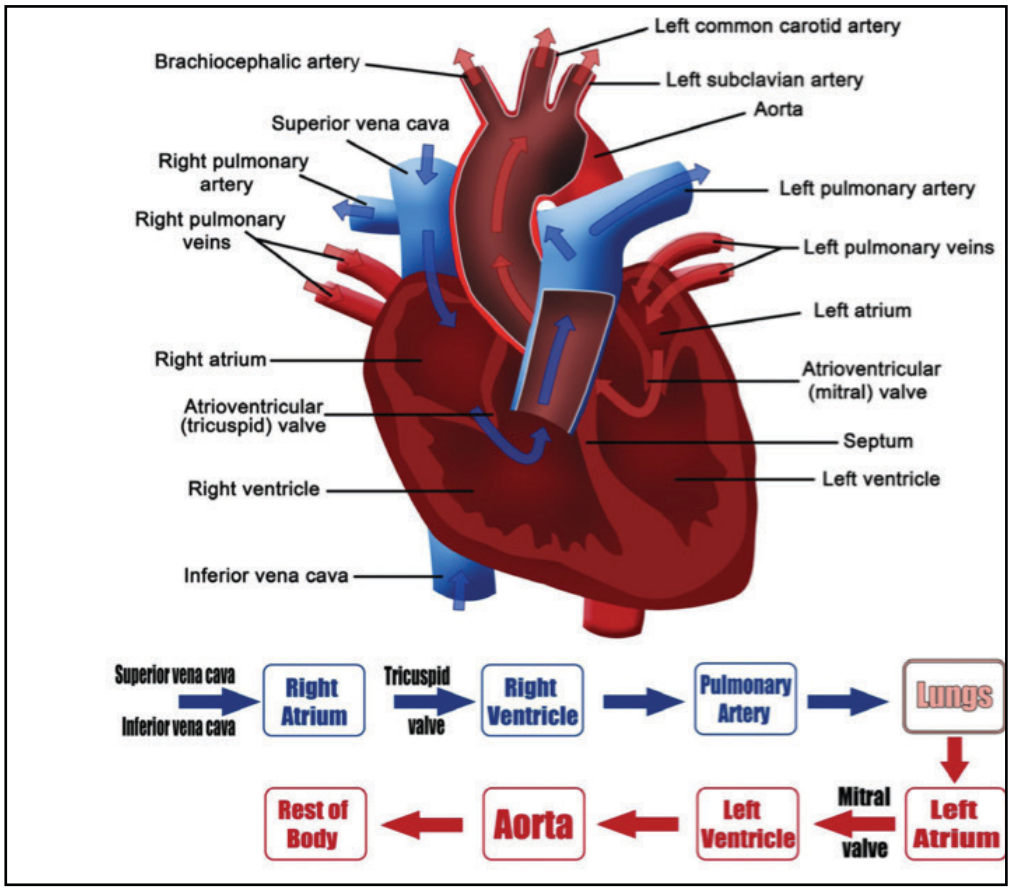

Figure 1-2: *Blood circulation through the heart to the body. Adapted from[27]*

The heart is located in the thorax in the mediastinum, posterior to the sternum and between the lungs (Fig. 1-3). The heart is surrounded by a double walled sac called the pericardium [28], which provides protection and helps to fix it inside the chest. In the pericardial cavity,

serous lubricating fluid is present between the pericardium and heart. Its major function is to favor the motion of the heart and to prevent friction. The heart wall is composed of three layers: the epicardium, myocardium, and endocardium (Fig. 1-4).

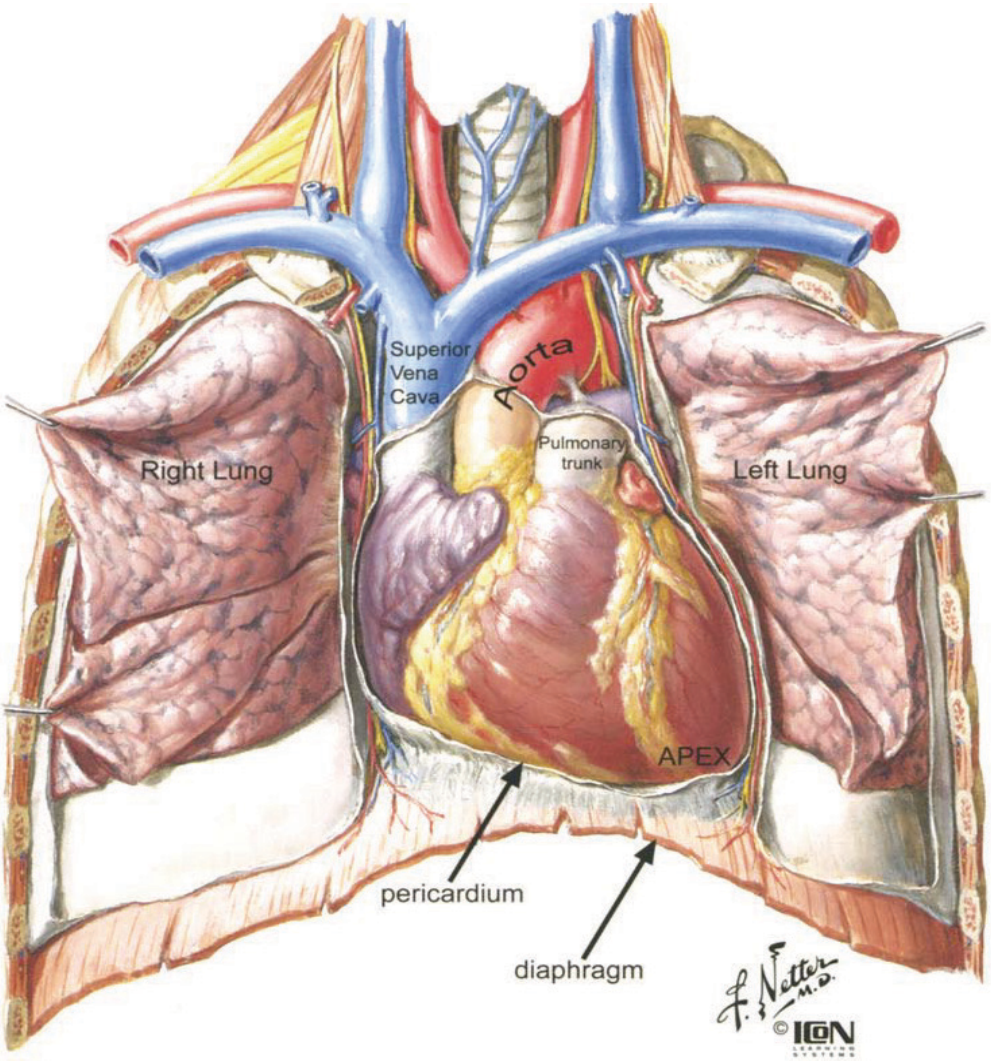

Figure 1-3: *Heart location between the lungs (Mediastinum). Adapted from [29]*

1.1.1 Histological and structural properties of the pericardium

The pericardium is a closed sac made of connective tissues that contains the heart, the roots of the great arteries and 5-30 ml pericardial fluid. It is also called the parietal pericardium [30]. The

parietal pericardium is composed of serous and fibrous layers (Fig. 3). The fibrous layer is fused to the serous one, forming a single layer with two surfaces, i.e. *fibrosa* and *serosa* [30]. The outer layer, *fibrosa,* is covered with adipose tissue, which anchors the heart to the mediastinum, while the inner layer, *serosa,* consists of continuous lines of mesothelium producing pericardial fluid [31]. The main functions of the pericardium are to:

- Provide stabilization to the heart in its anatomic position through the maintenance of geometry by preventing its adhesion to other structures in the thorax [32].
- Maintain the volume/pressure ratio in the heart chambers [32].
- Protect the heart against the spread of infections by generating a physical barrier [31].
- Lubricate the surface of the heart with serous fluid, preventing damage to the epicardium and reducing friction with surrounding elements [33].

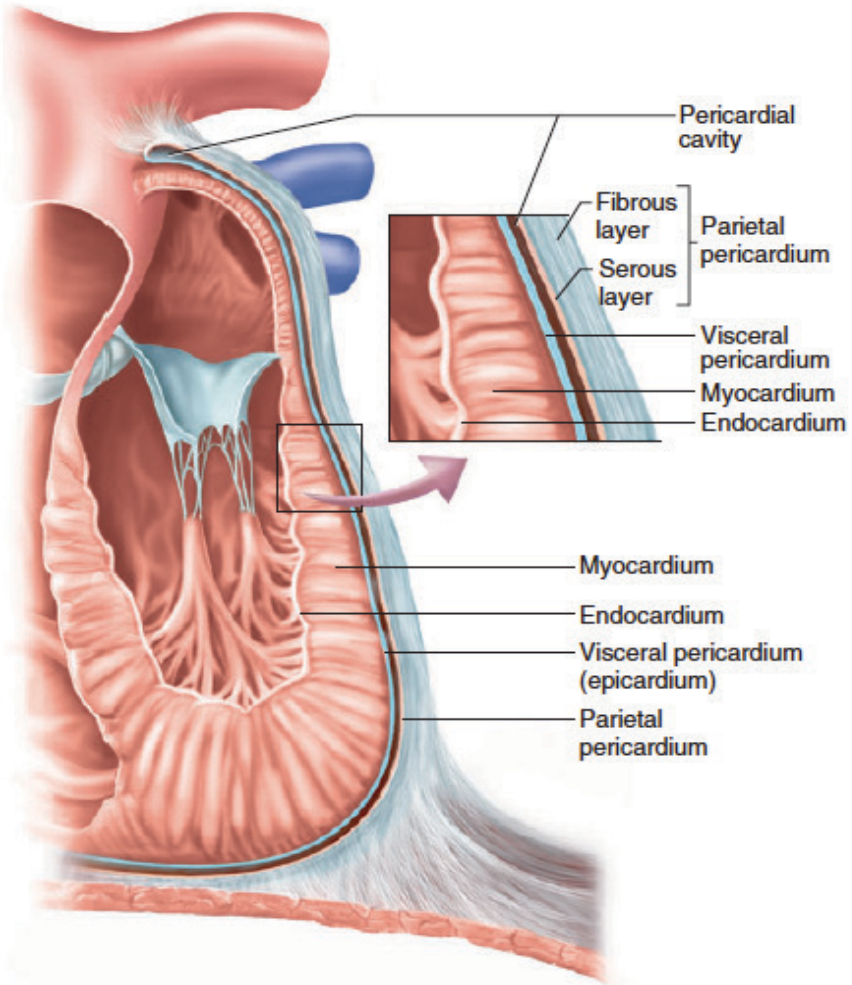

Figure 1-4: *Heart wall layers. The insert illustrates the pericardium's layers. Adapted from*[26].

The microscopic structure of the human parietal pericardium consists of three layers: the *serosa*, the *fibrosa* and the epipericardial connective tissue layer (Fig. 1-4). The serosal surface contains a continuous layer of mesothelial cells with microvilli, whose major function is the formation and regulation of serous fluid. The cells lie on the basement membrane supported by wavy collagen fibers in the submesothelial layer (Fig. 1-5a and b). *Fibrosa* is composed of a small number of connective tissue cells, well-organized compacted collagen, and unimposing elastic fibers, including small vessels coming through in oblique plane. Different layers of collagenous bundles can be identified in the *fibrosa (Fig. 1-5D)*. The fibers in close proximity to the mesothelium seem to have cephalo-caudal orientation [31], whereas

the dense *fibrosa* showed anisotropically-oriented collagen bundles with crimped pattern and thin elastic fibers perpendicular to the collagen [34]. Their external elastic fibers are larger than those closest to the mesothelium. Elongated and narrowed cells are resident in the connective tissue of the *fibrosa.* The multidirectional orientation and wavy appearance of collagen permits some degree of stretching and elongation. By contrast, the epipericardial layer is rich in elastic fibers and contains blood vessels, adipose tissue and neuronal elements (Fig. 1-5a and b)[31].

Ultrastructural examination of the mesothelial cells shows two differently shaped cells - flat and cuboidal ones - which may differ in their function. The flat cells consist of thin cytoplasm, few mitochondria and poorly developed endoplasmic reticulum and Golgi apparatus, whereas the cuboidal-shaped cells are rich in organelles, Golgi apparatus, mitochondria and well-developed endoplasmic reticulum. Both cell forms carry occasional cilia and are covered with 3µm long microvilli (Fig. 1-5a). The latter increase the surface area for the transport and production of pericardial fluid. The presence of few vesicles along the luminal surface was observed. Mesothelial cells are attached to each other through desmosomes, which build junctional complexes reinforcing and tightening the intracellular adhesion. Traditionally, flat mesothelial cells have been identified as the most abundant cell type in parietal pericardium, whereas cuboidal cells seem to appear as single cells or in small groups and are most commonly located in the visceral part of pericardium [34,35].

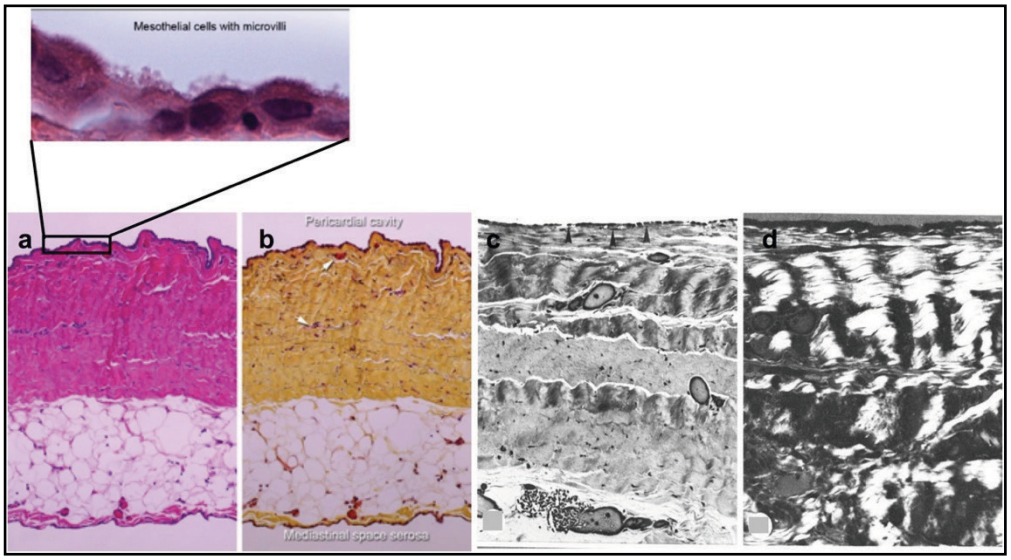

Figure 1-5: *Histological sections of parietal pericardium: H&E (A) and Movat pentachrome (B). The insert (X800 magnification), mesothelial cells with microvilli are visible. Adapted from [31]. (C) Parietal histological section of human pericardium showing mesothelial layer (arrow), (D) Polarized light microscope section showing orientation of collagen fibers through entire thickness. Adapted from[34].*

1.2 Heart valves

The heart is composed of four chambers: the left and right ventricles and the left and right atria. The role of the heart is to collect blood from the lungs and pump it throughout the body in a unidirectional way, carrying it through four valves (Fig. 1-2). The atrioventricular valves (AV, tricuspid and bicuspid) allow blood to flow only from atria to ventricles in order to prevent regurgitation. The semilunar valves (SL, pulmonary and aortic) enable blood to flow only from the ventricles out of the heart in order to prevent backflow [36].

The four heart valves are supported by a cardiac framework made of dense connective tissue (collagen), which forms the base of the heart (Fig 1-6a). This area remains stationary during the heart's motion, whereas the flaps of the valves, along with the myocardium and arteries, belong to the heart's dynamic component. Figure 1-6b shows the close relationship of the heart valves to each other, which is important for their individual dynamical function. The four valves are composed of two or three mobile fibrous tissues called leaflets or cusps, lined with endothelium [37].

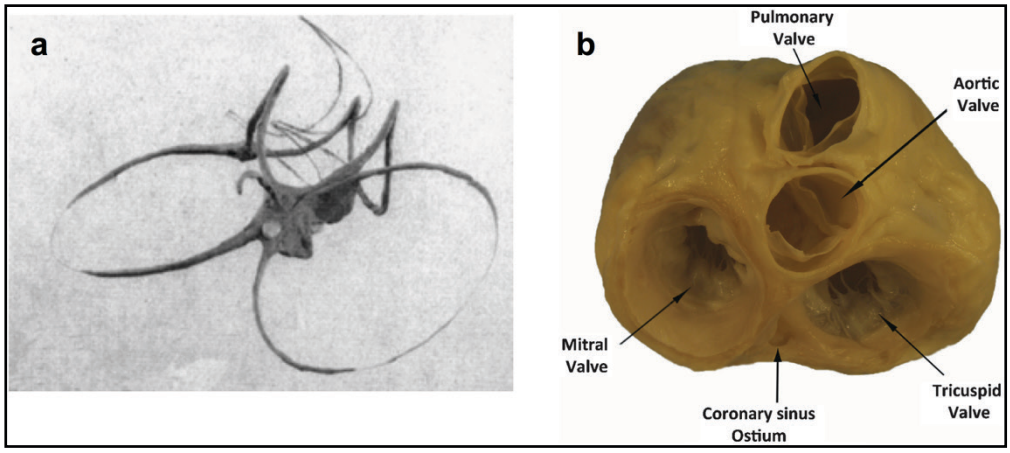

Figure 1-6: *A: Cardiac skeleton supporting the four heart valves. Adapted from [38]. B: anatomical view of the four heart valves showing their relationship to each other. Adapted from [37]*

1.2.1 Atrioventricular Valves

The AV valves are composed of large asymmetrical, thin, soft and pliable leaflets situated between the atria and the ventricles. The number of leaflets has been traditionally defined by the commissures. The mitral valve (Fig. 1-7) is composed of just two leaflets, anterior and posterior, and is responsible for the left atrioventricular performance. The triscupid valve (Fig. 1-7) consists of three irregular flap-like leaflets referred to as anterior, posterior and septal leaflets, and monitors the right atrioventricular opening [39]. Their general anatomical structure is similar and comprises the annulus, leaflets, tendinous cords, and papillary muscles [40]. The leaflets are attached to their respective annulus as a solid ring-like fibrous cord defining the opening area of the valve. The chordae tendineae, a tendinous cord of white collagen, attaches the free edge of the leaflet to the papillary muscles.

The ECM composition and structures of the cardiac valves ensure their functionality and durability. The AV valves share very similar ECM structures. However, the mitral leaflets differ from the triscupid ones in that they are thicker and there are twice as many nerves in the anterior leaflet as in the posterior one. Architecturally, the leaflets can be dived into lamina *atrialis* (facing the atrial side) and lamina *fibrosa* (facing the ventricle side), surrounded by endothelial cells. Lamina *atrialis* consists of fibrocytes lying between the collagen fibers and histocytes. By contrast, the lamina *fibrosa* of the triscupid valve is composed of dense collagenous fibers, and forms the backbone of the valve. Furthermore, mitral leaflets contain other cells types such fibroblast, smooth muscle and myocardial cells [37]. Both valves also show remarkable differences due to their position in the high and low-pressure system of the circuit. Thus, their structural design considers these specific flow characteristics.

The chordae tendineae of the mitral valve have a similar composition to the tricuspid valve. They are mostly composed of

collagen, elastic fibers and endothelial cells [41]. Collagen, one of the main load-bearing components, is arranged parallel to the long axis of the chordae in order to maintain the competency of the cardiac valves. Elastic fiber alterations or modifications in the collagen arrangement may lead to chordal rupture [38].

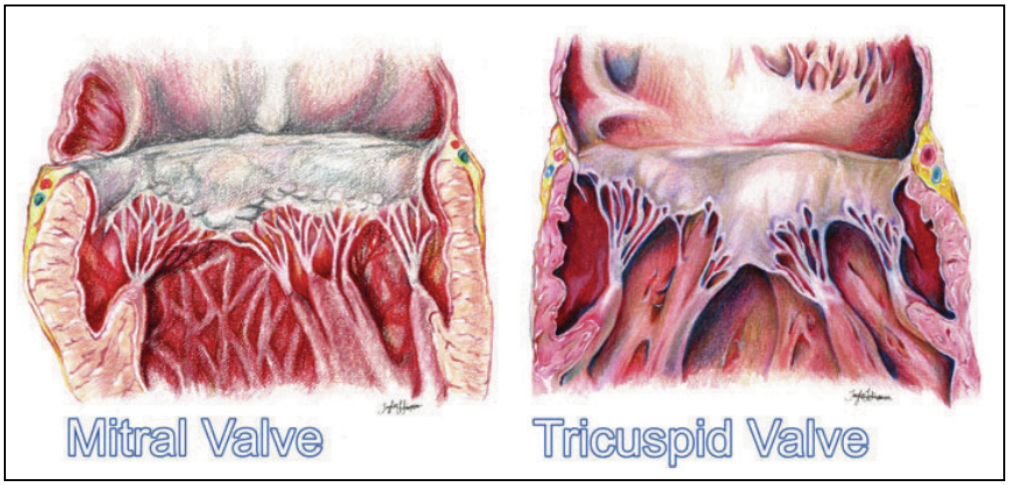

Figure 1-7: *Illustration of Mitral and Tricuspid valves showing the annulus, chordae tendineae and papillary muscles. Adapted from [37].*

1.2.2 Semilunar valves

The semilunar (SL) valves' structure and anatomy is much simpler and more elegant than that of the AV valves. The unique shape of SL valves gives them an autonomous structure without need for chordae tendineae to maintain their performance. The SL valves connect the ventricles to the great arteries. Anatomically, three cusps form the SL valves and provide them with distinct mechanistic functions. Each cusp is attached to its respective annulus (crown-shaped fibrous structure), resulting in a "semilunar" shape [38]. The aortic valve connects the left ventricles to the ascending aorta. The cusps of the aortic valve are named for their relationship to the coronary arteries, which branch from its sinuses as follows: left coronary, right coronary and non-coronary cusps (Fig. 1-8a) [39]. In contrast, the pulmonary valve connects the right ventricle to the pulmonary root. Its cusps are defined by their relationship to the aortic valve and called right and left-facing cusps and non-facing cusps (Fig. 1-8b). The aortic valve is seen

as the “centerpiece” of the heart [37]. However, both valves show comparable architecture. The pulmonary valve is employed as a substitute for the malfunctioning aortic valve in Ross’ procedure [42]. The differences seen in histological investigations might only be due to their exposure to different pressures and not to their mechanical performance.

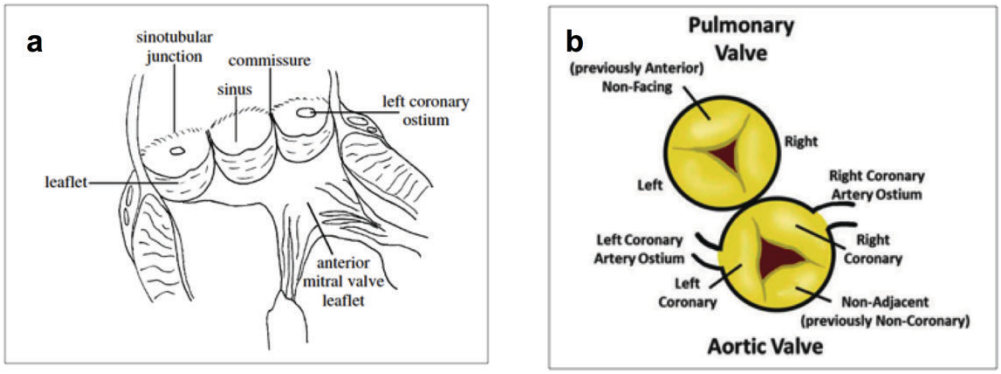

Figure 1-8: *SL valve structures a: Aortic root drawing. b: Pulmonary and aortic valves showing their relationship to each other. Adapted from[38]*

1.3 Valves' ECM structures and components

The ECM components and structure of a valve are important factors for its function and durability. All four valves share a highly organized leaflet structure with unique mechanical properties, which is divided into, *spongiosa*, *fibrosa* and *ventricularis* for SL or *atrialis* for AV valves [39]. The principal ECM components of the leaflets are collagen type I (70%), II (24%), V (2%), elastin (10%) and proteoglycans (20%) offering exceptional durability, flexibility and strength for each valve type [43–45]. *Fibrosa* provides the stress-bearing fibrous layer. It is mostly composed of circumferentially-oriented collagen type I and III, responsible for mechanical strength [46]. The *spongiosa* or central layer consists predominantly of a high concentration of proteoglycans and glycosaminoglycan (side-chains of proteoglycans), with little contribution from collagen and elastic fibers. It works as a barrier between the two layers, allowing the absorbance of the generated stresses during valve closure [45]. The ventricularis and atrialis layers of SL and AV are composed of radial and circumferentially-oriented elastic fibers surrounding lose collagen fibers, allowing the cups/leaflets to resist deformation and reformation and maintaining the collagen configuration [47,48]. Proteoglycans are distributed throughout the leaflet layers. The flexibility of these layers permits the leaflets to recoil during valve closure [49]. Their major role is to enhance viscoelasticity and to withstand compressive loads [50].

1.4 Heart valve disease: Stenosis & Regurgitation

Valvular heart disease is characterized by the manifestation of stenosis or regurgitation. Any of the four cardiac valves can be affected, compromising heart function and resulting in high mortality (200,000 death every year) [1]. Stenosis is the failure of the valve to successfully open or close, due to a decrease in the orifice area of the valve, leading to obstruction of the blood flow (Fig.1-10). Regurgitation is a defective closure of the valve leading to leakage of blood back into the left atrium during systole (valve incompetence) [37] (Fig 1-11a).

The functional modification of the valves is closely linked to structural change, which is probably mediated by interaction of ECM components, valvular cells and environmental conditions. Genetic predisposition may play a role as well. However, aortic valves are the most frequently diseased valves. When considering only severe aortic stenosis, its frequency of occurrence is around 2–4 % in the elderly (over 65) and increases to 25 % when aortic sclerosis is implicated.

1.4.1 Pathology of heart valve disease: mechanism

Three types of pathological modification of the valve can be distinguished: (1) congenital deformities leading to dysfunction of the valve (bicuspid aortic valve); (2) myxomatous valve degeneration attributed to collagen degradation, proteoglycan accumulation and elastic fiber fragmentation [39], consequently causing weakness and prolapse of the leaflets and, hence valve regurgitation and incompetence [13,39]; and (3) fibrotic degeneration as a consequence of collagen accumulation, proteoglycan degradation, and elastic fiber fragmentation. These structural changes result in an increase in the stiffness of the leaflets (decrease in compliance) leading to an obstruction of the movement of the valve known as stenosis. Valve stenosis is considered as a continuum from sclerosis to advanced

stenosis, characterized initially by valve thickening, followed by formation of calcium nodules and neovascularization [51].

1.4.1.1 Aortic valve stenosis

The aortic valve is the most commonly affected valve with stenosis caused by calcification termed as calcific aortic valve disease. Its etiology in industrialized countries has undergone a fundamental shift from rheumatic to degenerative calcification [52]. In order to remain pliable, the aortic valve must be exposed to continuous repair throughout life, which occurs by means of the cells residing within the tissue. Valve interstitial cells (VICs), as the predominant cell type, are distributed in different sub-populations that control the homeostasis within the three layers of valve cusps (Fig. 1-9), whereas valve endothelial cells (VECs) form a line in the outer layers (*fibrosa* and *ventricularis*) of the cusps and function as a barrier to prevent inflammatory cell infiltration and lipid accumulation [25].

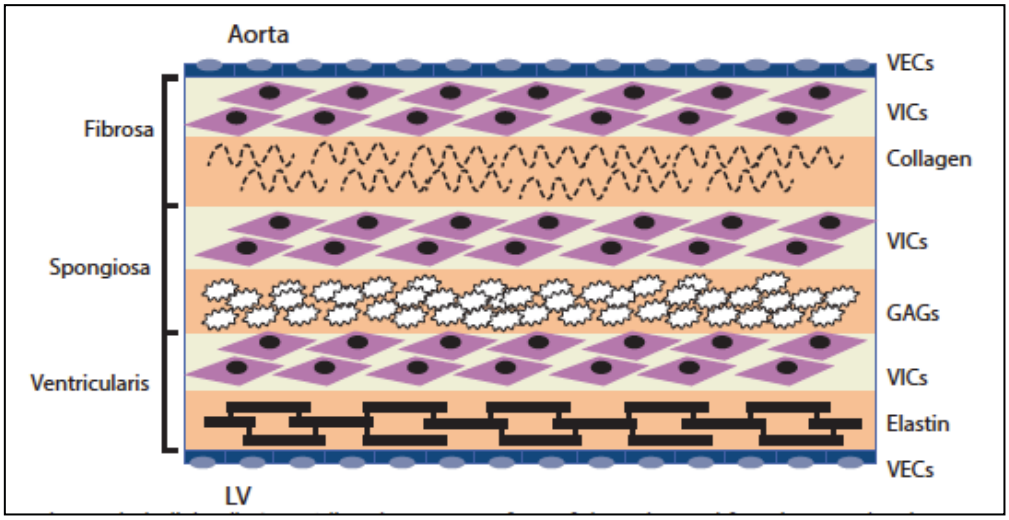

Figure 1-9: *Cellular architecture of the Aortic Valve. Adapted from [25]*

Calcific aortic valve disease (CAVD) is a degenerative process mediated through alterations of valve interstitial cells (VIC). They are responsible for repair of damaged collagen and other ECM components during valve remolding. VICs are known to be highly plastic and able to transit from one phenotype to another when it is

needed, for example in response to injury, pathology, or during hemostasis [13]. The main cause of CAVD is believed to be initiated through the activation of VICs by increases in proliferation and trans-differentiation to myofibroblast and osteoblasts promoting calcification and bone formation (Fig. 1-10) [13,39,51]. On the other hand, the second mechanism that has been suggested is related to mechanical stress caused by blood crossing the aortic valve, which damages the basement membrane of the cusps (Fig.1-9). The damage caused to the basement membrane in turn results in infiltration of inflammatory cells such T-lymphocyte, and deposition of low-density lipoprotein (LDL), causing the initiation of a chronic inflammatory process [53].

In more recent years, many studies have implicated atherosclerosis in the development of CAVD. Atherosclerosis is an extremely complicated process involving several factors that lead to a lesion composed of lipids, macrophages, proliferating smooth muscle and apoptosis [25]. A wide variety of factors (cholesterol, LDL, male sex, diabetes mellitus, smoking) have been identified as being associated with an increase in the incidence of valve stenosis, and likely play a role in structural leaflet damage. A recent study proposed that valvular calcification is an active process, not a passive one as was originally believed, and that it is based on activation of pro-osteogenic signaling pathways. The existence of osteoblasts with lipoprotein deposition and chronic inflammation in atherosclerotic vascular lesions as well as in CAVD also supports the hypothesis of a common cellular mechanism [25]. Moreover, the progression of CAVD has also been strongly associated with hereditary factors. Malformation of the aortic valve (bicuspid aortic valve (BAV)) is one of the most common congenital heart diseases, characterized by two cusps rather than three. The valve with two cusps is forced to sustain far more mechanical stress, resulting in stenosis (Fig.1-10). 50% of adult patients and 70 to 85% of children with valve stenosis possess a BAV [54]. BAV occurs frequently with other cardiovascular malformations such coarctation of the aorta [54].

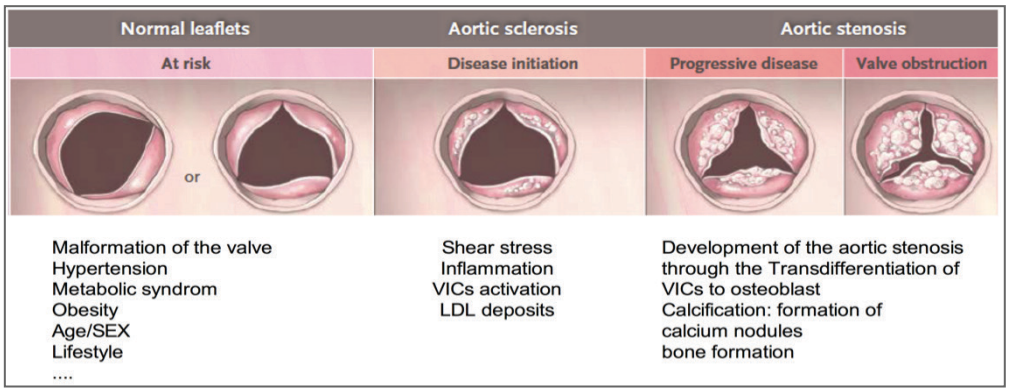

Figure 1-10: *Disease progression of aortic valve stenosis from normal or bicuspid aortic valve. Adapted from [55]*

1.4.1.2 Mitral valve regurgitation

Myxomatous degeneration of the mitral valve is the most common valvular disease, causing frequent heart failure [56]. The structural degeneration described in 1.41 leads to a floppy valve (Fig. 1-11A). Mitral valve prolapse is characterized by a decrease in collagen in the *fibrosa* layer and an increase in glycosaminoglycan concentration in the middle part (*spongiosa*), which in turn results in a thickening and rise in extensibility in the *spongiosa* and a decrease in stiffness in the *fibrosa* (Fig.1-10B2). These structural changes are on account of alterations in ECM remodeling (Collagen, GaGs) through the activation of VICs [13]. There is clear evidence that mitral valve prolapse is also linked to some heritable disorders such as Marfan and Ehlers-Danlos syndromes and to gene mutation characterized by connective tissue dysfunction affecting the hemostasis and remodeling of the ECM. Taken together, the pathogenesis of mitral valves by regurgitation may develop, caused by ECM dysregulation due to a cellular alteration or based on genetic conditions, ultimately causing a major alteration to the biomechanical function of the valves.

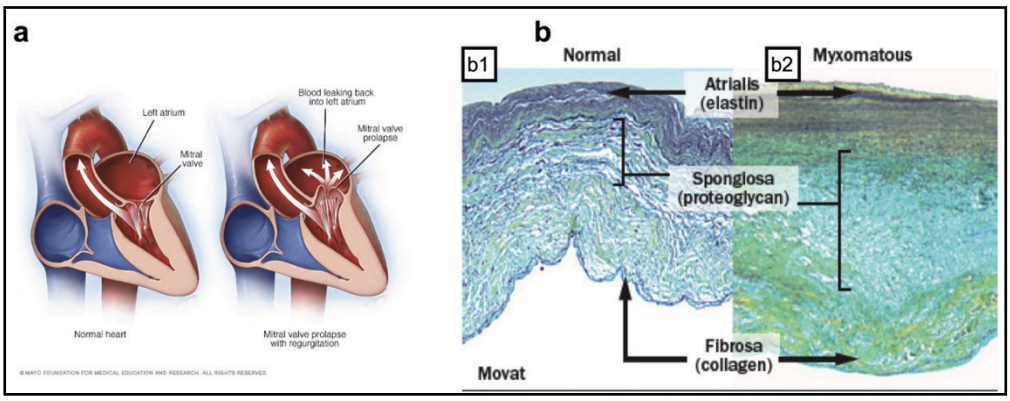

Figure 1-11: *a: Mitral valve prolapse and regurgitation. b: Histological characterization of healthy (b1) and (b2) Myxomatous Mitral leaflet using Movat pentachrome stain (collagen, yellow; proteoglycans, blue-green; and elastin, black). a Adapted from[57]. b adapted from [58]*

The treatment of heart valve disease usually depends on the clinical condition of the patients. The current pharmaceutical therapies are able to treat the symptoms but do not solve the main health problem and may only delay surgical intervention (valve repair or replacement). Degeneration of the valves is an irreversible event. In most cases, surgical treatment remains the sole solution for these patients.

1.5 Heart valve substitution

Cardiovascular disease is recognized as one of the main causes of mortality in industrial countries. It affects more than 100 million people worldwide [59]. Each year, 280,000 valve substitutes are implanted globally [60]. The disease etiology has gone through a transformation from rheumatic heart problems to degenerative ones. Rheumatic heart disease is still considered the most common malady in developing countries [59]. The high demand for surgical substitution of degenerative diseased heart valve has created a large market for manufacturing prosthetic substitutes, which would ideally mimic the function of the native valve characterized by an excellent hemodynamic performance, long durability, and low thrombogenicity.

Nowadays, the increase in life expectancy, which is accompanied by frequent comorbidities, will increase the prevalence of valvular surgeries over the coming years. Three types of cardiac valve substitutes are used for heart valve replacement.

- Mechanical heart valves, which are implanted surgically;
- Bioprosthetic heart valves (BHV), which can be implanted via a surgical or transcatheter approach [61];
- Cryopreserved allografts, which are implanted surgically.

Currently, application of heart valve replacement worldwide is estimated to be approximately 70% mechanical valves, 28% bioprostheses, and 2% cryopreserved allograft heart valves [62]

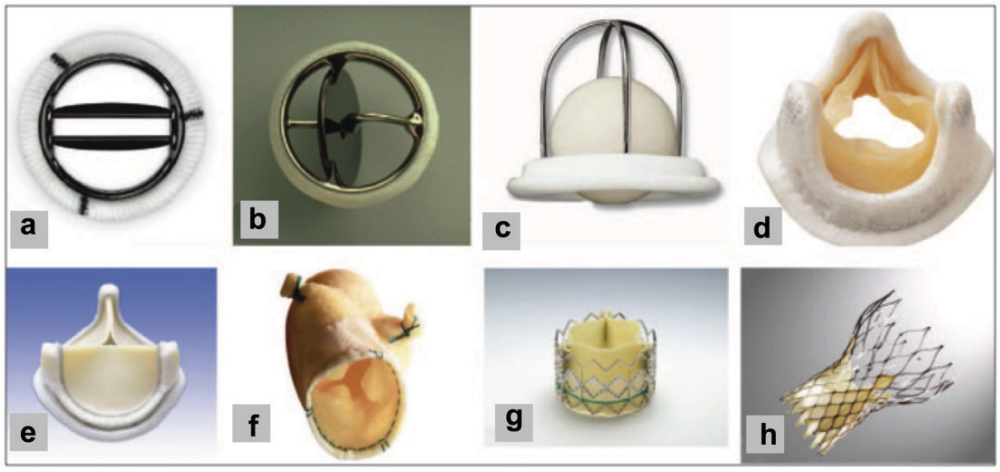

Figure 1-12: *Different types of prosthetic heart valves divided into mechanical (a-c) and bioprosthetic (d-h). a, Bileaflet mechanical valve (St Jude); b, monoleaflet mechanical valve (Medtronic Hall); c, caged ball valve (Starr-Edwards); d, stented porcine bioprosthesis (Medtronic Mosaic); e, stented pericardial bioprosthesis (Carpentier-Edwards Magna); f, stentless porcine bioprosthesis (Medtronic Freestyle); g, percutaneous bioprosthesis expanded over a balloon (Edwards Sapien); h, self-expandable percutaneous bioprosthesis (CoreValve). Adapted from [60]*

1.5.1 Mechanical heart valves

The choice of prosthetic heart valve is usually defined by the age and the medical history of the patient. Traditionally, guidelines recommend the implantation of a mechanical valve for patients under 60 with life expectancy over 10-15 years [63]. Mechanical valves are durable and last over 20-30 years but they are thrombogenic. Therefore, patients require lifelong therapy with anticoagulation drugs such as warfarin [63]. This thrombogenicity is due to the metallic material used for valve manufacture. In order to overcome this limitation, major advances have been made in their material composition, design and surface processing (coating). Since the first valve developed by Starr and M. Lowell Edwards, different materials have been fabricated such as metal or carbon alloys.

Mechanical valves are divided into three models according to their design [60]:

- Caged-ball valves: the first successful mechanical valve was implanted in the early 1960s. It was commonly made of metal

alloys; this model is no longer implanted because of its high thrombogenicity. The design basically comprises a silastic ball with a circular sewing ring and a cage formed by 3 metal arches (Fig.1-12c). It is characterized as having the smallest effective orifice area [60];

- Single-tilting-disk: the “Monoleaflet valve”. This was introduced in 1970s. It is composed of a single flat, free-floating circular disk ensured by two metal struts. However, some models showed intermediate thromboembolic complications. The most used monoleaflet valve in Europe is the “Björk–Shiley Disc valve” and the most implanted worldwide is the Medtronic Hall (Fig.1-12b). Tilting valves can create an opening angle from 60° to 80°C, thus achieving two different sizes of orifices [60,64];
- Bileaflet valves: this substitute class was implemented for the first time in the 1980s. This two-disc technology is capable of excellent hemodynamic performance and provides low thrombogenicity in comparison with its counterparts. This enables the bileaflet valve to be the most frequently implanted mechanical replacement in the world. The structure is composed of two semicircular leaflets that are attached to a rigid ring by small hinges or open pivots. The disks can open and close simultaneously. The opening angle of the leaflets ranges from 75° to 90°, resulting in three orifices. The most commonly employed valve substitutes in this category are the St. Jude Medical valve (Fig.1-12a) and Bileaflet Bicarbon–Sorin (Fig 1-13) [60,65].

Figure 1-13: Composite image of examples of mechanical valves from the major manufacturers. Adapted from[65].

1.5.2 Bioprosthetic heart valves

Bioprosthetic heart valves (BHV) are usually manufactured from animal heart valves or pericardium isolated from bovine or porcine origin. The great advantages of the use of BHV become evident in the cardiovascular field following the implantation of the first allograft aortic valve by Donald Ross [11]. Low thromboembolic risk and excellent hemodynamic performance led to hope for new generation of biological cardiac valves for all patient populations. But the lack of donor tissue has prompted the search for other biological substitutes. The first attempt with xenogeneic tissues preserved in mercurochrome-and-formalin was tested in five patients with poor durability in 1965. Later, in 1969 Carpentier introduced the use of glutaraldehyde (GA) as an oxidizing agent, which prevents collagen denaturation, stabilizing the structure of collagen and masking the xenoantigens in the porcine aortic valve. The use of GA treatment together with the metal frame would ensure the tissue's three-dimensional shape, which is of major importance for the functioning of the valve. The stent-mounted porcine valve was termed a bioprosthetic valve [5]. On the other hand, Ionescu introduced GA-fixed bovine pericardial valves mounted on a Dacron-covered titanium frame. The so-called Ionescu-Shiley Pericardial Xenograft was tested later in clinics in patients with an encouraging success rate [9].

Bioprosthetic substitutes can be fabricated as stented or stentless valves. The aim of the design is to mimic the anatomy and function of the native valve. Therefore, various aspects have to be considered in

the design of the substitute such as the assembly of the valve, techniques used for surgical implantation and the biocompatibility of the chosen material [66].

1.5.2.1 Stented valves

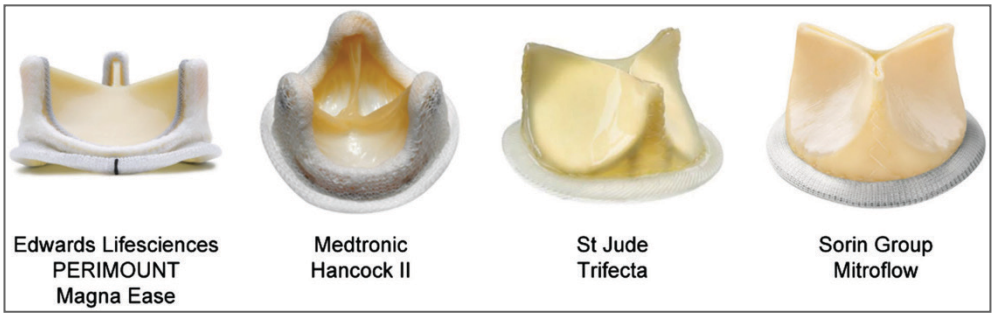

Figure 1-14: *A composite of bioprosthetic valves from each of the four major manufacturers. Adapted from[65]*

Stented bioprosthetic valves are the most commercially produced substitutes for heart valve replacement. Pericardial valves are produced from GA-fixed sheets of pericardium forming valve leaflets mounted inside or outside metallic or polymer stents (Fig. 1-14 (Carpentier-Edwards Magna)). The stent consists of three posts resulting in a semilunar shape, surrounded by a swing ring enabling the fixation of the implant in valve annulus. GA-treated porcine leaflets are mounted directly on the supporting stent (Fig. 1-12d (Medtronic Mosaic)). It has been reported that the stent could result in obstruction of the left ventricle, a decrease in the opening area of the valve and increase in stress at the stent sites. These facts may impact the cardiac function and durability of the valve [60]. The most famous stented valves from several manufacturers are shown in figure 14.

1.5.2.2 Stentless valves

The concept of stentless valves was introduced following in the footsteps of homograft aortic valve replacement, which was seen as the first stentless implanted biological valve. The main aim was to improve hemodynamic performance. The bioprosthesis is sewn

directly at the site of the implantation either as full root or using a modified subcoronary-technique [60]. The stentless design is foreseen for implantation of larger prostheses, leading to a larger effective orifice area, resulting in better hemodynamics and decreasing the risk of valve prosthesis-patient mismatch [67] (Fig. 1-15b). Recently it has been shown in a randomized trial that the use of stentless Freestyle (Medtronic) for aortic root replacement is more suitable than a homograft. Progressive valve dysfunction and the need for reoperations were significantly lower in Freestyle [68] (Fig. 1-15b). However, stentless valves with a semilunar shape cannot be applied for mitral valve replacement.

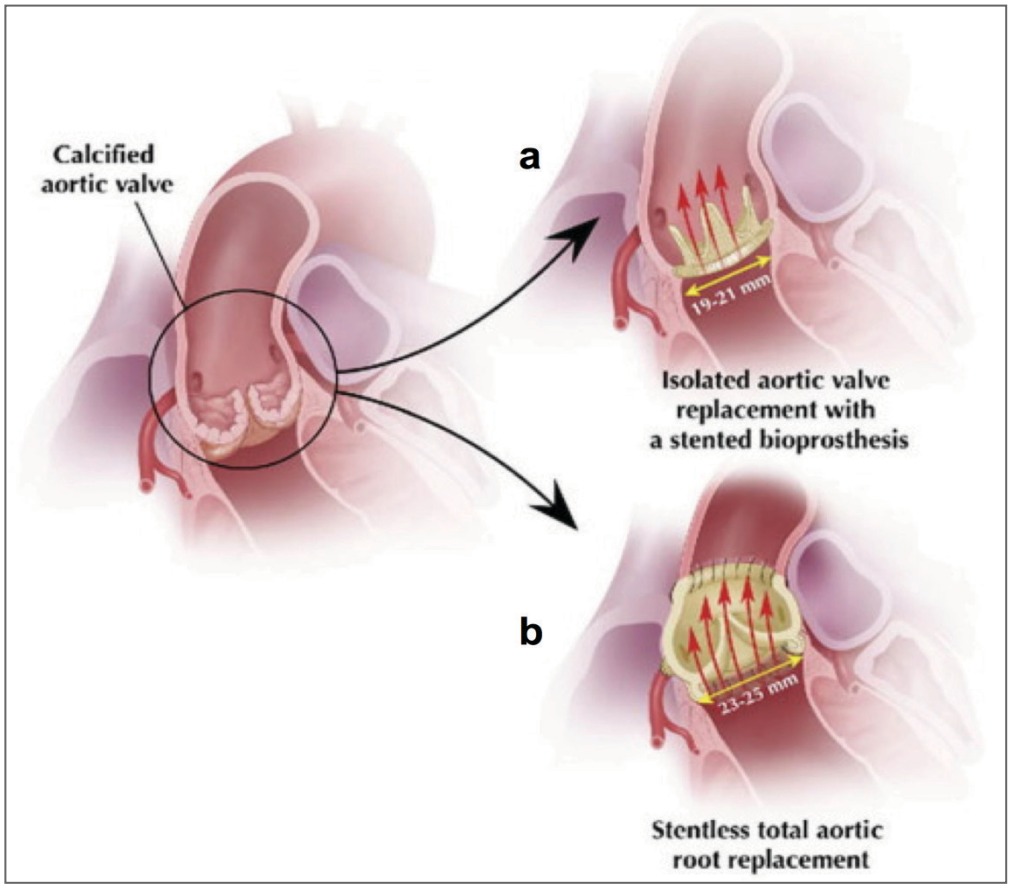

Figure 1-15: *Aortic valve replacement with stented (a) and stentless bioprosthesis (b) for total aortic root replacement. Adapted from [68]. Figure illustration by Rob Flewell. Stentless total aortic root replacement provides a lower rate of structural valve deterioration and reoperation as observed in homograft.*

1.5.2.3 Percutaneous valves

Percutaneous heart valve implantation has recently been introduced into clinical practice as an alternative to open surgical replacement. It provides minimal invasive intervention without the need for heart-lung bypass machines. The implantation is performed on a beating heart. It is intended for high-risk patients with severe aortic stenosis. The valves are usually mounted into a balloon-expandable (Fig. 1-12g) or elastic-memory Nitinol stent (Fig. 1-12h) and delivered via catheters employing mostly transarterial or transapical approaches (Fig. 1-16b) [69]. Several companies offer bioprosthetic valves for transcatheter implantation produced with bovine or porcine pericardium. The latter is thinner, enabling the size of the delivery system to be decreased. Among the commercial available percutaneous valves are [70]:

- Engager™ System (Medtronic Inc., Minneapolis, MN), with bovine valve pericardial bioprostheses;
- JenaClip (JenaValve Inc.,Germany) based on porcine aortic valve;
- CoreValve (developed by Medtronic Inc.) realized with porcine pericardium (Fig.1-12h);
- Edwards Sapien valve (Edwards Lifesciences) made of bovine pericardium (Fig.1-16a);

Percutaneous heart valve implantation provides major advantages over bioprosthetic valve implantation, such as superior hemodynamic performance, safety and reproducibility. It can be used for a variety of valve replacements in the aortic, pulmonary and mitral position in most patients. However, transcatheter technology is one of the most expensive heart valve replacements today [71]. Some options for commercial percutaneous heart valves are illustrated in figures 1-16.

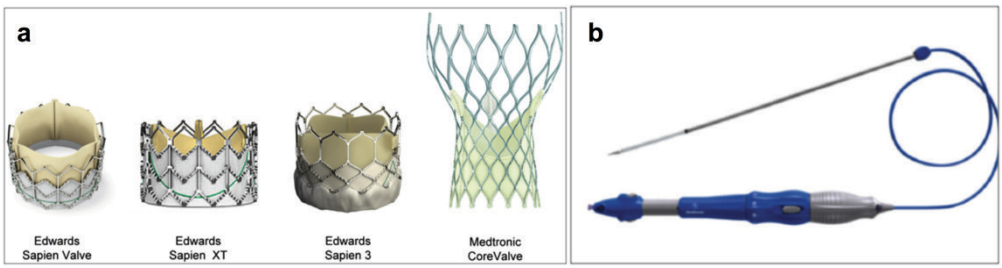

Figure 1-16: *(a) Edwards Lifesciences have developed three transcatheter heart valves. The first successful designed heart valve - CoreValve - was from Medtronic. Adapted from [4](b) delivery system. Adapted from [72]*

1.5.2.4 Allograft heart valve

The idea of using a human cadaveric heart valve to replace a diseased native one is quite old. The application of allograft implantation was initiated by the experimental work of Lam [73], who performed an allogeneic implantation of an aortic valve in the descending aorta of a dog. Later, Murray et al. [74] applied this technique in patients for the replacement of regurgitating aortic valves, showing satisfactory results. Based on these works, a few years later Donald Ross in Europe [75] and Sir Brian Barratt-Boyes [12,76] in New Zealand reported independently about a similar procedure able to successfully replace aortic valves in humans. Follow-up of the treated patients showed excellent hemodynamic performance and durability [77]. Generally, allograft valves are preferred in patients with endocarditis, since they perfectly match a recipient's damaged valve annulus. The patient populations that are most likely to benefit from these valves are women of childbearing age, children and young patients. They are employed frequently for the reconstruction of the right ventricular outflow tract in pediatric patients (Fig. 1-17). Allograft heart valves combine various advantages such as remarkable performance, resistance to infection, and a low incidence of thromboembolic complications [78]. However, due to the limited availability of tissue donors (valve scarcity) [79], allograft valves are less used than bioprosthetic and mechanical prostheses in surgical intervention. The lack of human donor valves is owing to several attempts at prolonging their storage time and keeping them free from

pathogens. In the 1960s-1970s the use of harsh sterilization and preservation protocols including gamma irradiation [80], incubation in GA and flash freezing negatively impacted their durability [77], which was found to be inferior compared to that of mechanical valves. Later on, allograft heart valves were mostly aseptically stored wet with prolonged refrigeration at 4°C for implantation purposes [81]; subsequently this 4°C storage was replaced by cryopreservation methods and establishment of allograft heart valve banks. A more detailed description of banking procedures will be provided in paragraph 1.8.

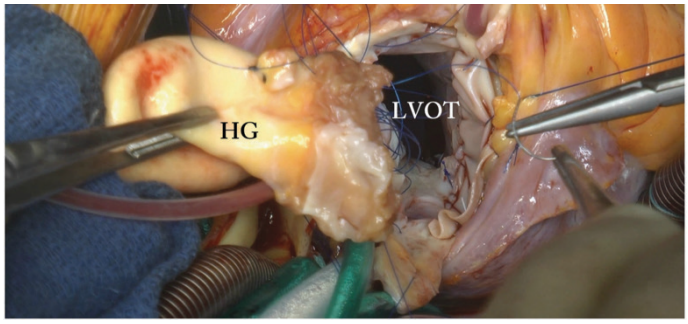

Figure 1-17: *Aortic valve replacement with aortic homograft. Adapted from [82]*

1.5.3 Structural degeneration of biological valves

About 30% of xenogeneic bioprostheses and 10-20% of homograft heart valves failed within 10-15 years of implantation [63,83]. In the young patient population, this degeneration is stronger and rapider due to accelerated calcification, which is probably related to the recipient‘s age [84,85]. The key elements of tissue degeneration of biological valves involve factors related to (1) recipient metabolism, (2) the structure and chemistry of the implant, (3) preservation and processing methods, (4) mechanical load, and (5) surgical technique used for suturing the valve to the annulus [84]. Bioprosthetic valve failure was attributed to two main mechanisms: structural and non-structural degeneration [86] (Fig. 1-19). Non-structural deterioration is mainly induced by extrinsic diseases such as pannus ingrowth, endocarditis and leaflet thrombosis, including patient-implant

mismatch or flawed attachment of the stent to the valve annulus (Fig. 1-18). In general, structural degeneration is the most common reason for failure of biological valves. Interestingly, the allograft and bioprosthetic valves share the common mechanism of structural deterioration of the native cups due to calcification. The pathophysiology of mineralization in cardiovascular tissues is a complicated issue, and one which is not fully understood. However, the mechanism behind the intrinsic modifications works the same way in both cases. Both undergo tissue degeneration marked by narrowing and thickening of the cusps, calcification and tears limiting their hemodynamic performance and durability (e.g. stenosis and regurgitation). In general, biological valves are characterized by their low/absent regeneration potential. While allografts are devoid of viable valvular cells caused by their harvesting and processing in ischemia conditions, and by cryopreservation trauma [87], xenogeneic valves are chemically treated with GA, devitalizing the cells and blocking the collagen fiber rearrangement. Both are unlikely to have any capability of ECM remolding and thus any endogenous matrix regeneration is rendered unfeasible. Moreover, the remaining fragments of the dead cells (cellular debris, and subcellular vesicle-like organelles) in the tissues were identified as a source of calcium-binding sites [88].

Both allogeneic and xenogeneic valves are prone to collagen degeneration. Their durability depends on the quality of the original isolated collagen. The loss of cells which are usually involved in ECM remolding results in progressive collagen degradation [13]. Besides this, the fixation of collagen with GA in the case of bioprostheses allows only one configuration/orientation of the fibers, compromising the structural reorganization of the cusps during valve function.

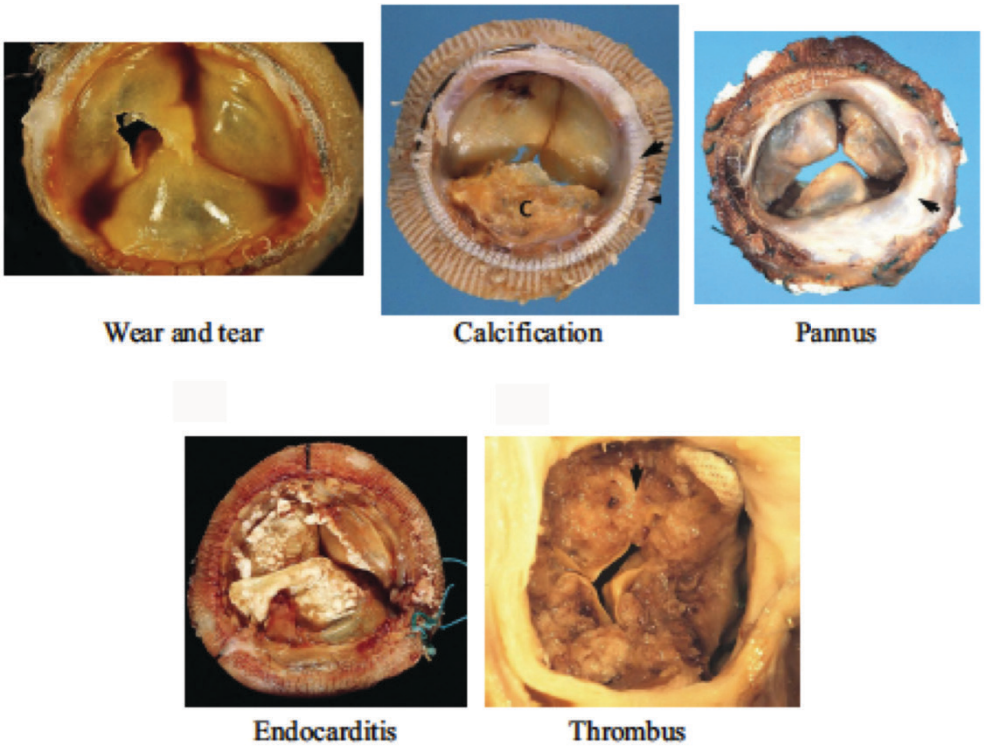

Figure 1-18: *Failure modes of bioprosthetic heart valves: the most common reason is calcification. Adapted from [89]*

Addressing the topic of calcification, collagen and elastin can serve as nucleation sites for calcium phosphate minerals [90–92]. In fact, clinical and animal studies demonstrated structural calcification of ECM components, i.e. collagen and elastin in allograft and bioprostheses, which seems to occur independently from cell-mediated ones.

The degeneration of bioprosthetic implants has also been associated with the immunological response to the xenogeneic epitopes galactose-α1,3-galactose (alpha-gal), since the GA fixation does not really remove the antigenicity of xenogeneic-tissues. Crosslinking renders the tissue only immunologically acceptable for in-human implantation, partially shielding the antigens and delaying the immune response. It has been demonstrated that immunologic activity against the implanted bioprosthesis plays a role in the acceleration of the calcification process [93,94]. In addition, the phospholipids and residual free aldehyde functional groups can react with the free

calcium ions in the blood, and contribute as well to bioprosthetic tissue calcification [95]. In the counterpart, the immunological issues related to the use of cryopreserved allografts are not fully elucidated. It has been shown that allografts may induce immunological reaction upon implantation. Kneib at al. [96] reported that patients with homografts developed a humoral response to human leukocyte antigens (HLA). Theoretically, this reaction can contribute to accelerate degeneration of allograft valves, but it is still not yet clear to what extent this immune reaction impairs valve dysfunction. Schoen et al. claimed in many studies that the typical degeneration seen in allograft valves cannot be attributed to immunological responses [87,97], whereas some evidence [98,99] has confirmed the involvement of an immunological response phenomenon to structural valve degeneration.

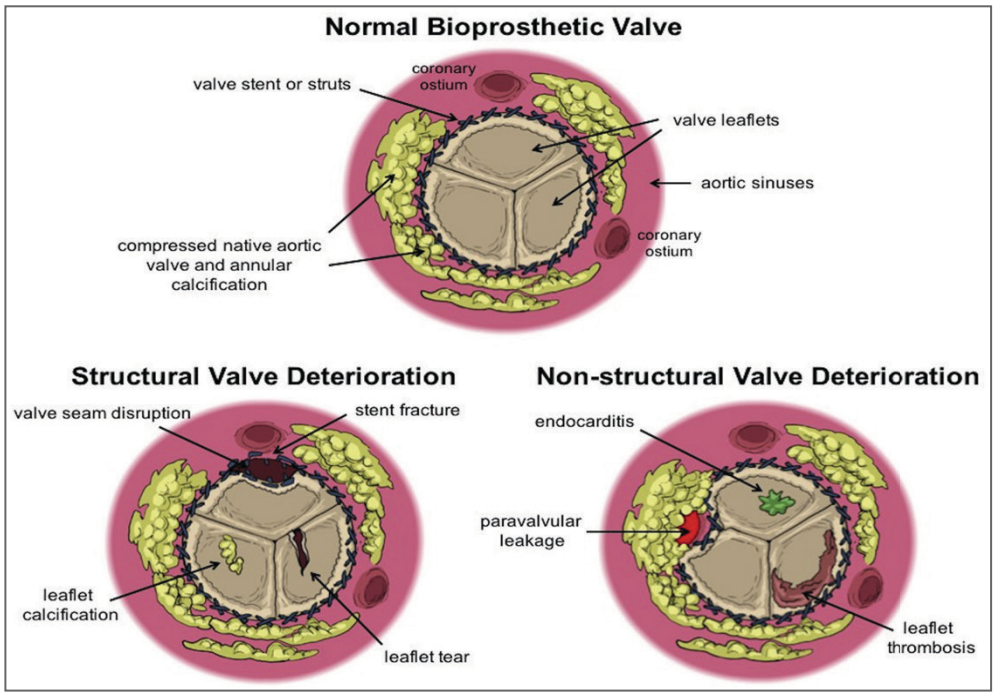

Figure 1-19: *Structural und non-structural degeneration of bioprosthetic valves. Adapted from [86]*

1.6 Scaffolds for cardiovascular tissue engineering

Cardiovascular tissue engineering (TE) aims to repair and replace tissues and organs damaged by disease, aging or trauma with new ones that mimic (at least partially) the function and structure of the original tissue. Body tissues and organs such as the skin or liver have the potential to renew and restore themselves through a regeneration process. This feature relies on the body's endogenous capacity for self-healing. Nevertheless, this capacity of the organism is limited to a certain extent. In general, two main strategies are used in tissue engineering, namely an *in vitro* and *in vivo* approach.

In vivo relies on the use of resorbable implants, which have the potential to induce the body's endogenous regenerative capacity in order to gradually restore the graft and convert it into an autologous-like tissue, while *in vitro* TE applies the strategy of using cell-seeded scaffolds in static (Incubator, two dimensional) or dynamic (Bioreactor, three dimensional) conditions. Generally, the media are supplemented with growth factors and proteins that are needed for cell maintenance and differentiation. This approach aims to develop a mature implant equivalent in the laboratory, ideally using the patient's own cells.

Traditionally, three types of scaffold have been suggested for cardiovascular TE: porous scaffolds, fibrous scaffolds, and hydrogels (Fig. 1-20) [100].

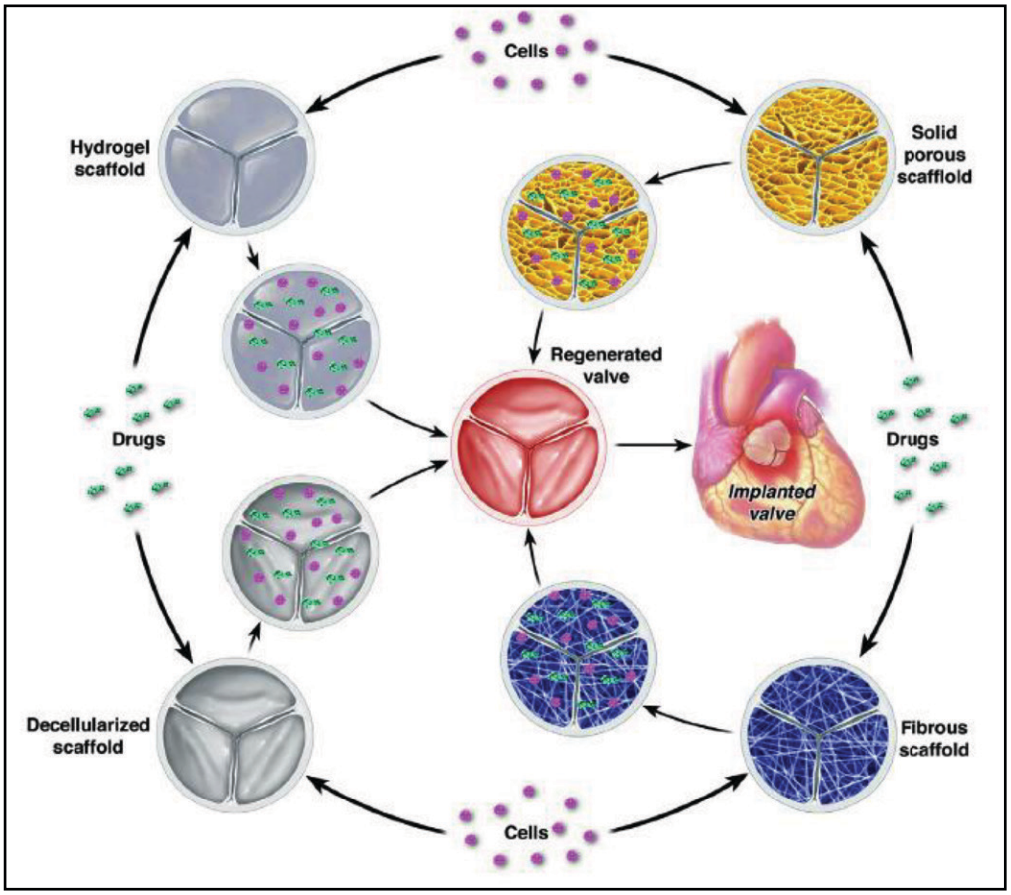

Figure 1-20: *Cartoon of the principle scaffolds that have been utilized for heart valve tissue engineering research. Adapted from [100]*

1.6.1 Scaffolds

Scaffolds constitute an important component for tissue engineering strategies. A wide range of options can be considered when choosing the best biomaterial for cardiovascular TE. All biomaterial types have strengths and weaknesses related to their structure and composition and chemical modifications, though ideally scaffolds must meet the following basic requirements [101]:

i) Cyto/biocompatibility: Ideally scaffolds should not provoke any immune reaction upon implantation, in order to prevent tissue rejection. In addition, they must provide a 2/3D structure for cells to attach, proliferate, differentiate and migrate onto and through the scaffold. For cardiac TE

applications it is of major importance that scaffolds should be bio-compatible with their surrounding environments such as cells and tissue components and in contact with blood, where induced thromboembolism can lead to severe complications;

ii) Bioactivity: It should possess a bioactive surface and physical cues such as topography to facilitate cell alignment, organization and promote faster regeneration;

iii) Architecture: any TE biomaterial should have a porous structure which allows cell penetration and migration and enables new tissue formation and remodeling. Additionally, the structure must promote nutrient and metabolite transport and have a predictable biodegradable rate that matches *in vivo/vitro* tissue growth and regeneration (balance between tissue degradation ≈ tissue formation). The by-products should not be toxic;

iv) Biomechanical properties: the scaffolds must have appropriate mechanical properties, which should match closely those of the native tissue. This is important on the one hand for *in vivo* functionalization of the implant and on the other hand because it influences the mechanosensitivity of the cells, determining the differentiation tendency.

1.6.1.1 Biodegradable synthetic scaffolds

Synthetic scaffolds include all materials that are chemically designed to mimic natural products but still can provide biocompatibility [102]. They were introduced as resorbable medical devices for tissue repair. However, they also offer many attractive advantages for TE applications. First, their degradation kinetics can be controlled to suit different applications in TE, supplying material with

superior biomechanical properties which has a greater advantage over natural polymers. Scaffolds can be fabricated into any design and shape with requested pore size, which allows selective control of their desirable stiffness and biomechanical properties. Generally speaking, mechanical strength is inversely proportional to porosity. Therefore, depending on the application, a compromise between porosity and biomechanical strength always has to be taken into consideration. Furthermore, manipulation of the surface with attractive chemical groups for cell attachment allows for improved interaction with the matrix surface. An attractive synthetic polymer used in cardiac TE (Fig. 1-21) with wide applications is polyglycolic acid (PGA). Depending on its medical applications, PGA can be produced in different forms: knitted, woven and non-woven meshes, foam, sponges and nano-fibers.

Another appealing synthetic polymer is poly(lactic acid) (PLA). One of its main advantages is the release of L-lactic acid, a naturally occurring byproduct of anaerobic metabolism in humans, which can be eliminated as carbon dioxide and water. Application of the polymer (PGA) in the cardiovascular field was initiated for construction of tissue-engineered heart valve leaflets *in vitro* and *in vivo* in ovine models [103,104]. The preliminary results were indicative of proper matrix generation, but the success of these valves was limited, partially due to animal infection and their short persistence. PGA and PLA are usually used in medical applications as absorbable sutures, known as Dexon and Vicryl. A combination of the polyester polymers PLLA and PGA (PLGA) is among the most frequently successfully applied biodegradable synthetic polymers for tissue engineering strategies [105]. They can be produced in different ratios, enabling tuning of their biomechanical behavior. The copolymer was also used for development of tissue-engineered heart valve leaflets *in vitro,* which showed high biocompatibility but poor valve performance and durability. Unfortunately, PLGA is characterized by limited bioactivity due to the release of large amounts of highly acidic byproducts. However, this drawback can be improved by using salt leaching

(sodium chloride particulates) to increase the pH, thus leading to better bioactivity [105].

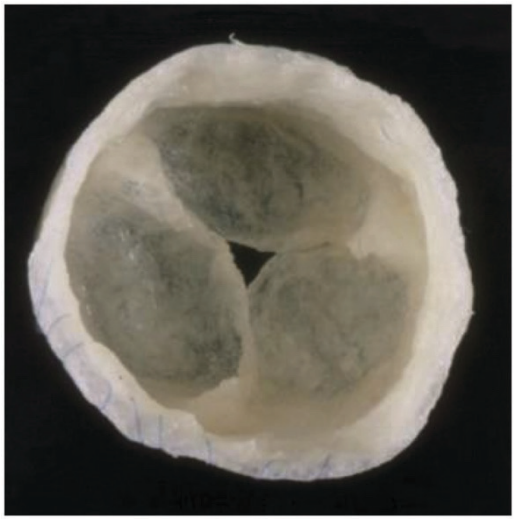

Figure 1-21: *TE heart valve of PGA mesh coated with poly-4-hydroxybutyrate after 14 days of conditioning in bioreactor. Adapted from [106]*

1.6.1.2 Natural scaffolds

Unlike synthetic polymers, natural occurring polymers are easily available, non-toxic and can be isolated from animals or plants. They consist of proteins or polysaccharides, which can be utilized to produce porous, fibrous and hydrogel natural scaffolds.

Natural polymers promise high biocompatibility and biodegradability without any adverse impacts on the environment or human beings. They are composed of natural binding sites for cells and are safe and free from side effects. However, they are characterized by poor biomechanical properties and rapid degradation *in vivo*, which must be taken into account during scaffold design. Among naturally occurring polymers, collagen, alginate, and fibrin are the most commonly used for cardiac scaffold applications. Hyaluronic acid, chitosan and silk have also been employed.

Collagen is by far the most abundant and predominant fibrous matrix protein in mammals. It accounts for 30% of the total protein found in the body and consists of a triple helical structure. It is slightly

immunogenic, due to a large degree of homology across species and has been used extensively in a wide range of TE applications. The variety of its parameters involving protein density, orientation and packing result in different but unique mechanical properties in a large number of tissues. Thus, its application ranges from soft tissues such as cartilage and skin to hard tissue like bone [105]. Collagen type-I is routinely used for research after extraction from rat or bovine tendons and bovine dermis [102]. Collagen has been produced in different forms, such as sponges, fibers or hydrogels. For fabrication of collagen scaffolds, a wide range of manufacturing techniques can be used to achieve the desirable properties [102]. For materials with high porosity, freeze-drying or phase separation are the techniques of choice, while electrospinning can be used to create aligned nanofibrous collagen scaffolds [107]. Collagen type-I can also be combined with glycosaminoglycans and processed through freeze-drying, for example, to generate scaffolds for skin in burned patients [108]. For heart valve repair purposes, collagen modeling (collagen gel) methods have been applied to manufacturing of valve cusps [109]. A lack of cell invasion and poor mechanical properties were observed when utilizing collagen gel. Further improvement of porosity and combination with synthetic polymers would enhance the strength of the scaffolds. Since the surface morphology of the biomaterial plays a role in the bioactivity of the scaffolds, it is crucial to take into account the optimization of the fabrication method. Available options for the fine-tuning of collagen stiffness are limited. However, crosslinking procedures have been widely used to prevent the degradation of collagenous scaffolds *in vivo* and to increase their strength, such as dye-mediated photooxidation and chemical, synthetic and natural agents. GA is a frequently applied crosslinking-agent in a variety of collagenous biomaterials. The most used form of collagen in clinical practice is provided by skin substitutes (Cosmoderm, [110]) and dermal fillers (Cymetra, [111]).

Fibrin gel is a natural scaffold that can be formed by the body after injury. It can also be produced from fibrinogen and thrombin as

scaffolds for TE applications. Fibrin-based biomaterials have been considered a particularly attractive material for medical application. Their unique polymerization mechanism enables the tuning of gelation times and manipulation of the network structure. The role of fibrin as a biological scaffold has been acknowledged both experimentally and clinically. It is widely used for speeding up wound healing or for repairing a large number of organs such as the heart [112] and urinary tract [113]. Fibrin is highly bioactive, and consists of many cell binding epitopes allowing interplay with different cell types and making its application extremely attractive for TE strategies. In fact, fibrin produced using the patient's own blood has been used in the cardiovascular field to bioengineer heart valves (Fig.1-22a1 and a2) [114]. This offers great advantages for its clinical use, since the autogeneic scaffolds are devoid of immune response-related complications. The most significant limitation of fibrin scaffolds is a lack of strength in their structure to withstand mechanical load *in vivo* [115]. Enhancement of mechanical strength is still under investigation. Different strategies are being tested to overcome this challenge, and fabrication of a composite using a synthetic/natural polymer for engineering vascular grafts [116] may be one of the possible routes. Current technology using aprotinin, a protease inhibitor of fibrinolysis, also holds significant promise for this field [117].

Alginate is a natural polysaccharide which is generally isolated either from brown algae or bacteria. This natural polymer has been largely used as hydrogels for TE applications. Arginine-glycine-aspartate (RGD) peptides are incorporated into scaffolds to boost their bioactive features, allowing matrix-cell interaction. Before use, alginate is further cross-linked with UV light or chemically with carbodiimide to improve its biomechanical properties. Alginate has attractive characteristics, making it interesting for cardiac regeneration. First, it is soluble in water as a viscose solution, facilitating its use as an injectable hydrogel. Moreover, it possesses the ability to build beats, fibers and films, thus broadening its experimental and clinical application. Alginate applications include cell transplantation, wound

healing and drug/protein delivery system. Most polysaccharides are biocompatible with blood, which make them strong candidates for the generation of cardiac failure [118] and construction of heart valve substitutes (Fig.1-22b1 and b2). Advanced alginate systems (Algisyl) are currently tested clinically in patients with moderate to severe heart failure [119].

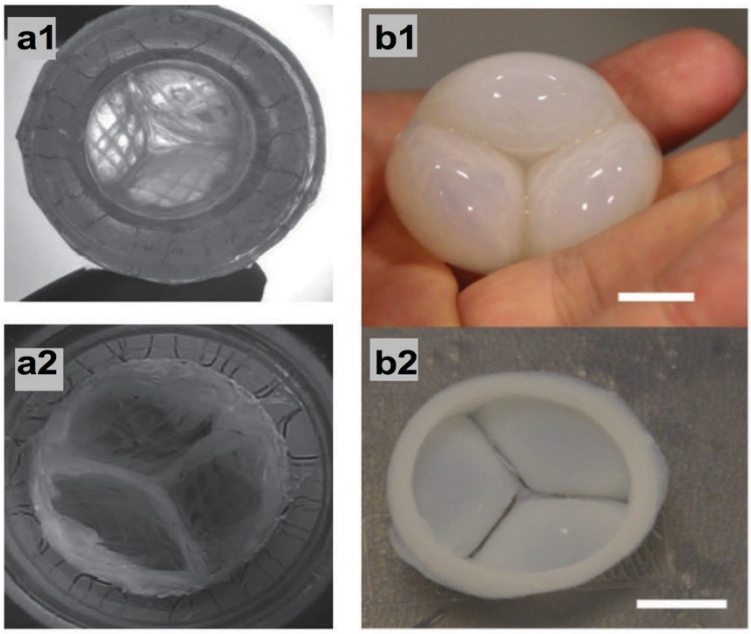

Figure 1-22: *Heart valve for TE strategies fabricated from natural scaffolds. a1 and a2 fibrin-based heart valve reinforced with textile, Adapted from [120]. (b1) and (b2)" Alginate shaped in tricuspid valve made from hydrogel. Adapted from [119]*

1.6.1.3 Decellularized scaffolds

There is a growing clinical need for readily available substitutes for a variety of cardiovascular surgical demands. Allogeneic tissues continue to represent the best solution for in-human transplantation. However, their application is limited in part by donors' scarcity and tissue failure due to the immunological-inflammatory processes caused by the remaining viable cells after cryopreservation.

In order to overcome this hurdle, decellularization has been initiated to improve first of all the durability and *in vivo* functionality of the scaffolds. The procedure can be employed on allogeneic and

xenogeneic tissues, ideally rendering them free of cells and immunogenic epitopes and hence making them potentially biocompatible for in-human implantation. The most appealing results today have been achieved using decellularized allograft heart valves. It has become evident that the removal of cellular components and especially HLA antigens from the endothelium ensures their longevity [121,122]. In xenogeneic tissues, GA-treatment was not capable of providing a long-term solution for antigenicity-related complications. The immune response against xenogeneic epitopes such as Alpha-gal and N-Glycolylneuraminic acids (Neu5GC) can be detected after heart valve replacement [123]. Alpha-gal provokes a hyperacute rejection, while with Neu5GC the response is delayed.

Decellularization offers a solution to the use of animal tissue to obtain acellular scaffolds devoid from DNA and optimally foreign epitopes, while the original ECM and their components are maintained and hold the matrix bioactive properties necessary for cell adhesion, proliferation and differentiation. Xenogeneic heart valves and pericardium obtained from bovine and porcine animals are abundantly used as acellular scaffolds in cardiac vascular TE approaches aiming to solve the donor shortage issue. Thanks to its excellent biomechanical properties of withstanding load, bovine pericardium is preferred over other species, while porcine pericardium has the major advantage of lower thickness. Due to the possible risk for patients of developing Creutzfeldt-Jakob disease, bovine pericardium is harvested from prion-free animals.

1.6.2 Tissue guided regeneration *in vivo*

In the last decades, major efforts were made to develop cardiovascular substitutes by means of TE. The strategy of *in vivo* guided regeneration relies on the organism's endogenous capacity for regeneration and repopulation of the implanted graft, avoiding lab-expensive and time-consuming *in vitro* cell culture in bioreactors [124]. The *in vivo* TE approach was introduced to offer ready and easily

available substitutes in a short time. It is assumed that over time the scaffold would slowly degrade, ideally leading to a biological matrix with high potential for remolding and growth. Basically, the approach is based on an inflammatory response-driven functional regeneration, which can be divided into three phases (Fig. 1-23):

i. An inflammatory phase, which is characterized by:
   - material/blood contact allowing the formation of scaffolds rich in endogenous proteins, cytokine and growth factors initiated by the first steps of the wound healing process;
   - inflammatory response with prominent infiltration of immune cells, such as monocytes (e.g. macrophages), and the formation of a provisory matrix.

ii. A proliferation phase, which is composed of:
   - recruitment of various stem cells, progenitor cells and fibroblasts;
   - interplay between macrophages and cells leading to production of ECM components, angiogenesis, and re-endothelialization of the graft.

iii. A remodeling phase, which consists of
   - remodeling ECM components (Collagen, Elastin, GaGs);
   - resolution of the inflammatory response.

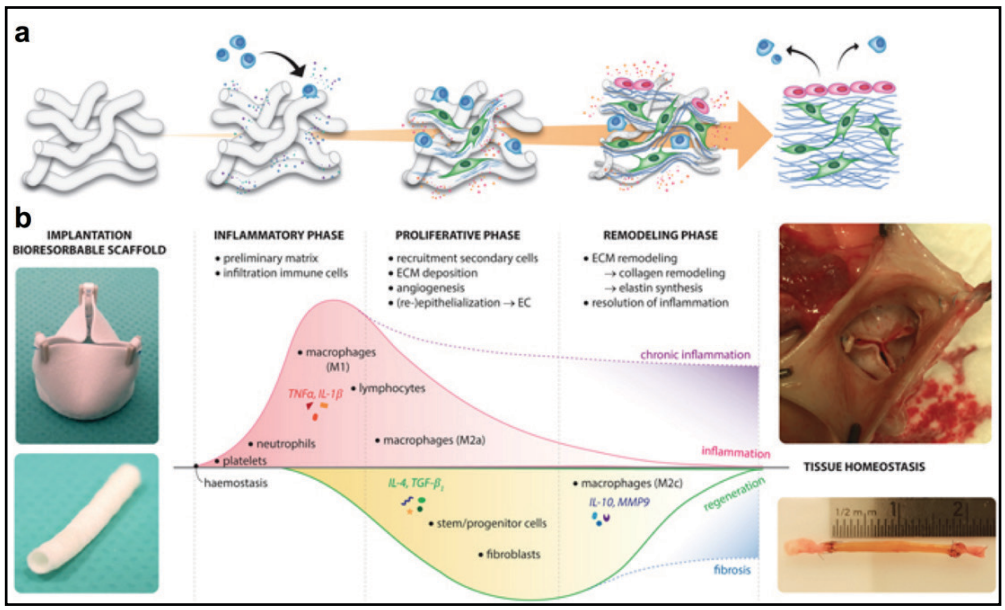

Figure 1-23: *Overview of different phases of tissue-guided regeneration from resorbable material toward a viable substitute. a: the natural phases of the wound healing response. b: Inflammatory phase characterized by several steps. Adapted from [124]*

In vivo cardiovascular TE applications include the regeneration of blood vessels, heart valves and cardiac patches. Polyurethane biodegradable scaffolds were attempted for arterial replacement. Unfortunately, the use of this synthetic polymer often shows poor mechanical properties *in vivo* leading to development of an aneurysm [125]. The main challenge for arterial substitution is that the implant should be able to withstand arterial pressure immediately after implantation. In order to overcome the lack of strength in the synthetic scaffold, Xeltis BV developed a bio-resorbable supramolecular polyester using electrospun for total cavo-pulmonary connection in pediatric patients. The initial clinical trial showed promising results in terms of scaffolds biocompatibility and remolding [126]. Other trials have been conducted using electrospinning technologies to produce new hybrid scaffolds made from biodegradable synthetic material and gelatin. The mixture of synthetic and natural polymers seems to significantly improve the elasticity and hence the compliance of the tubular grafts [127].

Regarding tissue engineered heart valves for *in vivo* settings, the most prepossessing outcomes have been achieved using acellular

scaffolds such as decellularized homografts [20,128,129]. In preclinical and clinical studies, decellularized heart valves for allogeneic implantation demonstrated self-regeneration potential, providing viable and functional tissues, excellent hemodynamic performance and even somatic growth in young patients [17,129–131]. These promising results underline the preference for allogeneic scaffolds for clinical use (Fig. 1-24b). However, clinical studies produced controversial outcomes in terms of their potential to stimulate endogenous cellular regeneration. SynerGraft valves demonstrated poor repopulation *in vivo* [132], while the Hannover group reported almost full repopulation of the arterial wall and partial recellularization of the cusps with the patient's own cells (Cebotari et al. 2011).

Cryolife Inc. (Georgia, USA) initiated the commercialization of decellularized heart valves upon the SynerGraft (SG) patent for decellularization technology. Their most prominent product is CryoValve SG (Fig. 1-24a), a cryopreserved allograft substitute, with good clinical outcomes [133]. According to the company, 5,700 heart valve replacements have been performed since 2000. Considering donor scarcity, decellularized xenograft heart valves [134,135], decellularized porcine and bovine pericardia [136,137], and decellularized porcine small-intestine submucosa [138] represent potential alternatives for the generation of novel heart valve replacements. Despite the reassuring results obtained from animal studies (500/700 SynerGraft porcine valves) carried out by O'Brien et al. [139], application of their product in clinical trials demonstrated high failure and detrimental consequences. Non-fully decellularized scaffolds with remaining xenogeneic epitopes resulted in the death of three pediatric patients [140]. Therefore, clinical application of xenogeneic scaffolds requires overcoming the stumbling block of the immune response to xenoantigens. Matrix P, a decellularized porcine valve substitute with a surprisingly positive clinical outcome [141], is commercially distributed by Autotissue Ltd. (Berlin, Germany). However, a recent investigation demonstrated that 38% of patients required reoperation due to graft failure after only 15 months [142].

Currently, other technologies are being tested in an attempt to overome the xenoantigen hurdle, especially alpha-gal. Epitope-free tissues are generated from transgenic knockout pigs for this antigen [93,134]. Moreover, coffee bean α-galactosidase and recombinant human α-galactosidase seem to be effective at removing alpha-gal in porcine aortic valves and pericardium [143]. It is likely that these new alternative methods are efficient, but they are also very costly and time consuming and need particular employees with highly specialized expertise. Apart from cardiac replacements utilizing valves of animal origin, decellularized xenogeneic pericardial patches have been extensively investigated for heart valve fabrication and cardiac reconstruction [144–146]. Although it promises success, clinical use is restricted due to the absence of proof showing the removal/deactivation of the xenoantigens and the lack of suitable preservation and sterilization methods. However, the commercialization of decellularized pericardial patches does not seem to be completely affected. (Matrix P Plus equine, (Autotissue Ltd, Berlin, Germany) and PhotoFix decellularized bovine pericardium and CryoPatch Pericardial Sheet, (Cryolife Inc.) (Fig. 1-24c).

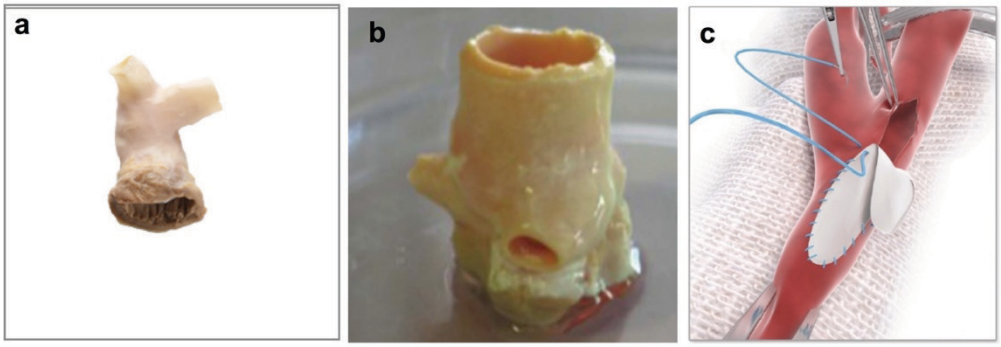

Figure 1-24: *Decellularized scaffolds. A: Synergraft CryoValve B: TRICOL aortic graft (porcine) for allogeneic implantation applied successfully in preclinical study, C: PhotoFix decellularized bovine pericardium. a and c adapted from[147]. b Adapted from[17]*

1.6.3 Decellularization in the cardiovascular field

Decellularization procedures have been introduced to overcome the current drawbacks of cryopreserved allografts and bioprosthetic heart valves. This modality allows removal of all endogenous cell

elements including cell membranes, organelles, and DNA, which are involved in structural deterioration and valve failure (inflammation, immune reaction and calcification) [84,148]. Ideally, the native structure, components, and physical properties should be preserved for proper function *in vivo*. In addition, these scaffolds should be biocompatible for cell colonization and repopulation. A variety of protocols were applied to decellularize tissues or organs. The approach is based on the lysis of cell membranes using either ionic solutions or physical treatments followed by detergent extraction steps to solubilize the nuclear and cytoplasmic cellular elements and finally combined with enzymatic treatments, mechanical agitation and/or perfusion. At the end, washing steps are carried out to remove residues of the chemicals used during the procedure. The effectiveness of the agents used for decellularization depends on the tissues cellularity, density and lipid content [149]. Frequently used chemical agents include: hypotonic and hypertonic solutions, detergents, and alcohols. Treatments with hypotonic and hypertonic solutions or their alternation are responsible for the induction of cell lysis through simple osmotic shock. Hypertonic solutions separate DNA from proteins and may also cause dramatic damage to some proteins, especially for those carrying the contractility function [150]. For efficient removal of DNA from the tissue, ionic, non-ionic, and zwitterionic detergents are used for decellularization. These detergents can easily solubilize the membrane and isolate DNA from proteins. Sodium dodecyl sulfate (SDS) is among the strongest chemicals used for this approach. This ionic agent is very effective in removing cell residues from dense tissues compared to other detergents but is also much more detrimental to ECM (loss of GAG and growth factors, denaturation of collagen and precipitation of elastin). Alternatively, sodium cholate offers a better option for preserving the ECM, while removing the cellular elements from the tissues [149]. The most commonly used nonionic gentle detergent for tissue delipidation is Triton X-100. Its general targets are lipid-lipid and lipid-protein interactions [151], whereas zwitterionic detergents are

specially selected for thinner tissues, and their application is accompanied by disruption of the ultrastructure. A balance between the exposure times, extraction of cellular components and the loss of ECM proteins should be taken into consideration during the procedure.

Chelating agents, such as ethylenediaminetetraacetic acid (EDTA), are able to disrupt cell adhesion to ECM, therefore they are usually supplemented to the detergents in the first steps of decellularization to boost the effect of the subsequent extraction treatments. It is likely that this cell disruption leads to the release of autolytic activities and metalloproteinase. Serine protease inhibitors such as phenlymethylsulfonyl fluoride (PMSF) are employed to prevent adverse damage to ECM [152,153]. Moreover, biologic agents such as enzymes are frequently utilized to break cell-cell binding and proteins by cleaving peptide bonds. In order to enhance the effectiveness of decellularization, enzymes such as nucleases are used as a terminal step in order to remove the remnants of nucleic acids. Endonucleases are preferred over exonucleases. The cleavage of the nucleotides occurs in mid-sequence and thereby they can easily fragment DNA. Trypsin, a serine protease, is another enzyme that can be used for tissue decellularization. However, it should be used with caution. Elastin and collagen possess limited resistance to this enzyme.

Alcohols, such as isopropanol, ethanol, and methanol, are effective for removing lipids. They should be used carefully, due to their fixative potential.

Freezing/thawing cycles and force/pressure can be applied as well as physical technique, allowing cell lysis within thin tissues, such as pericardium, urinary bladder and intestine [149,154]. However, the freeze-thaw process causes ice crystal formation, which does not lead to the loss of ECM proteins but might minimally alter its histoarchitecture.

Additionally, perfusion and agitation are additive techniques used during decellularization. Perfusion is preferred over agitation for the

vascular tissue network. It has been shown to be highly effective in such tissues. Regarding non-vascular tissues, immersion combined with agitation has been described as successful in heart valves, pericardium, tendon and other targets [149]. The exposure time of such approaches depends on tissue thickness, density, detergent used, and intensity of agitation.

1.6.4 Decellularization procedures for pericardium

Pericardium can be easily obtained from different biological sources. It can be autologous, allogeneic or xenogeneic. In general, human pericardium is for some surgeons the best choice for cardiovascular surgery. It possesses several advantages over its xenogeneic counterpart, because it is free from animal-derived pathogens and shows growth potential [155,156]. However, its clinical application is currently restricted in cardiovascular surgery due to shrinkage, thickening, degeneration and its tendency to form aneurysms [157]. Several groups experienced negative and failed outcomes using autologous pericardium to repair heart valves [158–160]. Valve deterioration was caused by thickening and retraction of valvular leaflets.

Human pericardial patches are commercially distributed by CryoLife but limited scientific information is available on these products. In order to prevent retraction, cryopreserved human pericardium has been stabilized with GA and used for replacement of cusps or valves. Although processing the tissues with GA stabilizes the ECM components and provides low antigenicity, the use of cross-linked tissues has also been associated with several limitations, including altered mechanical properties, calcification, cytotoxicity and early clinical failure in patients [158,161]. In order to produce acellular biocompatible pericardium for cardiovascular surgery, a wide variety of protocols have been established and performed in different ways [136,137,144]. Courtman et al. suggested a four-stage detergent and enzymatic extraction process for bovine pericardial tissue. The

preliminary results revealed acellular scaffolds composed of well-preserved collagen, elastin and GaGs [162]. Interestingly, Courtman reported that the deletion of the use of 1% SDS as a final extraction step was beneficial for the outcome.

During recent years, many other groups have compared a variety of decellularization protocols in order to find the most suitable method for decellularizing pericardium. Yang et al. performed and compared three protocols on bovine pericardium, namely the detergent and enzyme extraction (DEE), trypsin (TS), and Triton X-100 and sodium-deoxycholate (TSD) methods. They reported that all the protocols were effective in the removal of DNA, although the TS and TSD approaches resulted in severe damage to the matrix, altering the biomechanical properties [163]. Other comparative work was carried out by Mendoza-Novelo et al. The principal chemical agents utilized in this experiment were: Triton X-100, tridecyl polyethoxy ethanol (ATE), and alkaline treatment combined with nucleases. They also found that all protocols were able to effectively remove DNA. A decrease in GAGs content was observed after all three treatments, while no significant differences were observed between Triton X-100 and ATE in terms of maintenance of histoarchitecture and biomechanical behavior [164]. Recently, two other decellularization treatments for bovine pericardium have been investigated [165]: 1) 0.25%Trypsin-EDTA, TritonX-100, Deoxycholic acid, Peracetic acid/Ethanol and 2) Deoxycholic acid, DNase, RNase, Ethanol. Sahijt's work revealed that treatment with trypsin is damaging to the collagenous matrix. These results are consistent with these previous works [149,163].

Additional studies evaluated the impact of decellularization using SDS as a detergent, showing discrepancy in the literature. Mirsadraee et al. performed decellularization on human pericardium, applying SDS in combination with a hypotonic buffer solution and a nuclease and reporting excellent results. The decellularization with SDS succeeded in retaining all the major components and mechanical properties of the native matrix [166]. Conversely, in calf pericardium, SDS induced

swelling and a drop in the denaturation temperature, as well as modification of the biomechanical properties, also indicating a fall in the strength of the scaffolds [167]. This finding confirmed previous published work from Courtman et al. Decellularization protocols should therefore be optimized for specific tissues to achieve maximal cell removal with preservation of ECM integrity and biomechanical and bioactive properties.

Numerous post-decellularization treatments have been developed to improve biocompatibility of the graft upon implantation and potentially regulate host cell proliferation and differentiation. The functionalization of the pericardium using cell-adhesive peptide sequences today represents a promising strategy. The bioactive sequences are chemically defined peptides with high stability, and are devoid of immunogenicity [168]. Among the polypeptides applied in functionalization, the tripeptide Arg-Gly-Asp is the most common cell adhesion motif. Recently, Aubin et al. demonstrated the great functionalization potential of three different bioactive sequences on cell attachment of human umbilical vein endothelial cells and a trend toward increased *in vivo* endothelialization of decellularized ovine pulmonary and aortic valves [168]. Similar results have been achieved by Dong et al. utilizing RGD-functionalized pericardium. Increased cell colonization, proliferation and migration was achieved with this cell adhesion motif [169]. In the past, a protein-based coating approach to decellularized scaffolds (fibronectin, vitronectin, etc.) has been applied, inducing enhancement of endothelialization and recellularization of the autologous cells *in vivo* [170]. However, the coating with fibronectin and RGD was associated with an increase in neointima formation in vascular grafts [171,172]

1.7 Tissue banking of cardiovascular grafts

Since Ross and Barratt-Boyes introduced the use of human allografts and homografts into clinical practice there has been a clinical need to store available donor tissues to ensure their off-the-shelf availability for emergency or elected patients. Currently, heart valves and pericardium stored in tissue banks are cryopreserved human allografts ranging from newborn to elderly donors (> 65). The last overview published by the European Homograft Bank (EHB) in Brussels stated that between 1989-2008, 5,133 valves were cryopreserved, of which 4,600 were implanted in Europe. During the same period, 4,511 were discarded due to atheromas and fat deposits and a lack of sufficient decontamination (Table 1) [173].

Table 1: *Valves and arteries processed and discarded during last 20 years in Europe. Adapted from [173].*

	1989–1998				1999–2008			
	Valves		Arteries		Valves		Arteries	
Country	Processed	Discarded	Processed	Discarded	Processed	Discarded	Processed	Discarded
Belgium	2,207	834	655	139	2,950	1,300	1,857	617
France	693	237	57	13	1,490	634	130	47
Germany	454	200	13	1	166	93	6	0
Luxemburg	14	3	1	0	44	18	2	0
Switzerland	394	158	70	15	418	206	40	14
Netherlands	2	0	0	0	4	0	0	0
Italy	69	20	1	1	61	22	31	16

The initial tissue selection is carried out according to strict exclusion criteria focused on tissue quality, such as malformation, dilatation and calcification. It is performed by trained cardiosurgeons with the help of laboratory technicians from the tissue bank. Moreover, the quality control includes blood screening for transmissible diseases like HIV (human immunodeficiency virus), AIDS (acquired immune deficiency syndrome), hepatitis B/C, syphilis, enteroviruses and a series of histological and bacteriological examinations. Dissection, decontamination, cryopreservation and storage of the allografts are performed in separate workstations under laminar flow and sterile conditions. Usually, the tissues are procured from heart-beating multi-

organ donors, recipients of heart transplantation (domino heart), and non-heart-beating deceased patients (cadavers). The tissues are transported in sterile conditions in wet ice at 4°C in a triple bag filled with tissue culture medium or saline solution. Following their decontamination with antibiotic cocktails and negative bacteria sampling, the valves are exposed to 10% DMSO and frozen by slow-rate freezing and stored in the vapor phase of liquid nitrogen for a maximum of 5 years. When an allograft is needed, the tissue bank is contacted by a surgeon stating the emergency level and patient indications. On agreement with the tissue bank's proposal, a graft meeting the suitable criteria is sent to the clinic using dry ice shipment [173]. Alongside allograft heart valves, other tissues such as pericardium, arteries and veins are issued. Over the last few years, the activities of cardiovascular tissue banks in Europe have remained relatively stable. However, the number of donor tissues has decreased while demand has not. Among the European tissue banks, there are very large methodological differences regarding microbiological testing, decontamination and preservation of cardiovascular grafts. There is a high need for standardization of the protocols and procedures within European cardiovascular banks [174].

Given the recent advances of decellularized human valves undergoing clinical trials in Europe such as Espoir (decellularized pulmonary) [175] and Arise (Aortic valves)[176], crucial basic questions in tissue banking need to be revised:

- Is cryopreservation suitable for decellularized scaffolds?
- What properties should the preserved scaffolds ideally have?

Currently, decellularized heart valves are implanted shortly after accomplishment of the decellularization procedure. It was reported that they are stored in saline solution at 4°C for up to 3 weeks [129].

Table 2: Tissues issued by tissue banks, Adapted from [174]

Other tissues issued		2007	2008	2009	2010
Pericardium	banks	3	3	3	3
	in % of all banks	19%	18%	17%	17%
	tissues	39	50	54	81
Arteries	banks	7	7	7	9
	In % of all banks	44%	41%	39%	50%
	tissues	307	305	423	481
Veins	banks	3	3	3	4
	in % of all banks	19%	19%	17%	22%
	tissues	245	229	314	286

1.7.1 Cryopreservation of cardiac tissues

Cryopreservation relies on the use of cryogenic temperatures to preserve structurally intact living cells and tissues. Cryopreservation protocols have been established based upon knowledge acquired from the cryobiology of single-cell suspensions, which have later been applied to tissues. The main aim of this technique for tissue preservation is to ensure high cell viability and the genetic stability of cells after thawing, as well as to preserve the structure of the ECM. The most commonly used cryopreservation techniques are slow freezing and vitrification. These are two fundamentally different methods. Whereas conventional cryopreservation permits ice formation, vitrification is based on preventing it. Both methods, however, share the same physical and chemical relationships.

Basically, the principle of cryopreservation is dominated by the freezing of water, which represents 80% of tissue mass. The extent of damage caused by this process depends on the amount of free water in treated cells or tissues and on its ability to crystalize during the cooling process. In slowly cooled conditions, ice formation generally starts in the extracellular solution surrounding the biological material.

Many protocols are available to successfully cryopreserve different types of cells and even cell aggregates, but the most challenging task

is to achieve reproducible results for more complex tissues such as heart valves and engineered scaffolds, which requires knowledge of the important variable parameters involved in tissue cryopreservation. Among cryoprotective agents (CPAs), glycerol and DMSO are the most frequently applied cryoprotectants. Dextrans, glycols, starches, sugars, and polyvinylpyrrolidone have also been used as cryoprotective agents, but they are only used in combination with aforementioned low molecular weight cryoprotective agents. Additionally, fetal bovine serum (FBS) is often supplemented to cryopreservation solutions. The latter do not have any specific protective potential. CPAs protect during slow freezing by decreasing the rate of cell shrinkage and the ice fraction of the frozen solution, inhibiting solute effect injury due to too high salt concentrations, and minimizing intracellular ice formation [177]. Furthermore, they decrease the freezing point, providing more time for dehydration. However, they are cytotoxic at high concentrations. Toxicity can be reduced by decreasing the CPA loading temperature and using short exposure periods. Therefore, cryoprotectants should be used with caution. Their selection should first be based on their degree of toxicity and secondly on their membrane permeability. It has been shown that for vitrification a combination of CPAs leads to a synergistic increase in cell viability [178]. The chemicals utilized for cryopreservation approaches can be dived into intracellular and extracellular cryoprotectants [179]:

- intracellular cryoprotectants are penetrating agents with low molecular weight, such as DMSO or glycerol. They permeate the cells, minimizing damage and ice formation, and preventing membrane rupture;
- extracellular cryoprotectants that do not penetrate cells are characterized by relatively high molecular weights, such as sucrose, hydroxyethyl starch. They are used as bulking agents to increase the glass transition temperature.

Successful cryopreservation includes maintenance of intact metabolizing cells that possess the ability cell division ability. In order to reduce the cytotoxic effect and cell/ECM injuries during freezing, precooling of CPA solution to 4°C is crucial. The biological material is frequently transferred into a precooled cryoprotective solution and moved to a precooled cryopreservation device. Cooling rate is one of the most important factors affecting cell survival. It has been shown that cell-specific controlled-rate freezing maximizes the viability of several types, particularly when it is used for freezing single-cell suspensions. In tissues, however, this is difficult to accomplish due to the heterogeneous combination of cells, each of which has its own optimal cooling rate [180].

Ice formation is considered to be one of the major causes of cryoinjury to cells and tissues (Fig. 1-25a and b). Conventional cryopreservation is optimized to avoid intracellular freezing, whereas vitrification aims to avoid any ice formation (intra and extracellular). Dehydration in vitrification occurs by chemical substitution, while in slow-rate freezing dehydration is achieved by both osmotic dehydration and chemical substitution. Extracellular ice is formed in frozen tissue during slow freezing (low cooling rates), which results in an increase in solute concentration triggering osmotic dehydration of the cells. Under these conditions, the cell contents actually vitrify due to the combined processes of dehydration and cooling, thus the vitreous phase and freezing phase can coexist within the same system [181].

Potentially serious damage caused by dehydration and ice formation can be minimized by the following factors:

1. Use of cryoprotectants in appropriate concentration;
2. Freezing container;
3. Cooling/thawing rate;
4. Combination of CPAs;
5. Maintenance of the appropriate storage temperatures.

Storage and shipment temperatures may impair the graft quality if they are performed above the glass transition temperature of the freezing solution. Brockbank et al. reported that valve leaflets frozen slowly were negatively affected by storage at -80°C [182].

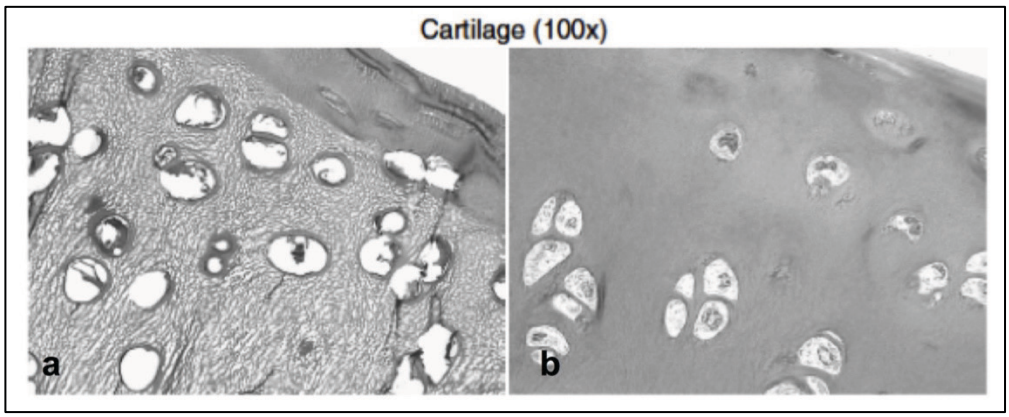

Figure 1-25: *Light microscope of cryosubstituted frozen (a) and vitrified cartilage (b) intensive ice formation. Frozen cartilage contained ice within the cells and the matrix, while vitrified is free from ice. Adapted from[181]*

1.7.1.1 Cryopreservation by controlled-rate freezing

Cell viability and the ECM integrity of cardiovascular tissues such as heart valves and arteries can be preserved by controlled-rate freezing. The optimal survival of single cell suspensions and tissues occurs at a cooling rate somewhere between 0.3°C and 10°C per minute. Usually, the cooling rate is only controlled between 4°C and -40°C. Slow cooling permits significant cell shrinkage (dehydration) and avoids formation of intracellular ice, if sufficient CPA is used. Thanks to its unique properties (inert, inflammable, readily available, relatively cheap and non-toxic), liquid nitrogen is often used to regulate controlled-rate freezers either by Direct Temperature Feedback or via Timed Pulse methods. Both rely on the control of the temperature of the chamber using a continuous supply of liquid nitrogen. The careful monitoring of the freezing rate is regulated by the programming capability of the device. Step Down Freezing is another method which is often practiced in the labs. Samples are placed in a precooled

freezing container and transferred to a freezer (-80°C) overnight. For long-term storage the samples are moved to nitrogen vapor. It is disputed if this simple device can provide the controlled cooling rates and ice nucleation associated with a true controlled-rate freezer [177].

Another factor which would probably affect the outcome of cryopreservation (ECM integrity or cell viability) is the warming rate. Most cryopreservation procedures apply rapid warming. The prevalence of works on cryopreservation performed using a rapid warming rate is probably due to the fact that priority has been given to the investigation of the cooling rate [177]. Rapid warming is carried out by simple immersion of the samples in a warm water bath. Recently, the warming rate topic has been addressed, e.g. nanowarming using nanoparticles has been developed to increase warming rates. This new technology holds promise to improve cell viability and tissue function after cryopreservation [183]

The utilization of culture media in tissue banking as the base solution for preservation is a common practice. However, these media do not suit optimal preservation at cryogenic temperatures. They are predominantly used to maintain cellular function at normal physiological temperatures. When tissues are exposed to cold, it is more appropriate to use media which are designed for reduced temperatures [184,185].

Clinically, the evidence for the survival of donor cells in cryopreserved cardiac valves is not strong; moreover, they do not appear to have any beneficial effect. On the contrary, cell remnants and the immunological incompatibility of graft and recipient were associated with reduced durability and valve dysfunction [62,98]. Many other studies highlighted the key point that intact connective tissue structure is of major importance for proper valve functioning while the remaining viable cells in allografts are useless [186,187]. Typically, 10% dimethyl sulfoxide is added to cells and tissues before freezing. Extensive ice crystal formation was observed in the ECM of frozen tissues following cryopreservation [179]. Ice crystal formation may

disrupt the histoarchitecture of the ECM. Therefore, it remains questionable whether standard cryopreservation is suitable for decellularized grafts, or, indeed, any grafts, since there have been conflicting results reported in the literature. Gerson et al. reported that SynergraftTM cryopreserved allograft valves did not show signs of structural damage using two photon-laser scanning confocal imaging [188]. On the other hand, performing similar microscopic imaging, conventional cryopreservation of porcine heart valves demonstrated a dramatic loss of autofluorescence and SHG within the frozen samples [189]. Evidence for the damaging role of ice in tissue cryopreservation has been previously reported by Brockbank and coworkers [18,190] and confirmed by other studies [186,191,192]. This finding led to the development of an alternative ice-free cryopreservation approach also referred to as vitrification.

1.7.1.2 Vitrification

Vitrification is the solidification of a liquid without crystallization. This method relies on the use of extremely high concentrations of cryoprotective agents and rapid cooling rates to avoid ice formation during cooling to cryogenic temperatures and rewarming. Vitrification allows successful preservation for a wide range of cells and tissues, including sperm [193,194], ovarian tissue, oocyte, embryos and blastocysts [195,196]. Vitrification can be applied to a wide variety of biological systems. The procedure is in many regards similar to that of conventional cryopreservation. Precooled CPAs are added in a stepwise or gradient manner to ice in order to reduce toxic side effects. Rapid cooling rates are typically applied down to around −100°C. This is normally done above the vapor phase of liquid nitrogen or in a precooled 2-methylbutane bath. Once the sample temperature reaches −100°C, slower cooling rates are used to further decrease the temperature down to cryogenic levels to avoid cracking. This can be performed by transferring the sample to a −150 °C mechanical freezer or placing it near the top of a vapor- phase

nitrogen-cooled freezer [197]. Finally, the tissues are stored well below the glass transition of the solution, typically between –135°C and –160°. In these conditions, a stable vitreous state reigns. This is crucial for the retention of vitrified tissue integrity and cell viability. Warming is performed in a similar manner, slowly to –100°C and then rapidly to 0°C by immersing the tissue in a water bath. A thermocouple is usually used to monitor cooling and warming. Rapid warming is generally beneficial for cryopreserved samples and even more important for vitrified tissues due to the need to avoid injury from devitrification and subsequent recrystallization [198]. Vitrification procedures can be performed with a simple apparatus composed of polystyrene box, metallic rack, and liquid nitrogen and rely on the application of mixtures of high levels of penetrating CPAs, such as glycerol, DMSO, ethylene glycol, formamide, propanediol and butanediol. Three main factors need to be taken into consideration for the formulation of a vitrification solution: the total solute concentration (higher than 40%), cryoprotectants' ability to form glass, and the cooling/warming rate rapid [199] .

The vitrification protocols established by Brockbank et al. for heart valves [197] as well as other tissues [200,201] are based on a protocol (VS41A) that was originally designed for preservation of mouse embryos by its originators [202]. VS41A is also known as VS55 [201]. The formulation consists of 8.4 M CPAs mixture of 3.1M formamide, 3.1M DMSO, and 2.2 M propylene glycol, which reflects its 55 % (w/v) of cryoprotective agents. VS55 was intended for organ preservation [203]. However, the application of this protocol for heart valve tissues showed some limitations. It is only suitable for small sized tissues, ice is formed during rewarming, and produced cracks in the sample below the solution glass transition temperature. To overcome these drawbacks, the solute concentration (w/v) was increased from 55% to 83% to formulate VS83 [197]. The VS83 appears to be extremely stable below and above the glass transition temperature, and even allows stable storage at -80°C (Fig. 1-26). VS83 has previously been applied to native aortic porcine heart valves [204]. Brockbank and

coworkers reported that the second protocol is cytotoxic to valvular cells, but preserves the ECM [204,205]. However the application of this protocol demonstrated excellent ECM integrity and maintenance of the matrix components (collagen, elastin, and GAGs) and high hemodynamic performance in several studies [189,204,206,207]. Interestingly, large animal studies within these works pointed out that ice-free, cryopreserved heart valves were only slightly immunoreactive and resistant to calcification, whereas cryopreserved ones calcified. In fact, it seems that vitrification masks or modifies immunoantigens. The loss of cell viability appears to be beneficial for the reduction of immunogenicity as was observed *in vivo* [204] and *in vitro* [205]. Recellularization with myofibroblasts and fibroblasts was detected after 20 weeks *in vivo* [197].

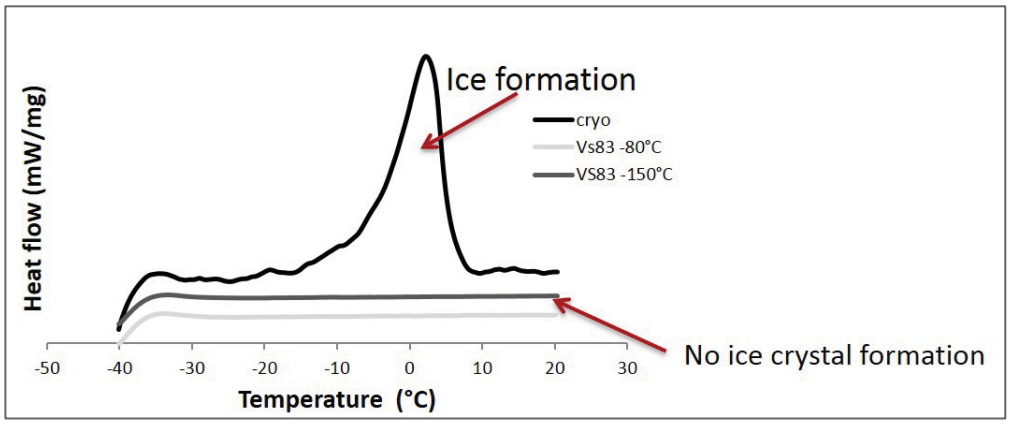

Figure 1-26: *Differential scanning calorimetry (DSC) of cryopreserved and vitrified DBP stored at -80°C and -150°C using VS83*

In summary, cryopreservation and VS55-based vitrification may both result in high cell viability, but studies carried out by Brockbank in collaboration with other groups showed that VS83-realized vitrification is superior for rabbit and porcine cartilage plugs, and human biopsy specimens [181]. In cardiovascular tissues the utilization of VS83 protocol allows better preservation of ECM structures. This positive effect has been demonstrated in several tissues such as vessels [201], veins [208] and heart valves [197] (Fig. 27). Among cryopreservation approaches, vitrification/ice-free preservation seems to be the best choice to preserve the ECM integrity of decellularized scaffolds for

cardiovascular surgical purposes. Moreover, vitrification is cheaper and does not require expensive equipment. Its simplicity and economic advantages may make it attractive for application in tissue banking. The disadvantages of this technology are the use of cytotoxic CPAs, and the costs associated with low temperature storage and shipping.

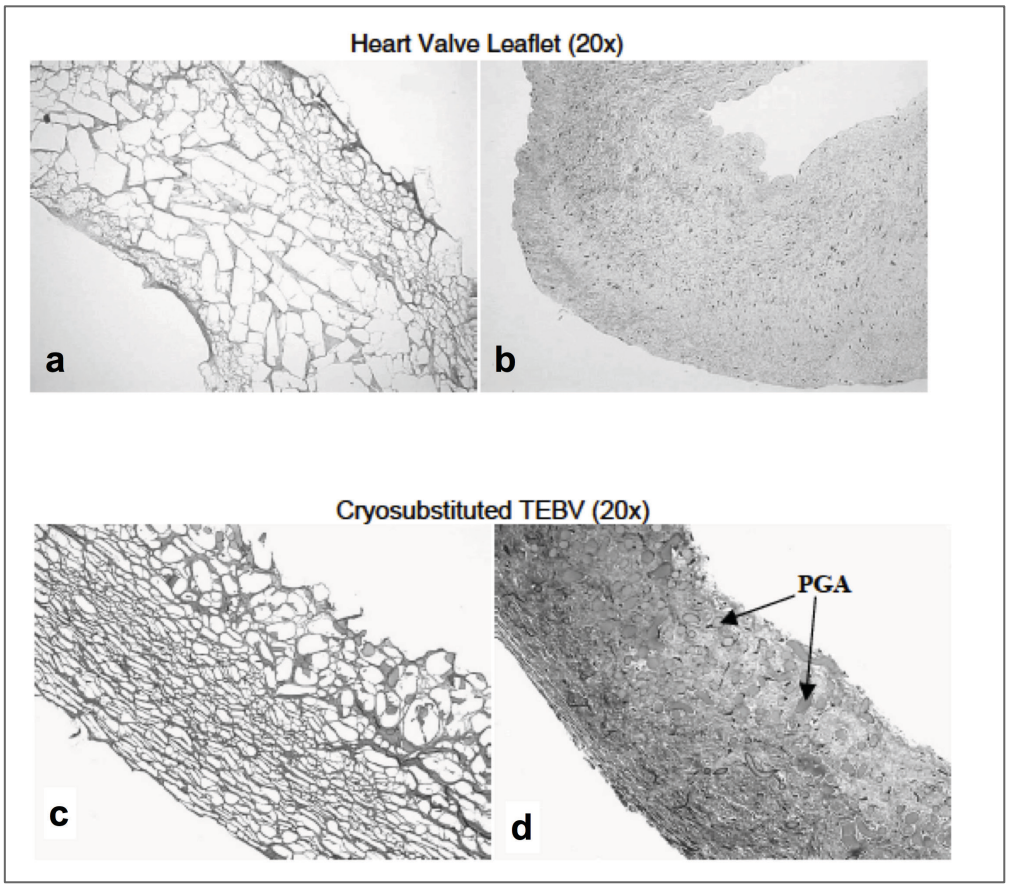

Figure 1-27: *Cryosubstitution of conventional cryopreserved and vitrified heart valve leaflets and TE blood vessels (TEBV). A: frozen leaflets B: vitrified leaflets. C: Frozen TEBV. D: Vitrified TEBV. Extensive ice formation is present in the frozen tissues. Adapted from[181]*

1.7.1.3 Freeze-drying

Freeze-drying is a controllable method for dehydrating frozen biological products under vacuum. It is also referred to as lyophilization. It can be traced back to prehistoric times, when it was used for food storage. It combines the benefits of both freezing and drying to offer a dry, shelf-stable, and readily available product [209].

Freeze-drying is widely applied in the pharmaceutical industry for processing of active proteins but is less used for cells and tissues. This is due to its irreversible damage to cell viability and ECM structure. Compared to cryopreservation, freeze-drying causes much more damage. Freezing and drying are both severe stress factors for tissues. Therefore, special protectants (lyoprotectants) need to be added to the solution to avoid damage during the process. When water is removed, lyoprotectants replace the water by forming hydrogen bonds with proteins, stabilizing the proteins and permitting them to maintain their original configuration [210]. Additionally, lyoprotectants need to be capable of forming a glassy state at room temperature. Sucrose and trehalose are non-reducing disaccharides and good glass formers. Both sugars possess the properties to be employed as lyoprotectants for dry preservation.

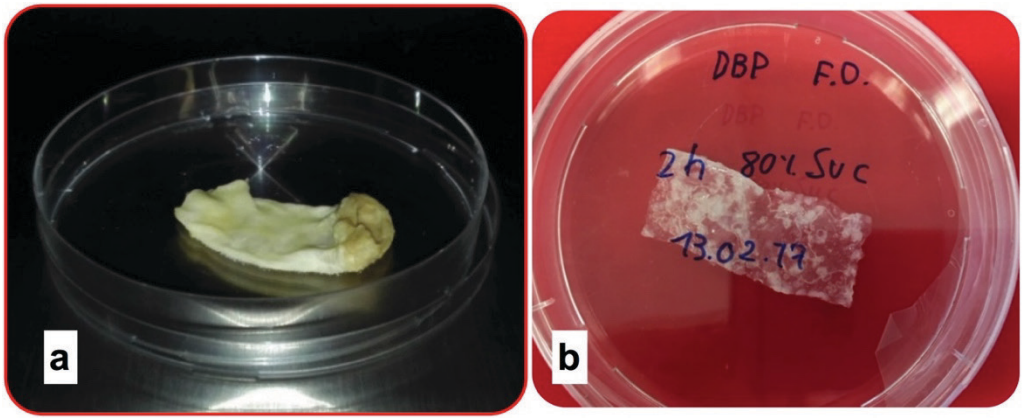

Figure 1-28: *Freeze-drying of decellularized scaffolds using 80% sucrose. a: freeze-dried decellularized porcine pulmonary heart valve and. b: Freeze-dried DBP*

There are 4 steps to complete the freeze-drying of biological tissue scaffolds [211] (Fig. 1-29). The whole process time ranges from several hours to days.

- Pretreatment: Includes incubation of the biological material with lyoprotecant. This step is important for protecting a material from freezing damage during the process;
- Freezing (Solidification): Scaffolds are cooled, and water is converted into ice until maximum freeze concentration occurs:

- Primary drying (Sublimation): Biological material is dried under low pressure, below its glass transition temperature to avoid sample collapse and to minimize damage during drying;
- Secondary drying (Desorption): the temperature is slowly increased to higher than in the primary drying phase, keeping the samples below glass transition temperature. The aim of this step is gradual dehydration of the sample while the glass transition temperature increases (removing unfrozen water).

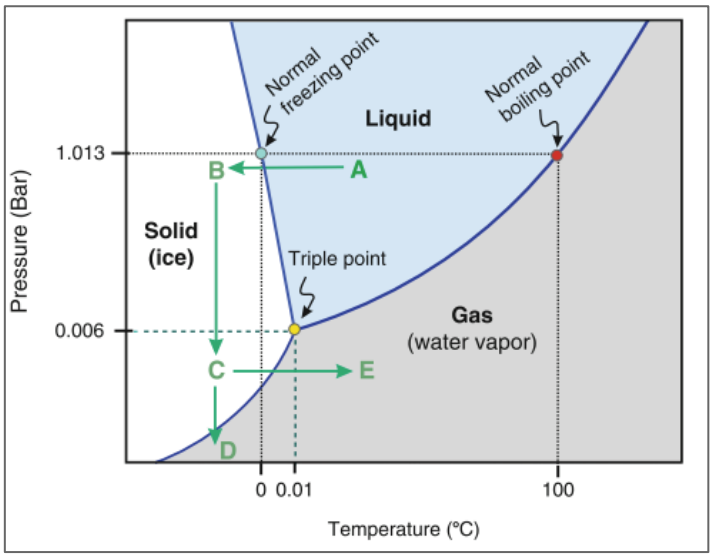

Figure 1-29: *Hypothetical freeze-drying paths consisting of solidification and sublimation of ice avoiding the direct liquid-gas transition. Paths A to B to C: solidification of liquid below the triple point and paths C to E/D: sublimation of ice to gas (water vapor) C to D: lowering the pressure, C to E: supplying heat. Adapted from*[212]

Freeze-drying in the cardiovascular field it is not a new topic. Freeze-dried allografts are convenient to store and transport. Several decades ago, the efficacy of freeze-dried allograft (without lyoprotectant) was evaluated by Ross' group in a long-term clinical study [77]. A high incidence of cuspal tears was observed along with deterioration of the mechanical properties [75,213]. Several other groups reported that freeze-drying causes drastic structural and mechanical alterations when applied to the preservation of native bovine pericardium [214–216] or decellularized arteries [217].

However, all these freeze-drying studies appear to have been performed without using any type of lyoprotective agent. Recently, Wang et al. reported on the freeze-drying of decellularized porcine pulmonary heart valves using sucrose as a lyoprotectant. The work showed that freeze-drying allows for storage and transport at room temperature, by using specific protectants that form a glassy state in these conditions [218,219]. The sucrose-protected freeze-dried valves demonstrated a well-preserved histoarchitecture after rehydration [220], and excellent performance, coupled with cell repopulation potential, in juvenile sheep [221] (Fig. 1-30). To sum up, freeze-drying allows storage at room temperature, eliminating the need for liquid nitrogen and reducing infrastructural costs for shipment. This technology has the potential to compete with cryopreservation approaches. Both standard and ice-free cryopreservation require storage at ultra-low subzero temperatures and frozen transport. Once the damaging effects of freeze-drying can be overcome, freeze-drying can be applied to a variety of decellularized scaffolds (Fig. 1-26a and b), holding promise for its application in biobanking.

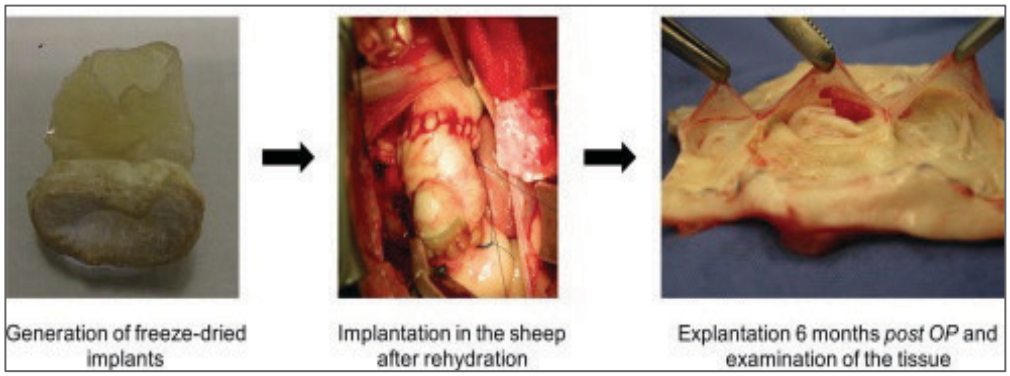

Figure 1-30: *Successfully implanted freeze-dried porcine heart valve in large animal model (sheep). Recellularization and no calcification were observed after 6 months. Adapted from [221]*

1.7.2 Summary

The utilization of the above-mentioned preservation strategies has been largely described in the literature for native cardiovascular tissues, especially heart valves. Only a few studies focused their

attention on studying the impact of preservation on decellularized biological materials. Conclusive investigations on the adverse impact of preservation methods, such as for instance decellularized xenogeneic pericardial scaffolds, are still missing. Utilization of preservation methods for decellularized scaffolds may impair ECM integrity and biomechanical properties leading to poor graft durability and tissue degeneration and eventually graft dysfunction *in vivo,* as has been previously observed for native tissues. At present, decellularized grafts have reached a point where development of adequate preservation strategies is urgently needed for clinical application. Therefore, evaluating the impacts of preservation technologies on the *in vitro* properties of scaffolds is of major importance.

1.8 Aim of the project

The aim of this PhD project was to investigate the feasibility of several preservation strategies for decellularized pericardial scaffolds in order to ensure off-the-shelf availability and their routine use in the clinic. The work is focused on the evaluation of the suitability of three different preservation methods to preserve decellularized bovine and porcine pericardial scaffolds: cryopreservation as the gold standard preservation method, vitrification, and freeze-drying.

In order to achieve this main goal, this PhD thesis addresses the following objectives:

- Decellularization of bovine and porcine pericardial scaffolds applying TRICOL technology;
- Analysis of maintenance of their ECM structure and mechanical behavior;
- Investigation of the preservation methods tailored for decellularized scaffolds;
- Evaluation of their impact on ECM integrity (histologically, microscopically and biochemically), biomechanical properties and cytocompatibility.

2 **Material & Methods**

All reagents used for decellularization and preservation are from Sigma-Aldrich (Saint Louis, MO, USA) unless otherwise stated.

2.1 Decellularization of bovine and porcine pericardia

Native bovine pericardium was collected from 8-month-old animals (Piebald calves) in a local slaughterhouse (Bugin S.r.L, S. Maria di Sala, Venice), while porcine from 9-11-month-old animals (Duroc pigs) was obtained from a local slaughterhouse (Macello F.lli Guerriero, Villafranca Padovana, Padua). Both tissues were transferred in phosphate buffered saline (PBS). Dissection and additional washing in PBS/medium were carried out within two hours of arrival in the laboratory. Excess adipose tissue was carefully trimmed from the pericardium (Fig. 2-1b). Isolated pericardia were kept in sterile bottles of 200 mL or 400 mL according to the amount of tissue to be decellularized (≈ 100 cm^2/400 mL). Briefly, the first step of the decellularization protocol of pericardial patches was performed under continuous stirring with hypotonic buffer solution (pH 7.4) containing 10% (v/v) DMSO, 10 mM of sodium ascorbate, and protease inhibitors (PI) (2 mM of phenylmethylsulfonyl fluoride, 5 mM of N-ethylmaleimide,5 mM of benzamidine, 1 mM of iodoacetamide, and 5 mM of EDTA). After 8 hours, the solution was replaced with hypotonic washing solution without DMSO and PI. Then the pericardia were washed for the next 16 hours (8 hours each time) with 1% (v/v) Triton X-100 in the presence of PI and without PI in Triton X-100 0.1% (v/v). Further washing steps followed in PBS solution containing sodium chloride (0.5 M) at 4 °C for two 8-hour periods and in hypotonic PBS buffer. This was followed by replacing Triton X-100 with 10 mM of sodium cholate and the extraction was resumed for two 8-hour periods at room temperature. The pericardia were finally washed in 10% (v/v) isopropanol in 0.9% NaCl. All extraction steps were carried out in degassed solutions containing 10 mM sodium ascorbate and 5 mM ethylenediaminetetraacetic acid (EDTA) under nitrogen atmosphere (Fig.31c). Residual nucleic acids were digested using the non-specific

endonucleases Benzonase™ at a concentration of 1500 U $cm^{-2,}$ at 37 °C for 48 h. So-obtained DBP patches were maintained in antibiotics and antimycotic cold saline solution (100 U/mL penicillin, 100 mg/mL streptomycin and 25 µg/mL amphotericin B) for one week until further processing.

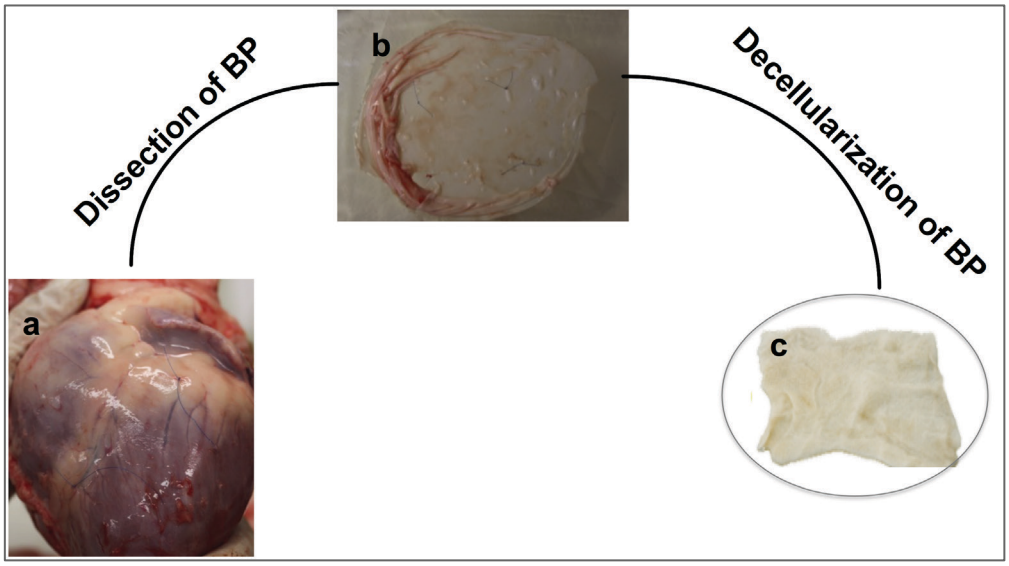

Figure 2-1: *Dissection and isolation of bovine pericardium for decellularization procedure. A: bovine heart, b: native BP marked using sutures to indicate area of interest. C: decellularized BP using TRICOL technology.*

2.2 Conventional cryopreservation

Decellularized pericardial patches were transferred into polyethylene vials with cryopreservation medium, containing 10% (v/v) dimethyl sulfoxide and 90% (v/v) medium 199. Slow-rate-freezing was conducted at ~1°C/min. in a controlled rate freezer (CM-2000; Carburos Metalicos, Madrid, Spain) at 40 °C min^{-1} down to −80°C. Then, samples were plunged into liquid nitrogen and stored at −150 °C. The cryopreserved pericardia were stored at −150°C for 1 month until further assessment. Rapid warming was carried out in a 37°C water bath. After thawing, the tissues were washed 5 times in PBS for 10 min each.

Table 3: *Step up of the freezing machine used for cryopreservation: cooling rate 1°C/min*

Temperature	**time**
4°C	0.1 min
4°C	10 min
−80°C	84 min
−80°C	10 min

2.3 Vitrification using VS83

DBP scaffolds were cut into rectangles with an area of 6 cm2. The patches subjected to vitrification were infiltrated gradually in precooled VS83 solution (4.65 mol/L formamide, 4.65 mol/L DMSO and 3.31 mol/L propylene glycol in Euro-Collins solution) in six 15 min-steps at 4°C [207,222]. Cryoprotectant concentrations of the diluted VS83 solutions were step-wise increased from 0 to 12.5, 25, 50, 75 and 100%, resulting in a final total concentration of 12.5 mol/L of protectants as previously described [197]. Scaffold patches were placed in bags (Caso vacuum bags, Arnsberg, Germany) containing VS83, while the top was covered with 0.5 ml of 2-methylbutane in order to prevent air contact and ice nucleation. A polystyrene box was filled with liquid nitrogen and two-racks were positioned above the liquid nitrogen. Rapid cooling at ~ -20 °C/min was achieved by placing the samples on the racks above the vapor phase of liquid nitrogen. A separate control specimen was prepared under the same conditions to measure the cooling rate of the samples with a T-type thermocouple (Fluke, Everett, USA). Upon reaching -100 °C, the sample bags with the DBP patches were transferred to a -150 °C mechanical freezer (MDF-1155ATN; Sanyo Electric Biomedical Co., Bad Nenndorf, Germany). Thawing of the tissue was achieved by placing the bags in a 37°C water bath for 1–2 min, followed by five washes in PBS solution for 10 min each

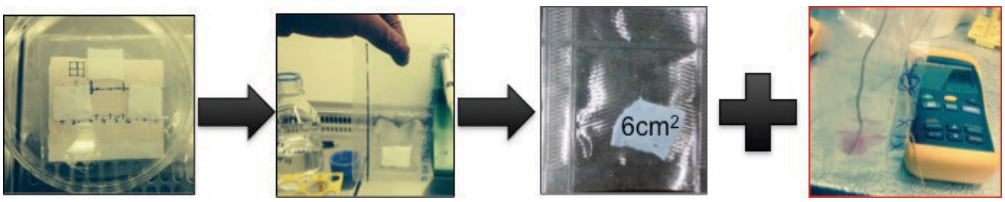

Figure 2-2: *Vitrification of decellularized scaffolds using VS83*

2.4 Freeze–drying

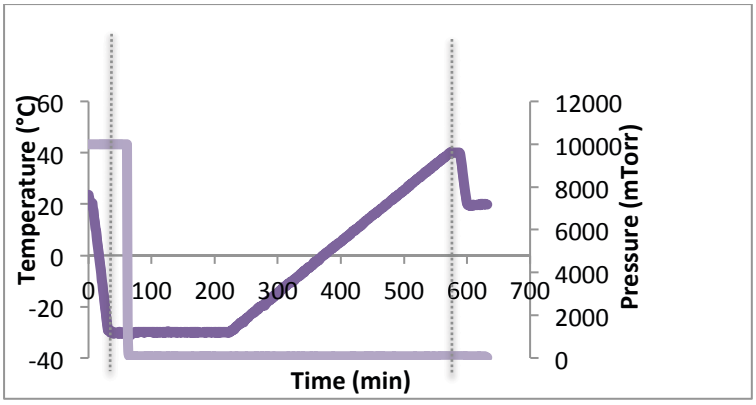

Figure 2-3: *freeze-drying program used for DBP and DPP. Slow freezing at 1°C/min to -30°C. Primary drying for 420 min at −30°C and 60 mTorr. Secondary drying: increase in temperature to 40°C at 0.1°C min$^{-1.}$*

In order to load patches with the lyoprotectant sucrose for freeze-drying, decellularized pericardial tissues were incubated in 5% (w/v) sucrose solution at 37°C for 4 hours and then transferred to a sucrose solution of 80% (w/v), in which they were maintained at 37°C for 60 min [220]. The 80% sucrose solution was refreshed three times (Fig. 2-4a). Sucrose-loaded tissues were placed in sterile petri dishes. Freeze-drying was achieved using a programmable freeze-drier with temperature-controlled shelves. The samples were subjected to slow freezing at 1°C/min until the temperature reached −30°C; primary drying was performed for 7 hours at −30°C and 60 mTorr. For secondary drying, the temperature was increased to 40°C at a rate of 0.1°C/min, while keeping the vacuum pressure at 60 mTorr (Fig. 2-3). The dried samples were stored at 4°C for 1 month until further assessment (Fig. 2-4b). Rehydration was carried out by washing out the sucrose using PBS. The samples were subsequently incubated in PBS overnight until further assessment.

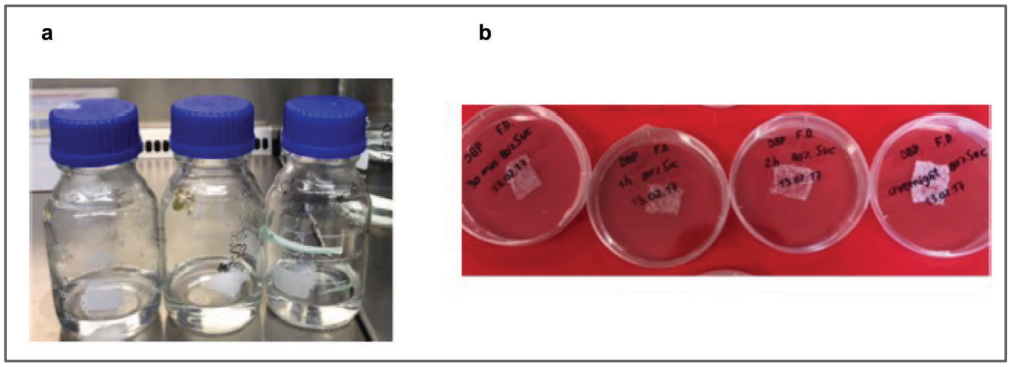

Figure 2-4: *Freeze-dried DBP loaded with 80% sucrose. (a) Incubation of DBP patches in 50 ml 80% sucrose solution. (b) Freeze-dried DBP before rehydration.*

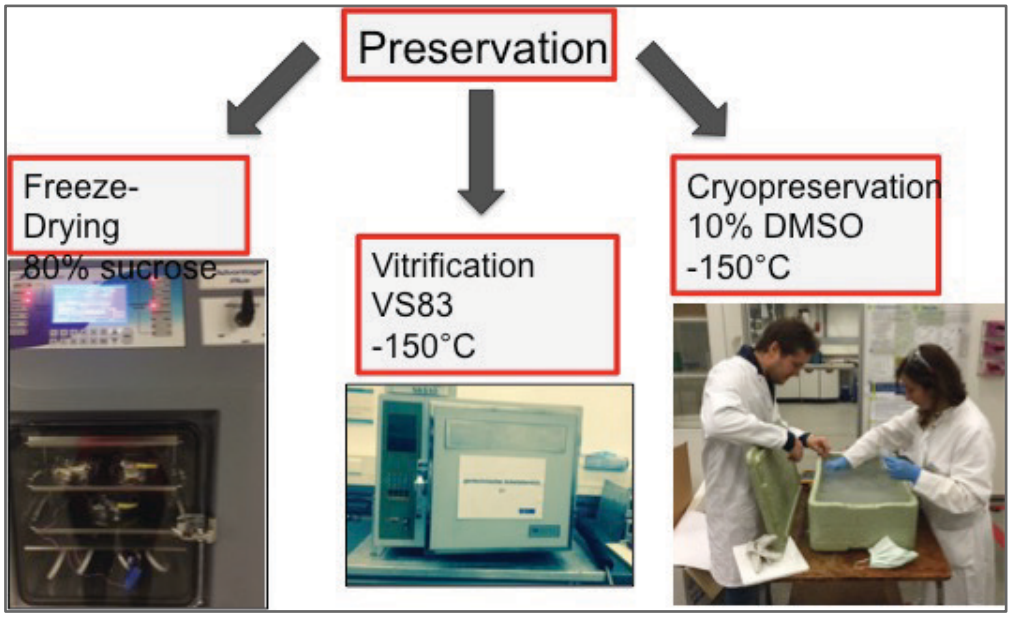

Figure 2-5: *Preservation strategies applied for decellularized porcine and bovine pericardium*

2.5 Histological analysis

2.5.1 Tissue sample dissection

Samples of the control and preserved tissues (n=3 in all cases) measuring 6-8 mm in diameter were cut using a biopsy puncher (Kai industries, Seki, Japan) for histology, Fourier-Transform Infrared spectroscopy (FTIR), Differential Scanning Calorimetry (DSC), Scanning Electron Microscopy (SEM), multiphoton microscopy and cytotoxicity assessment. Biomechanical and biochemical analyses were performed on six DBP scaffolds (n=6).

2.5.2 OCT embedding for decellularized scaffolds

Histological staining was carried out on native and decellularized scaffolds to evaluate a decellularization process. Prior to embedding, the samples were fixed in 4% paraformaldehyde (PanReac AppliChem, Chicago, IL, USA) in PBS for 20 min at room temperature in darkness and then incubated in 20% sucrose in PBS overnight at 4°C. The embedding of the samples was performed in a 1:1 solution of 20% sucrose and O.C.T (Optimal Cutting Temperature compound, Sakura, Japan). Subsequently, they were snap-frozen in liquid nitrogen and stored at −80°C until cryosectioning. Staining was performed on 5-6 μm sections using standard hematoxylin/eosin (H&E), Mallory trichrome (MT) and alcian blue (Bio-Optica, Milan, Italy). Images were captured using a Nikon Eclipse 50i light microscope equipped with a NIS-Elements D3.2 Software (Nikon Corporation, Shinagawa, Tokyo, Japan)

2.5.3 Paraffin embedding for preserved patches

The ECM structure of pericardial scaffolds was assessed by histological staining following preservation methods. Prior to paraffin embedding, the samples were fixed in 4% paraformaldehyde

(PanReac AppliChem, Chicago, IL, USA) in PBS for 20 min at room temperature in darkness. The analysis was conducted on 6–7μm sections using standard hematoxylin/eosin (H&E), Mallory trichrome (MT) and PicroSirius red (Bio-Optica, Milan, Italy) staining. The sections were inspected under a bright field (H&E and MT) and polarized light (Picrosirius red) microscope. Images were captured using a Nikon Eclipse 50i light microscope equipped with NIS-Elements D3.2 Software (Nikon Corporation, Shinagawa, Tokyo, Japan).

2.6 Scanning Electron Microscopy

Native, decellularized and treated samples were fixed and maintained in Karnovsky solution [8% (w/v) paraformaldehyde, 10% (v/v) glutaraldehyde (50%) in 0.2 M cacodylate buffer] at 4°C in the dark until the assessment. Prior to SEM analysis, Karnovsky solution was removed and the samples washed in physiologic solution (0.9 % NaCl) and dehydrated for 10 min with serial gradients of ethanol (70%, 80%, 90% and 100%). Subsequently the samples were critical point-dried (CPD) and coated with gold-palladium. Analysis of their surface was performed using a JEOL JSM-6490 electron microscope. The images were acquired using low vacuum mode 20 kV at low and high magnification (1,000x and 10,000x). Analysis of their surface was performed using a JEOL JSM-6490 electron microscope. The images were acquired using low vacuum mode 20 kV at low and high magnification (1,000x and 10,000x).

2.7 Multi-photon microscopy (MPM)

Multiphoton-induced auto fluorescence and second harmonic generation (SHG) were detected using two photon microscopy connected to a titanium:sapphire laser source (Chameleon Ultra 2, Coherent), with tunable emission wavelength of 700−900 nm at 80MHz, described in detail elsewhere [223]. Additionally, the major components of the basal lamina of DPP upon preservation were selectively captured by using indirect immunostaining on cryosections.

2.7.1 Evaluation of collagen and elastin fibers

Multiphoton-excited autofluorescence and SHG microscopy are powerful non-invasive imaging tools for studying ECM-ultrastructure components, such as elastic and collagenous fibers, without the need to previously label or fix the tissue. The chosen excitation wavelength was $800\,\mathrm{nm}$ in order to detect the SHG and the elastin autofluorescence signal separately (one excitation wavelength, two separate channels for detections). The SHG was detected at 400 nm while elastin had its autofluorescence centered around 525 nm. The images were acquired with a fixed resolution of $1024\mathrm{x}1024$ pixels and frame accumulation of one hundred and twenty frames, with a pixel dwell time of $0.14\,\mu\mathrm{s}$. To perform quantitative measurements, images were additionally acquired as RAW uncompressed files. Four different regions of interest (ROI) were taken to assess SHG intensities, which are measured as grey value intensities of tissue structure integrity. Besides that, quantification of the fiber waviness was implemented as previously described in [224]. Briefly, the distance between visible endpoints of a collagen bundle (L0) and the length of the fiber bundle (Lf) was measured using NeuronJ, (ImageJ plug-in). The quantification of the waviness of the fibers is defined as straightness parameter: Ps = L0/Lf.

Where Ps is restricted between 0 and 1. Ps= 1 indicates a straight fiber. The quantifications were conducted using ImageJ (NIH, Open Source Program).

2.7.2 Combined MPM and immunofluorescence

Basal lamina proteins - laminin, collagen type IV, and heparan sulfate - were detected together with collagen type-I SHG and elastin autofluorescent signals. The SHG was identifiable at an excitation wavelength of 1200 nm, while elastin and the secondary antibody's fluorophores at 800 nm. The images were acquired with a magnification of 25x, fixed resolution of 1024x1024 pixels, and frameaccumulation of 120 frames. Prior to the detection of the proteins, the slides were washed in PBS to remove OCT followed by incubation for 10 min with bovine serum albumin (BSA). Primary and secondary antibodies were also diluted in a 1% (w/v) BSA solution. The primary antibodies were incubated for 60 min at 37 °C in a humidified atmosphere and then washed in PBS. Incubation with the secondary antibodies, rhodamine (rhod)-conjugated anti-rabbit and anti-rat, was performed for 30 min at 37°C in the dark. The slides were washed again in PBS followed by mounting with aqueous mounting medium. The antibodies, dilution and supplier utilized for this technique are described in Table 4.

Table 4: Primary and secondary antibodies used for evaluation of basal lamina proteins using TPM

		Primary antibody
Antibody	**Dilution**	**Company**
Collagen IV	1:100	ab6586, rabbit (Abcam, Cambridge, USA)
Laminin	1:100	Z0097, rabbit (Dako, Santa Clara, USA)
Heparan sulfate	1:50	AB1948P, rat (Millipore, Burlington, MA, USA)
		Secondary antibody
Antibody	**Dilution**	**Company**
Rhodamine (rhod-conjugated)	1:100	AP132R, goat-anti-rabbit-IgG and AP136R anti-goat-rat-IgG (Millipore, Burlington, MA, USA)

2.8 Biochemical analysis

Prior to dissection the patches were washed with Milli-Q water (ultra-purified water) for 1-2 hours. Then were lyophilized using the freeze-drying machine for subsequent biochemical tests. Shortly before starting the assessments, the dry weight of the scaffolds (bovine and porcine, (n=5-6)) was recorded.

2.8.1 Sulfated glycosaminoglycans quantification (GAGs)

Lyophilized pericardial tissues were used for the quantification of chondroitin sulfate, one of four GAG groups, according to the protocol established by Farndale et al [225], Chandrasekhar et al [226] and improved by Barbosa et al [227]. Briefly, pericardial samples (n=6; 10-12 mg dry weight) were digested with 7 Uml^{-1} papain overnight at 60°C. A dimethylmethylene blue (DMMB) solution was prepared in a formate buffer pH 3.0 containing 5% ethanol and 0.2 M guanidine hydrochloride (GuHCl) to isolate the GAG-DMMB complex from tissues. The GAG-DMMB complex was obtained as a stable pellet after centrifugation of the treated samples. The dissociation of the complex was achieved using 4 M GuHCl solution at pH 6.8 containing 10% propanol. The UV absorption of the decomplexed DMMB was then proportional to the GAG amount complexed from the treated sample [227]. The absorbance was read at a wavelength of 656 nm. Dilutions of chondroitin sulfate (Sigma-Adrich) were used to generate a standard curve. The concentration of sGAGs was calculated by interpolation from the standard curve.

2.8.2 Hydroxyproline (HYP) quantification

HYP is one of the major components of collagen protein comprising 14% of total amino acid content. Therefore, the quantification of collagen was carried out by measuring it based on the

protocol established and described by Edwards & O Brien [228]. Briefly, lyophilized pericardial tissues (n=5; 5-6 mg dry weight) were digested using 4 ml 6 N HCl overnight at 120°C and the supernatant was collected after centrifugation The hydrolysate was neutralized at 96°C for 2 hours and an assay buffer (50 g/L citric acid monohydrate, 120 g/L sodium acetate trihydrate, 34 g/L sodium, 0.8% (v/v) glacial acetic acid and 20% (v/v) 1- propanol, at pH 6.5) was added to dried samples. 50 µL triplicates of standard (trans-4-hydroxy-L-proline amino acid; Sigma) and test solutions were incubated with 100 µl chloramine-T reagent (14.1 mg/mL). Following incubation, 100 µl Ehrlich reagent (200 g/L 4-(dimethylamino) benzaldehyde, 60% (v/v) 1-propanol and 26% (v/v) perchloric acid) was added and again incubated at 60 °C for 45 min. The optical density was measured in a 96-well plate at a wavelength of 565 nm. The HYP content was determined by interpolation from the standard curve.

2.8.3 Denatured Hydroxyproline (dHYP) quantification

The same groups described above for quantification of HYP were also used for the quantification of dHYP. The quantification of denatured collagen was carried out according to Bank et al. [229]. Moreover, autoclaved NBP and NPP samples were used as positive controls. Lyophilized preserved samples weighting (n=6; 10-15 mg dry weight) were incubated with 5 mg/ml α-chymotrypsin solution containing 0.1 M Tris and 2.5 mM calcium chloride overnight at 37°C. The digestion of the tissues by the enzyme led to the release of degraded collagen, which was quantified using hydroxyproline (HYP) as described above (2.8.2)

2.8.4 Elastin quantification

Elastin content was as quantified using the Fastin Elastin assay kit (F2000, Biocolor, Carrickfergus, United Kingdom). Samples with 3-6 mg dry weight were obtained from decellularized and preserved patches (n=4). The test was conducted following the steps described in the kit's protocol. First, the samples were treated with 0.25 M oxalic acid at 100°C overnight to extract α-elastin. The extract was added to fastin dye reagent (5,10,15, 20-tetraphenyl-21H, 23H-porphine tetrasulfonate (TPPS)) to form elastin-dye complex as a brown pellet. The dye dissociation reagents were then added to release the dye into the solution. Elastin was gained and its absorbance was measured at a wavelength of 513 nm in a microplate reader (TECAN Infinite M2, Tecan Trading AG, Männedorf, Switzerland). Standard curves were made from the reference solution of α-elastin prepared from bovine neck ligament elastin (1 mg/ml), in 0.25 M oxalic acid. Elastin content was determined by interpolation from the standard curve as µg elastin/mg dry tissue

2.9 Fourier transform infrared studies

The overall protein secondary structure of the various treatment groups was studied after immersing samples in deuterium oxide (D_2O) for 3-4 hours in order to reduce the contribution of interfering water bands in the protein amide-I region. FTIR spectra were recorded and analyzed using a PerkinElmer 100 FTIR spectrometer (PerkinElmer, Norwalk, CT, USA) equipped with a triglycine sulfate detector and an attenuated total reflection (ATR) accessory equipped with a ZnSe crystal/diamond and a pressure arm to position the sample on the ATR surface. The acquisition parameters were as follows: 4 cm-^{1}, 4 co-added interferograms and 4000-900 cm^{-1} wavenumber range.

Decellularized preserved samples were cut with the help of a biopsy punch (Kai industries) with a diameter of 6 mm and placed on the ZnSe crystal. Infrared spectra of the patches were recorded immediately. The region 1700–1600 cm−1 was selected from the acquired spectra to analyze the overall protein secondary structure. Second derivatives of the spectra were calculated using a 13-point smoothing factor (Omnic software (Thermo-Nicolet, Madison, WI, USA)) and normalized to resolve differences in peak intensities. Ratio-values of bands at 1650 (assigned to α-helical structures) and 1630 cm^{-1} (assigned to ß-sheet structure) were calculated to quantify differences in amide-I band profile among treatment and control groups using the following calculation: $R= \frac{\mathrm{Xi}\left(1630\ cm^{-1}\right)\mathrm{Beta}}{\mathrm{Xi}\ (1650 cm^{-1})\ \mathrm{Alpha}}$.

Where X represents the spectral absorbance value at 1630 or at 1650 cm^{-1}.

2.10 Differential scanning calorimetry studies

DSC measurements were performed using a Netzsch DSC 204F1 Phoenix instrument (Netzsch Geraetebau GmbH, Selb, Germany). Approximately 10-15 mg wet weight of tissues were cut using a biopsy punch (6 mm) and subsequently transferred into aluminum sample pans, which were hermetically sealed and placed in the DSC. An empty pan was used as a reference. In order to study protein denaturation profiles, the samples were heated from 20°C to 90°C at the rate of 10°C/min. Protein denaturation of the tissue is visible as an endothermic event in the DSC traces. The thermograms were analyzed using Netzsch Proteus analysis software in order to obtain the onset temperature (T_{onset}) of protein denaturation

2.11 Uniaxial tensile testing

Samples for mechanical testing (native, decellularized, decellularized preserved and GA-fixed) were isolated from the left anterior side of the bovine pericardium, where the collagen showed the most uniform fiber distribution, parallel to the heart circumferential direction [230], while porcine patches were cut along collagen fiber orientation. Their alignment was visualized using a light box and two polarized light filters (Fig. 2-5b). The investigation of the mechanical properties of the patches was conducted in an Instron® tensile machine (Instron 3365; Instron, Bucks, UK) equipped with temperature-controlled bath (Fig. 2-5c). The samples were tested in PBS at 37 °C. For this purpose, strips of pericardium measuring 10 mm in length by 5 mm in width were cut and their thickness was measured at three points using a Mitutoyo thickness gauge (Mitutoyo; precision: ±0.01 mm) (Fig. 2-5a).

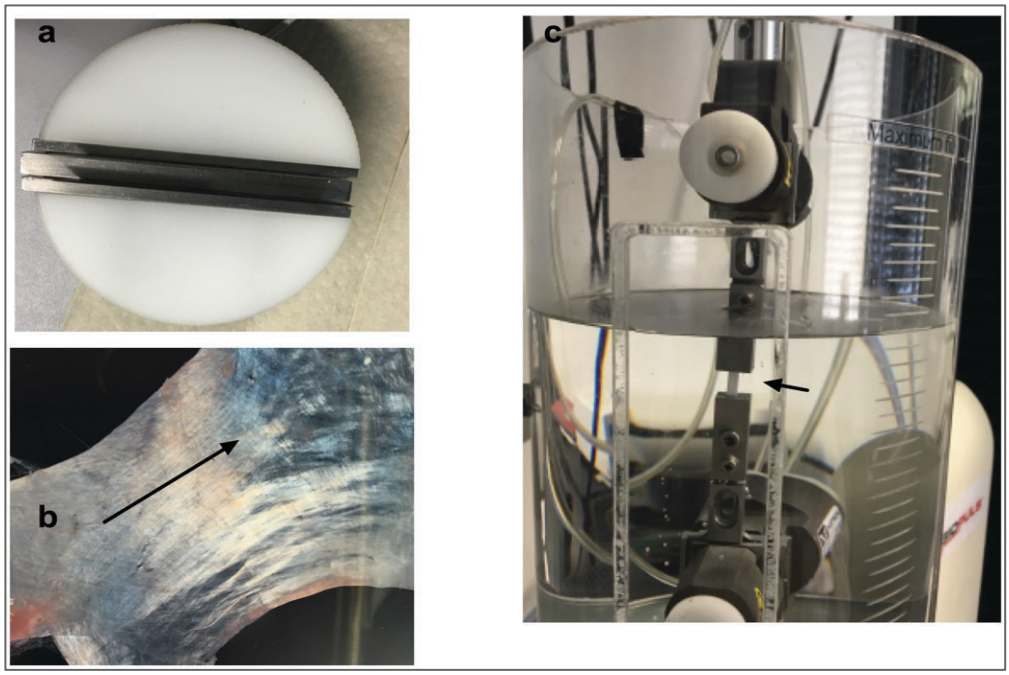

Figure 2-6: *a: Cutting block used for the dissection of specimen for uniaxial tensile testing. b: Decellularized pericardial samples were isolated parallel to the collagen fiber alignment. c: Biomechanical test set-up utilized for the uniaxial tensile loading to failure in the Instron tensile machine.*

2.11.1 Test procedure

Low-force uniaxial tensile testing was basically done as previously described in [231]. Decellularized (control), preserved groups and native GA-fixed pericardial specimens were subjected to low-strain-rate uniaxial tensile loading to failure. The average thickness value was used for testing. The specimens were preconditioned for 50 cycles at a rate of 20 mm/min, before being sequentially stretched to failure at the same rate. The test was stopped on occurrence of failure, as determined by the first significant decrease in load detectable during extension. During testing the load (F, in Newtons) and specimen extension (Δl, in mm) were recorded and subsequently converted to engineering stress (σ, MPa) and engineering strain (ε). The stress-strain curves of each sample were plotted and analyzed by the means of four parameters, elastin phase modulus (MPa), collagen phase modulus (MPA), failure strain (mm) and ultimate tensile strength (MPa), which has been characterized previously by Korossis et al. Finally, the calculated biomechanical parameters were averaged over the number of samples in each group and analyzed by means of four parameters: elastin phase slope (El-E), collagen phase slope (Coll-E), ultimate tensile strength (UTS) and failure strain (εUTS) (Fig. 2-6).

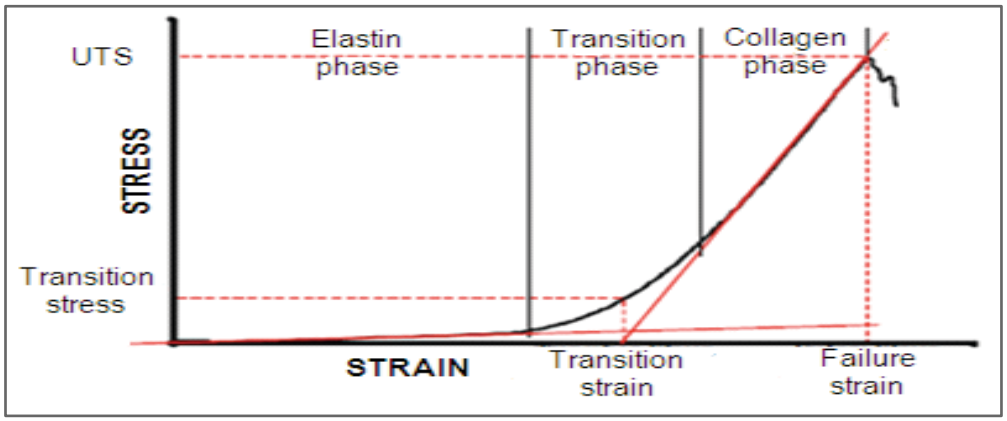

Figure 2-7: *Typical stress-strain behavior of soft tissue, which consisted of an initial linear region (elastic phase), followed by a secondary prolonged linear region (collagen phase), prior to failure. UTS: ultimate tensile strength. Adapted from[232].*

2.12 In vitro cytocompatibility assays

Following preservation methods, the cytotoxicity of the scaffolds was assessed with quantitative and qualitative assays according to ISO 10993-5 for biological evaluation of medical devices through contact and extract (only for preserved DPP patches) [233]. Two different cell lines were tested: umbilical vein endothelial cells (HUVEC) and human bone marrow mesenchymal stem cells (hBM-MSC).

2.12.1 Contact cytotoxicity assay

Scaffold cyto-compatibility following preservation was assessed with a contact cytotoxicity assay as described in ISO 10993-5 for the biological evaluation of medical devices. Preserved pericardia were cut with biopsy punchers (Kai industries, 8 mm diameter) and attached to a six-well culture plate (Corning Inc., Lowell, MA, USA) using steri-strip (3M, Maplewood, MN, USA). Prior to cell seeding, 24 h treatments with the antibiotic/antimycotic solution were performed to ensure scaffold disinfection, as previously described in [234]. The samples were then washed three times with PBS and kept overnight in basal or alpha MEM Medium at 37°C until cell seeding. HUVEC, P5, and hBM-MSC (Promocell, Heidelberg, Germany), P7, were seeded into each well at 1.5×10^5 cells in 2 ml of culture medium. The seeded punches were cultured for 3 days and stained with Giemsa to visualize the cell morphology and distribution under light microscopy. Wells with no scaffold samples and with cyanoacrylate glue were seeded with the same cell density and served as negative and positive controls, respectively. Images were acquired at phase contrast with a Nikon Eclipse 50i light microscope equipped with NIS-Elements D3.2 Software (Nikon Corporation, Shinagawa, Tokyo, Japan).

2.12.2 Proliferation assay (MTS)

A proliferation test was performed using an MTS assay (CellTiter 96®AQueous One Solution Cell Proliferation Assay, Promega, Madison, WI, USA). Viable proliferating cells have the ability to reduce MTS tetrazolium to a formazan-dye, which can be detected at 490 nm (FLUOstar Omega, BMG LABTECH, Ortenberg, Germany). The cell proliferation was assessed at two time points (24 h and 72 h).

2.12.3 Extract cytotoxicity assay

Preserved decellularized porcine pericardial samples were used to prepare soluble extracts. DMEM with 80% (v/v) DMSO served as positive (cytotoxic) control and cell culture medium as negative control. Prior to extraction, the samples underwent disinfection treatment for 24 h as described above (2.12.1) and were then minced with a scalpel (n=4 for each group). The minced tissues were incubated with cell culture medium for hBM-MSCs (alpha-MEM) and HUVEC (Basal medium) respectively (1 ml per 100 mg wet tissues) for 72 h at 37°C under agitation. The samples were subsequently centrifuged at 20.000 g for 15 min and the supernatants were collected immediately for further processing. In the meantime, hBM-MSCs P6 and HUVEC P8 were seeded at $1,5*10^5$ into a 24-well plate (Corning Inc) at 37°C in 5% (v/v) CO_2. After 48 h hours both cells lines reached a confluency of 80%. The cell culture media was aspirated and the soluble extracts, positive and negative control (0.5 ml) were added in triplicate to the wells. Cell morphology was observed at phase contrast with a Nikon Eclipse 50i light microscope equipped with NIS-Elements D3.2 Software (Nikon Corporation).

2.12.4 Cytotoxicity assay (LDH)

The supernatants from cell culture of HUVEC and hBM-MSC of contact and extract assay (only preserved DPP) were analyzed for extracellular lactate dehydrogenase LDH (Pierce LDH Cytotoxicity

Assay Kit, Thermo Fisher Scientific) at two time points (24h, 72h). Basically, in the case of cell lysis, LDH is released into the culture media. This allows its quantification using a colorimetric assay based on the conversion of tetrazolium salt into formazan following an enzymatic cascade. The absorbance was measured at 490 nm using a plate reader spectrophotometer (FLUOstar Omega) and calculated as previously described [235]

2.12.5 Live-dead staining

Preserved porcine pericardial patches were cut with biopsy punches (8 mm diameter) for live/dead staining to assess cytotoxicity of CPAs after 72h. Punch disinfection was performed to ensure scaffold disinfection according to (2.12.1). hBM-MSCs P7 were seeded into each well at 1.5 × 10^5 cells in 2 ml of culture medium. Live/dead staining solution was prepared with 1 µM calcein AM and 1 µM ethidium homodimer-1 (1.2 µl calcein and 5 µl of ethidium homodimer-1 in 5ml of PBS). After 72 h of cell culture, live/dead stain solution was added into each well to completely cover the tissue and samples incubated at 37°C in the dark for 30 min. The samples were washed 3 times in PBS and then wet mounted onto a microscope slide and covered with a glass coverslip. The visualization of living cells was carried out by means of MPM as previously described (paragraph 2.10). The images were acquired with a magnification of 25x, fixed resolution of 1024x1024 pixels, and frame accumulation of 120 frames but as Z-Stack. The Z-Stack images of all groups were converted to single image by Z-projection with the help of imageJ. This permits the visualization of 3-D datasets in 2-D. Live and dead cells were counted with cell counter (imageJ tool) and the percentage of viable cells was calculated as follows: $(Viable\ cells/total\ number\ of\ cells)\times 100$.

2.12.6 Statistical analysis

All data were expressed as mean ± standard deviation. Data were analyzed in Microsoft Excel, and GraphPad Prism for Mac, Version 6.0

(GraphPad Software Inc., California). One-way ANOVA using the Tukey test was performed to evaluate significant differences for all groups (native, decellularized, preserved) for both species. Significance was accepted at the 5% significance level.

3 **Results**

3.1 Evaluation of TRICOL bovine and porcine pericardial scaffolds

Sabra Zouhair, Eleonora Dal Sasso and Sugat R. Tuladhar performed the decellularization of bovine and porcine pericardial tissues. For this chapter of the thesis, Sabra Zouhair performed most of the analysis unless otherwise stated. Histological staining, as well the MPM imaging of the *fibrosa* layer of DBP and DPP scaffolds shown in this work, was carried out by Eleonora Dal Sasso,. Data evaluated and analyzed by Sugat R. Tuladhar are not shown in this paragraph.

First co-authors contribution statement

3.1.1 ECM evaluation after decellularization

3.1.1.1 Histological analysis

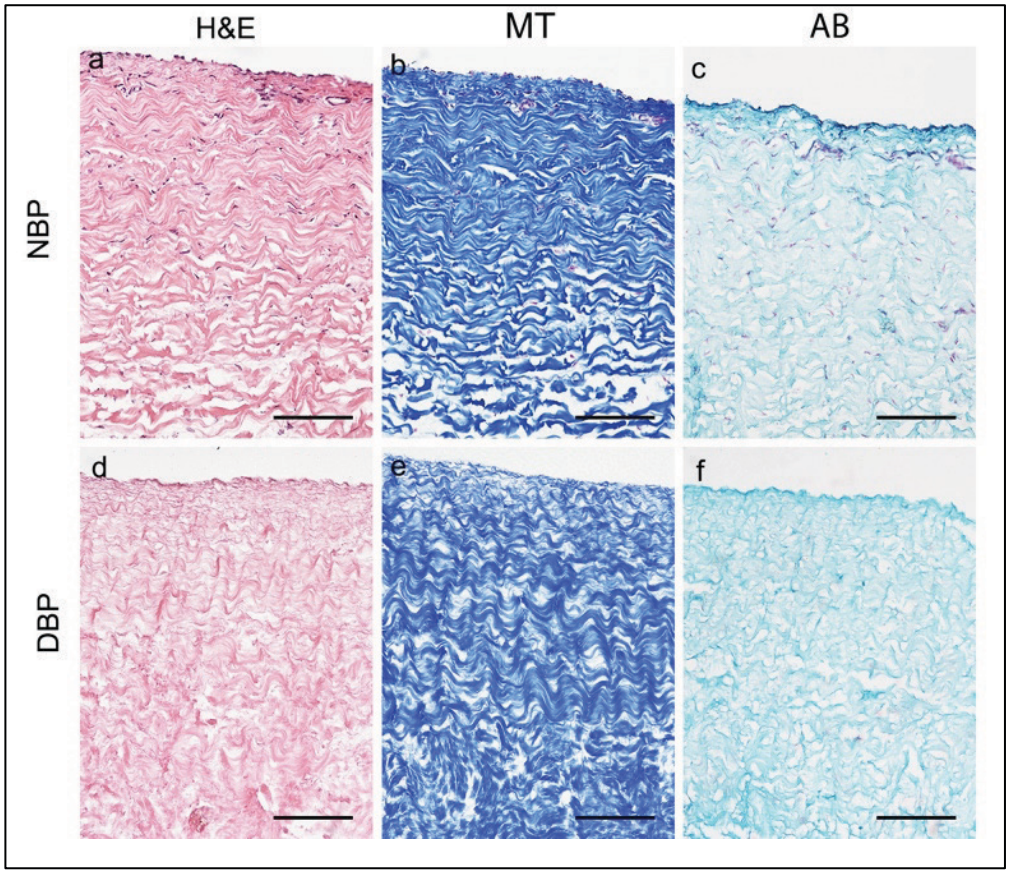

Figure 3-1: *Histological staining of NBP (a-c) and DBP (e-g). (d, f) H&E, (a, d) MT and (b, e) AB (c, f). Scale bars represent 100 µm.*

The ECM structure of pericardial scaffolds was assessed by histological staining. H&E staining revealed spatial distribution of cells within native bovine (Fig. 3-1a) and porcine pericardia (Fig. 3-2a). Mesothelial cells also were identified lining the *serosa* of the native pericardial sections. Broadly, the ECM structure was mainly composed of wavy collagen fibers and GaGs as observable by MT and AB (Fig. 3-1b,c and Fig. 3.2b-c) for bovine and porcine tissues respectively. After Tricol treatment, decellularized bovine and porcine samples appeared to be acellular and devoid of cellular fragments and nuclear residues as visible by H&E and MT, respectively (Fig. 3-1d-e and Fig.

3-2d-e), while collagenous matrix organization and structure were maintained in both species. Discoloration of GAGs was observed in both DBP (Fig. 3-1f) and DPP (Fig. 3-2f) samples in comparison to native sections (Fig. 3-1c, Fig. 3-2c).

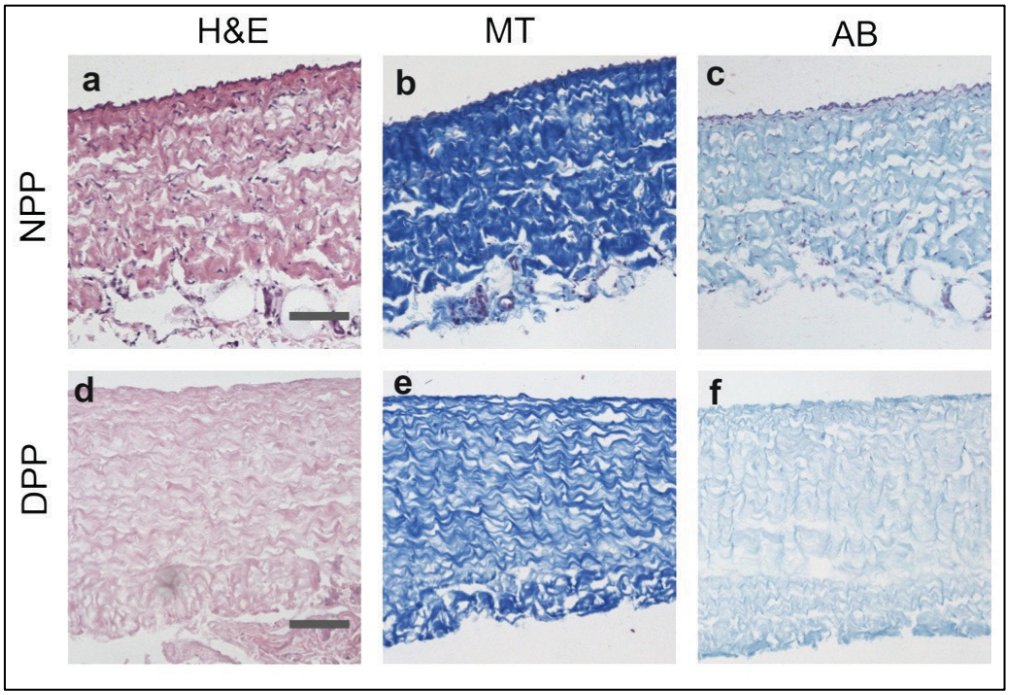

Figure 3-2: *Histological staining of NPP (a-c) and DPP (d-f), H&E, (a, d) MT and (b, e) AB (c, f). Scale bars represent 100 µm.*

3.1.1.1.1 Scanning electron microscopy

To further analyze the effectiveness of TRICOL decellularization, ultrastructural imaging was carried out using SEM. Surface analysis of *serosa* of NBP and NPP tissues revealed a cobblestone-like structure (Fig. 3-3a,b and e, f respectively), which was not observed in TRICOL DBP (Fig.3-3 c, d) and DPP samples (Fig. 3-3g, h). Cell removal leads to the exposure of the collagen bundles in bovine and porcine scaffolds in *serosa* and *fibrosa* layers (Fig. 3.3c, e and Fig.3.4c, e respectively). At higher magnification, collagen organization appears to be well-maintained after decellularization. Moreover, elastic fibers were detected on the *fibrosa* of DBP and DPP samples (Fig. 3-4c, d and g, h respectively).

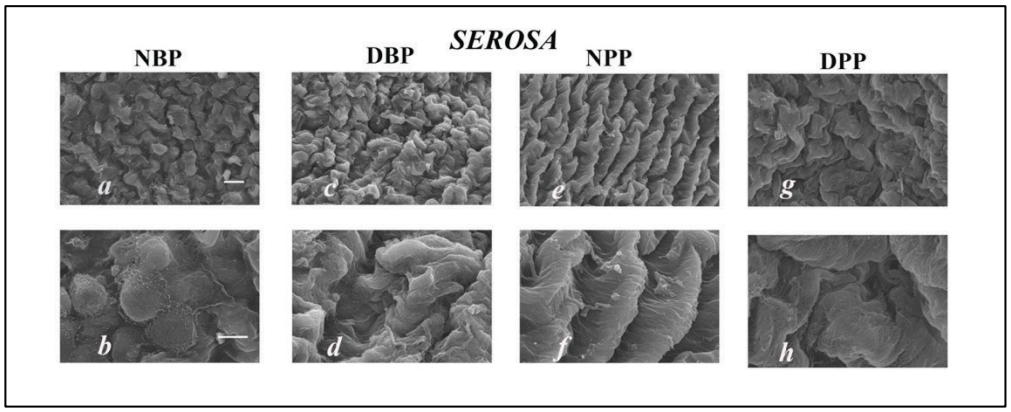

Figure 3-3: *Scanning electron microscopy analysis of the serosa surface of native and decellularized porcine and bovine pericardial tissues: micrographs are represented in two magnifications 1000X and 5000X. Scale bars indicate 5 µm and 10 µm*

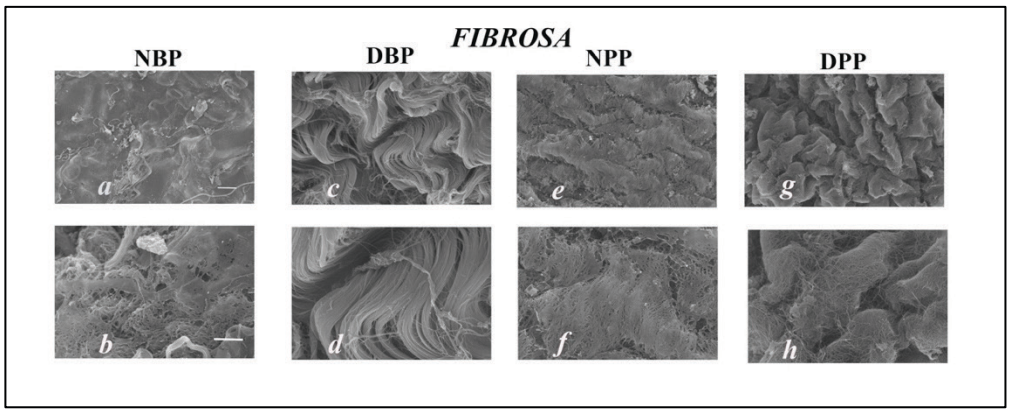

Figure 3-4: *Scanning electron microscopy analysis of the fibrosa surface of native and decellularized porcine and bovine pericardial tissues: micrographs are represented in two magnifications 1000X and 5000X. Scale bars indicate 5 µm and 10 µm*

3.1.1.2 Multiphoton imaging

Autofluorescence imaging and SHG revealed similar collagen and elastin structures in native and decellularized bovine and porcine tissues in *serosa* and *fibrosa* layers. Representative images of *serosa* surface showed the presence of green fluorescent cell nuclei and elastic fibers detected at 800 nm in native tissues (bovine and porcine) (Fig. 3-5b und h). This depends on two-photon excited reduced coenzyme NAD(P)H, whereas at the same excitation the nuclei were absent in decellularized scaffolds (Fig. 3.5e and k).

The SHG imaging confirmed the crimped pattern of collagen fibers, which were more evident and larger in the *fibrosa* of native and

decellularized bovine and porcine pericardia (Fig.3-6 a, d, g, j) and smaller and better organized on *serosa* (Fig. 3-5 a, d, g, j). Autofluorescence analysis on *serosa* and *fibrosa* layers displayed elastic fibers running parallel to collagen in NBP and DBP (Fig. 3-5b, e and Fig. 3-6b, e respectively) and wavy and branched elastic networks in NPP and DPP (Fig. 3-5h, k and Fig. 3-6h, k respectively). Cell removal seems to have induced more organized collagen structure. However, quantification of the SHG signal in the *serosa* and *fibrosa* layers did not show any statistically significant differences between the native tissues and their decellularized counterparts in either species (Fig. 3-7), suggesting that decellularization did not affect the quality of collagen.

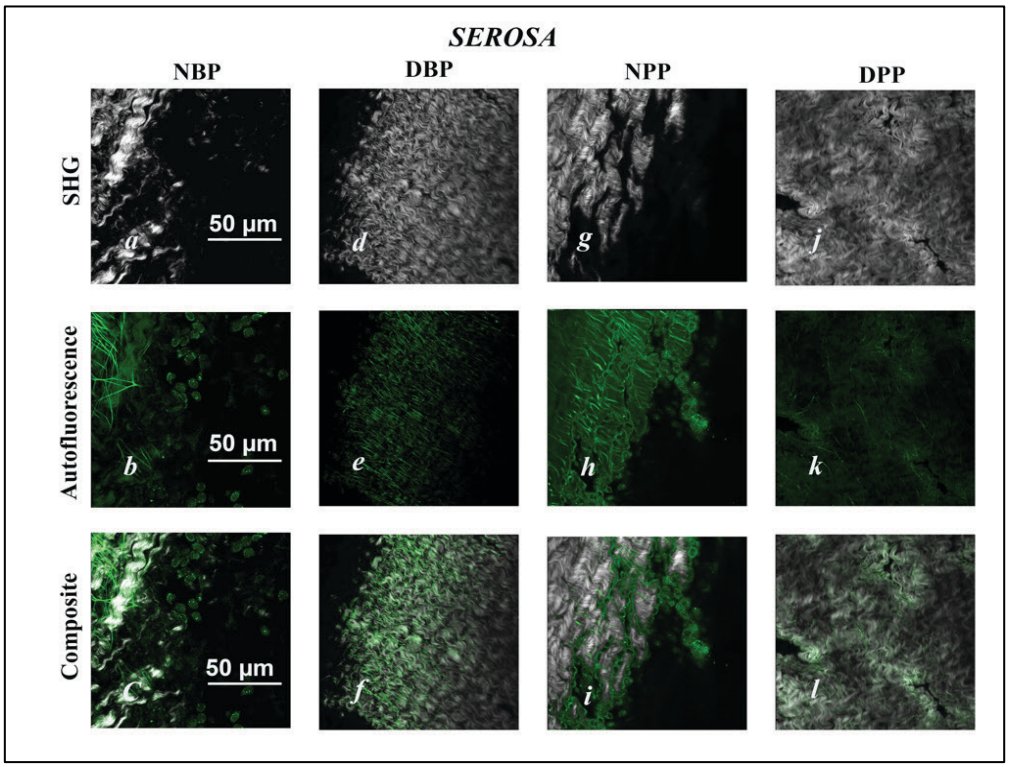

Figure 3-5: *Second harmonic generation (SHG) microscopy and Multiphoton-induced autofluorescence imaging of serosa of the native and decellularized bovine and porcine pericardial tissues. Both collagen (400 nm) and elastic fibers (525 nm) appeared clearly in native and decellularized porcine and bovine tissues. Moreover, cells were detected in natives of both species. Scale bars represent 50 µm.*

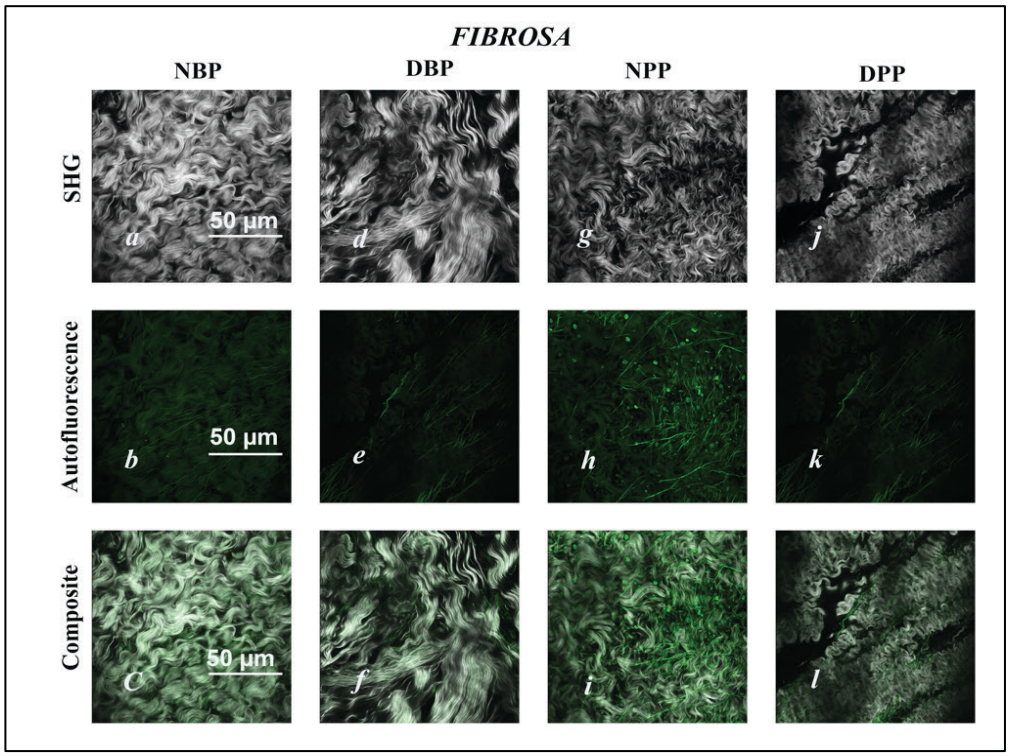

Figure 3-6: *Second harmonic generation (SHG) microscopy and Multiphoton-induced autofluorescence imaging of fibrosa of native and decellularized bovine and porcine pericardial tissues. Both collagen (400 nm) and elastic fibers (525 nm) appeared clearly in native and decellularized porcine and bovine tissues. Scale bars represent 50 µm.*

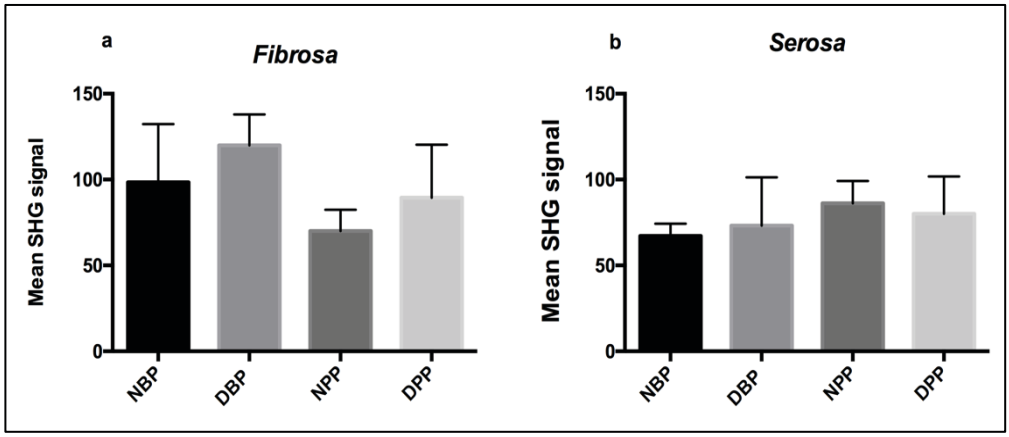

Figure 3-7: *Quantification of SHG signal intensities of collagenous structures (n=6). Data are presented as mean ± SD. No significant differences were found between the native and decellularized tissues in respect to serosa (a) and fibrosa (b) layers.*

3.1.2 Evaluation of protein stability and secondary structures

3.1.2.1 Analysis of the fingerprint region of the proteins with FTIR

FITR analysis was performed to investigate the impact of TRICOL on the overall protein secondary structures. The amide-I band region 1700–1600 cm^{-1} is used to correlate the band shape with secondary structure contents. Second derivative spectra of native and decellularized samples were calculated to reveal differences in the amide-I region assigned to the two main types of protein secondary structure. Figure 3-8 (a1) and (a2) shows typical spectra demonstrating the bands at 1650 and 1630 cm^{-1} more clearly, which likely indicate α-helical and β-sheet structures, respectively, in both tissues. The ratio of the bands at 1650 and 1630 cm^{-1} was used as a parameter to highlight differences among the treatment groups. The ratios in NBP and NPP tissues were found to be respectively 0.96 and 0.95 (Fig. 3-8 (b1) and (b2). The corresponding values for DBP and DPP tissues were respectively 0.96 and 0.98 Fig. 3-8 (b1) and (b2), suggesting that the overall protein secondary structure was not affected by the TRICOL decellularization procedure.

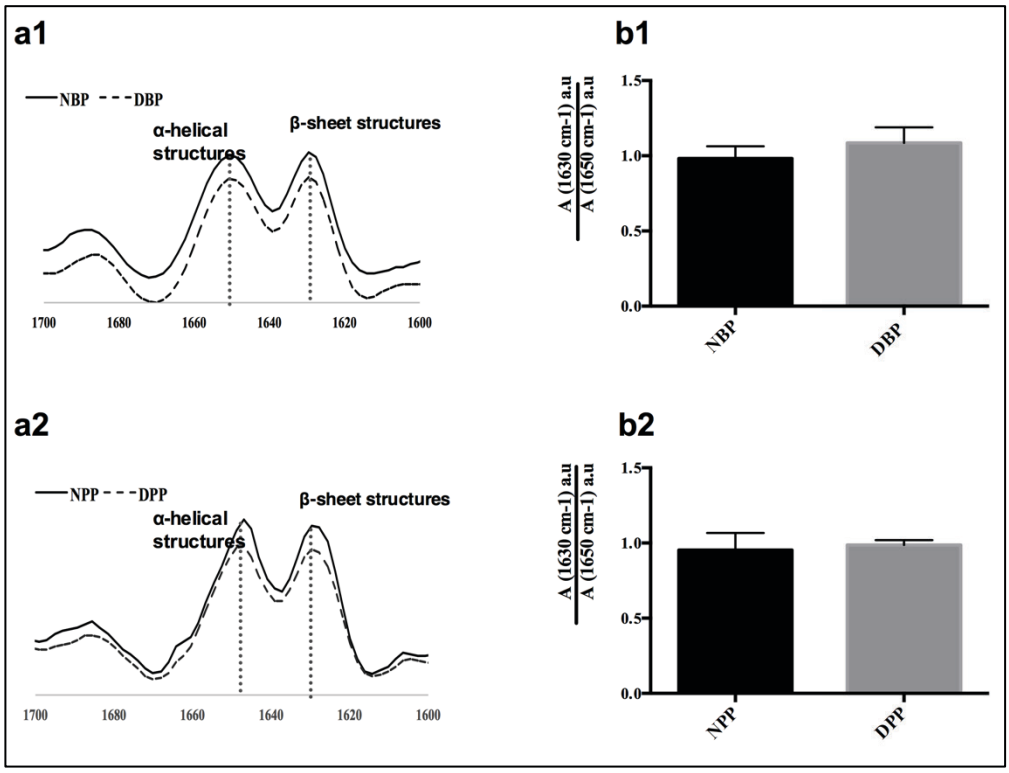

Figure 3-8: *The panel presents second derivatives of the recorded spectra between 1600 and 1700 cm^{-1} indicating α-helical structures at 1650 cm^{-1}, and β-sheet structures at 1630 cm^{-1} in bovine (a1) and in porcine (a2). The bars represent ß/α ratio from the different spectra of the native and decellularized groups from both tissues (b1 and b2). Data are presented as mean ± SD. No significant differences were found between the groups in both species.*

3.1.2.2 Analysis of denaturation profiles of ECM proteins using DSC

The denaturation profile of native and decellularized scaffolds was investigated using DSC, which provided thermal fingerprints of the scaffolds that were used to detect possible negative effects of the decellularization technology on matrix proteins such as protein denaturation, degradation or crosslinking. Figure 3-9 (a1) and (a2) shows DSC thermograms of native tissues and after decellularization in both species. The protein stability of bovine and porcine pericardia was assessed by means of T_{onset} and compared among native, decellularized and GA-treated pericardia in each species Fig. 3-9 (b1) and (b2); T_{onset} for the bovine group was determined to be 66.7 ± 0.9, 67.77 ± 0.07 and 83.55 ± 0.25°C, and for the porcine group 65.4 ± 0.25, 64.45 ± 0.15 and 86.45 ± 0.17°C. Statistically significant

differences were found for native DPP in comparison to decellularized DPP (P< 0.05) indicating a minor decrease in the denaturation temperature in this species. By contrast, GA-fixation significantly increased the protein denaturation temperature for both bovine and porcine tissues to respectively 83 and 86°C (p< 0.001).

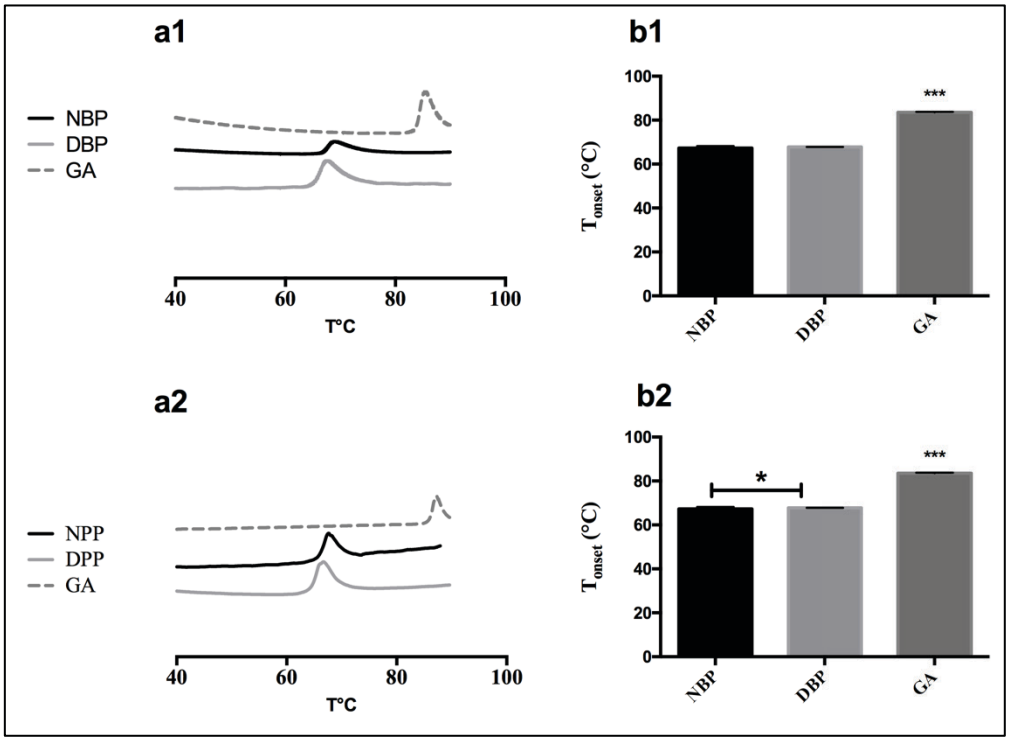

Figure 3-9: *Evaluation of protein stability after TRICOL using DSC. DSC thermograms of the tissues after decellularization and GA-fixation are shown in panels a1 and a2. Bars b1 and b2 show the onset temperature of protein denaturation (T_{onset}) for bovine and porcine tissues. Data are presented as mean ± SD. ***P<0.001, * p<0.05.*

3.1.3 Assessment of the biochemical properties of decellularized scaffolds

3.1.3.1 HYP content and sGaGs

Collagen and sGaGs are the main components of the ECM of pericardial scaffolds. Therefore, their quantification is important for studying the extent of the damage that might be caused by decellularization. The HYP content in decellularized porcine and bovine tissues (127.12±52 µg/mg dry weight) was estimated to be

higher in comparison to their native counterparts (119.55±26.12 µg/mg dry weight). This is likely due to the loss of cells and soluble proteins after decellularization. However, no statistically significant differences were found between native and decellularized tissue for both species (Fig. 3-10a). A decrease in the amount of sGaGs was observed after the TRICOL procedure; for bovine and porcine respectively (4.50±2,75; 5.97±1.01 µg/mg dry weight) compared to their native counterparts (13.71± 6,83; 8.23± 2.77 µg/mg dry weight) (Fig. 3-10b). However, differences were only found to be statistically significant for the bovine pericardium (P< 0.01). These results confirmed the maintenance of collagen and GaGs after preservation as observed with the ultrastructural analysis.

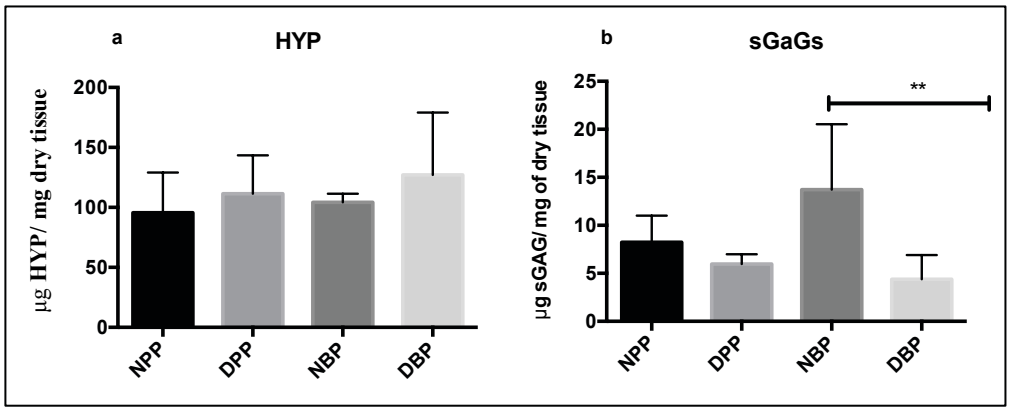

Figure 3-10: *Biochemical results: quantification of hydroxyproline content (a) and sulfate glycosaminoglycans (b) after preservation and reconstitution. Mean hydroxyproline (HYP) and sulfated glycosaminoglycans (sGAGs) content per dry weight of tissue (n = 6). No significant difference was found in HYP contents after the treatments. A decrease of sGAGs in DBP was confirmed statistically. Data are presented as mean ± SD. ***P<0.001*

3.1.4 Evaluation of the biomechanical behavior of bovine and porcine tissues

3.1.4.1 Uniaxial tensile testing

Biomechanical testing was performed on native and decellularized bovine and porcine tissues. For comparison, glutaraldehyde-crosslinked samples were also tested. The generated stress-strain curves are illustrated in Figure 3-11 (a1) and (a2), demonstrating the typical J-shaped curves of soft tissues [236]. Significant differences in

stress-strain behavior of bovine and porcine pericardia were observed after decellularization and fixation.

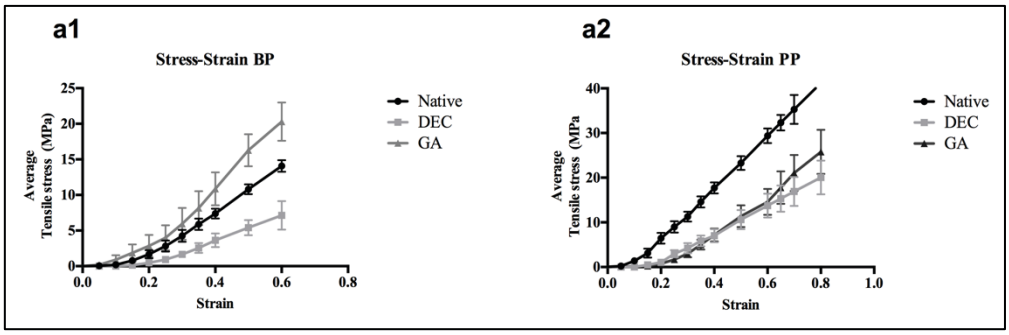

Figure 3-11: *Average of stress strain curves of native, decellularized, GA-fixed bovine and porcine tissues. Data are presented as mean ± SE.*

The calculated biomechanical parameters of bovine and porcine pericardia after treatments are illustrated in Fig. 3-12. The results primarily show a trend towards lower slopes in both the elastin and collagen-phase modulus, suggesting increased compliance. However, this decrease was only statistically significant for the collagen-phase modulus in DPP (59.07 ± 8.02 MPa) compared to NPP (37.33 ± 11.12 MPa, Fig. 3-11b, $p<0.001$). A similar tendency was observed for the failure strain parameter. The decellularized scaffolds (bovine and porcine) demonstrated higher values compared with their native counterparts, indicating a tissue with greater extensibility. Moreover, the ultimate tensile strength of DPP scaffolds (7.9 ± 2.88 MPa, $p<0.05$, Fig. 3-12c) was found to be significantly lower compared to NPP ones (13.65 ± 1.73 MPa, Fig. 3-12c). Additionally, a significant increase in thickness upon TRICOL was observed in porcine scaffolds (0.23±0.024 mm, 0.15±0.014 mm, $P< 0.01$; Fig. 3-11e). This finding is indicative of an increased scaffold compliancy after TRICOL.

Regarding GA-treatment, the tissue crosslinking resulted in a significant increase in the slope of the elastin-phase modulus for both bovine (1.19±1,13 MPa) and porcine (0.58±0.39 MPa) tissues in comparison with their decellularized counterparts respectively (0.24±0,11; 0.24±0.38 MPa, Fig. 3-12a), indicating a loss of compliance. A comparable trend has been observed for the slope of the collagen-phase modulus of decellularized scaffolds with respect to

native tissues, although the slope was found to be significantly higher only for bovine tissues (57.8±11.13 MPa, P< 0.001, Fig. 3-12b). In addition, GA-treated tissues demonstrated differences between native and decellularized scaffolds with regard to failure strain, though this was only statistically significant for the porcine group (0.58±0.51, p< 0.001, Fig. 3-12c). It appears that GA- treatment leads to a loss of extensibility in bovine and porcine tissues.

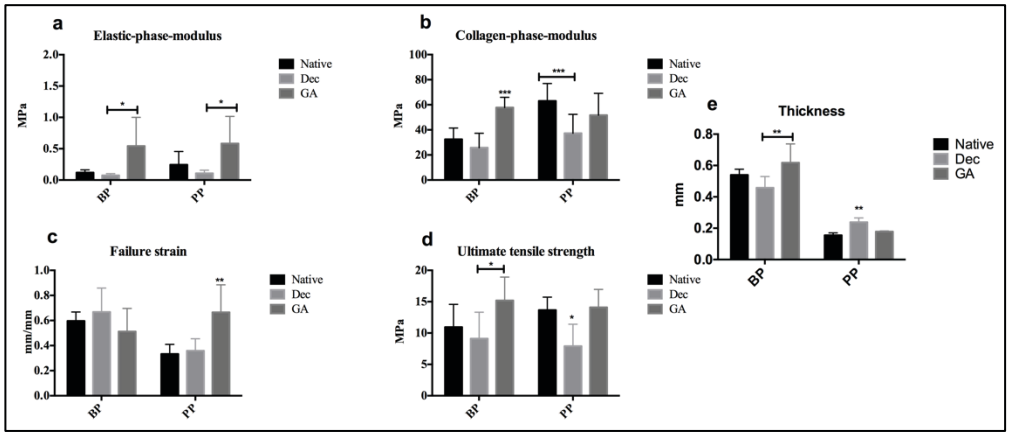

Figure 3-12: *Mean of biomechanical parameters for decellularized pericardial scaffolds compared to native and GA-treated tissues. (a) Elastic phase modulus, (b) Collagen-phase modulus, (c) Failure strain and (d), Ultimate tensile strength, (e) Thickness. Data are presented as mean ± SD; asterisks indicate significant difference of the treated groups compared to the control. *P<0.05, **P<0.01, ***P<0.001*

3.2 Evaluation of preservation methods on bovine pericardial scaffolds

3.2.1 ECM evaluation of preserved DBP patches

3.2.1.1 Histological analysis

Histological staining was used to analyze the ECM architecture of decellularized, FD, vitrified and cryopreserved DBP patches. Collagen was arranged in fibers showing their wavy and crimped appearance in red (Hematoxylin/Eosin) and blue (Mallory trichrome) in control (Fig. 4-1a and b), as well in the FD (Fig. 1e and e), vitrified (Fig. 4-1i and j) and cryopreserved (Fig. 4-1m and n) samples. PicroSirius red staining under bright field microscopy also demonstrated the typical structure of DBP, mainly composed of regularly structured collagen bundles (pink) and a few elastic fibers (brown) of both preserved and control DBP samples (Fig. 4-1g; FD, k; vitrified, o; cryopreserved, c; control). Under polarized light microscopy the PicroSirius red-stained sections revealed strong red-orange-green birefringence, which was correlated with collagen thickness and packing. The birefringence characteristic of collagen allowed visualization of fiber crimp. Thicker crimped collagen appeared red-orange, whereas thinner collagen fibers were detected in green. This appearance was maintained in DBP scaffolds after preservation and reconstitution (Fig 4-1d; control, h; FD, l; vitrified, p; cryopreserved). None of the applied preservation procedures affected the gross histoarchitecture of the ECM.

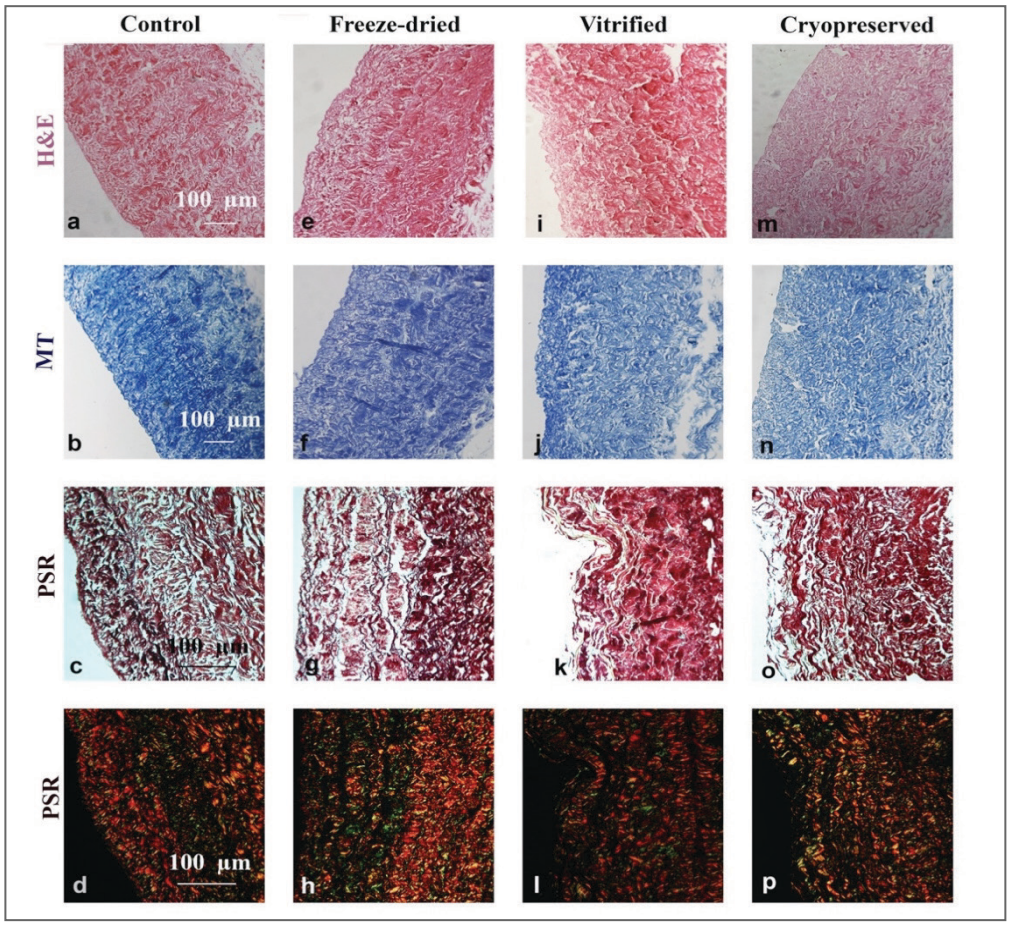

Figure 3-13: *Histological staining of preserved DBP patches. Representative light-micrographs of Hematoxylin/Eosin and Mallory Trichrome revealed well-preserved collagen structure in controls (a, b), FD (e, f), vitrified (i, j) and cryopreserved (m, n). PicroSirius red staining viewed under bright field or polarization contrast showed a crimped collagen profile and few elastic fibers in all investigated groups. Scale bars represent 100 µm.*

3.2.1.2 Scanning electron microscopy

Under SEM the DBP scaffolds showed a complex network of wavy fibers in the *fibrosa* layer, whereas a smooth and glistening surface with wavy morphology was observed on the serous side. Treated groups (Fig. 4-2e-p) demonstrated similar histoarchitecture compared to the control (non-preserved) (Fig. 4-2a-d), both on the *serosa* and *fibrosa* layers. At higher magnification, the collagen bundles also displayed a well-organized structure in all groups. (Fig. 4-2b, d for the control; f, h for the FD; j, l for the vitrified and n, p for cryopreserved groups).

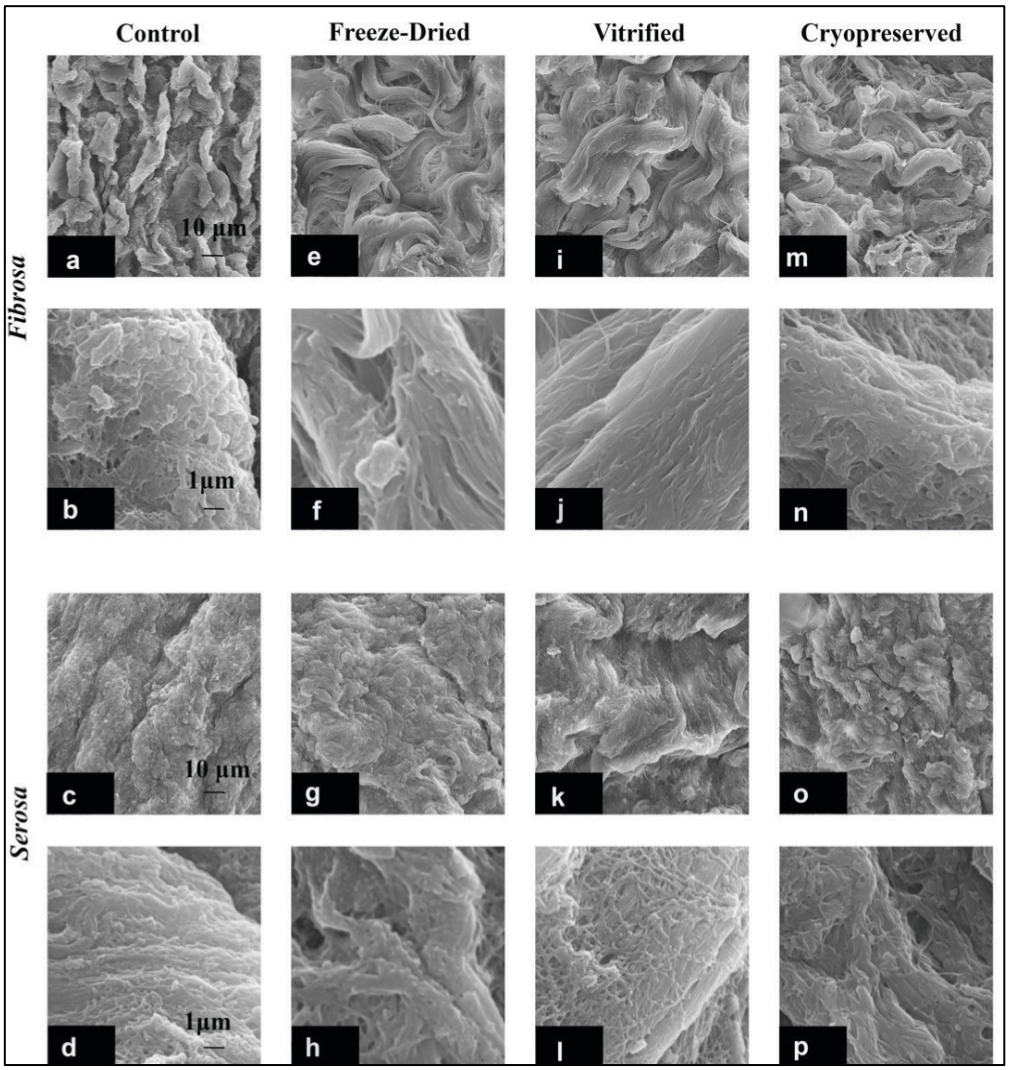

Figure 3-14: *Scanning electron microscopy analysis of the surfaces fibrosa and serosa of differently preserved groups: control (a-d), FD (e-h), vitrified (i-l) and cryopreserved (m-p). Micrographs are represented in two magnifications 1000X and 10000X. Scale bars indicate 1 µm and 10 µm.*

3.2.1.3 Multiphoton imaging

In order to investigate whether the preservation methods caused any damage to the ECM, two-photon excitation microscopy was used for three-dimensional tissue imaging directly on non-processed scaffolds without any labeling. This allowed visualization of elastin autofluorescence and detection of the collagen SHG signal. Autofluorescence imaging and SHG revealed similar collagen and elastin structures between the control (Fig. 4-3a, b) and the FD (Fig 4-

3d, e), vitrified (Fig 4-3g, h) and cryopreserved (Fig. 4-3j, k) samples. Wavy and branched elastic fibers varying from aligned to interweaving, together with crimped collagen fibers, could be visualized, as can be seen in the composite images (Fig. 4-3c, f, i, l). Qualitatively, collagen and elastic fiber organization and structure were similar in the FD (Fig. 4-3f), vitrified (Fig. 4-3i), cryopreserved (Fig. 4-3l) and control groups (Fig. 4-3c). Quantification of the SHG signal intensity and straightness parameter did not reveal any significant differences among the groups (Fig. 4-4a and b, respectively). Hence, bundle organization and fiber waviness of collagen were maintained after all preservation methods, confirming the MPM imaging results.

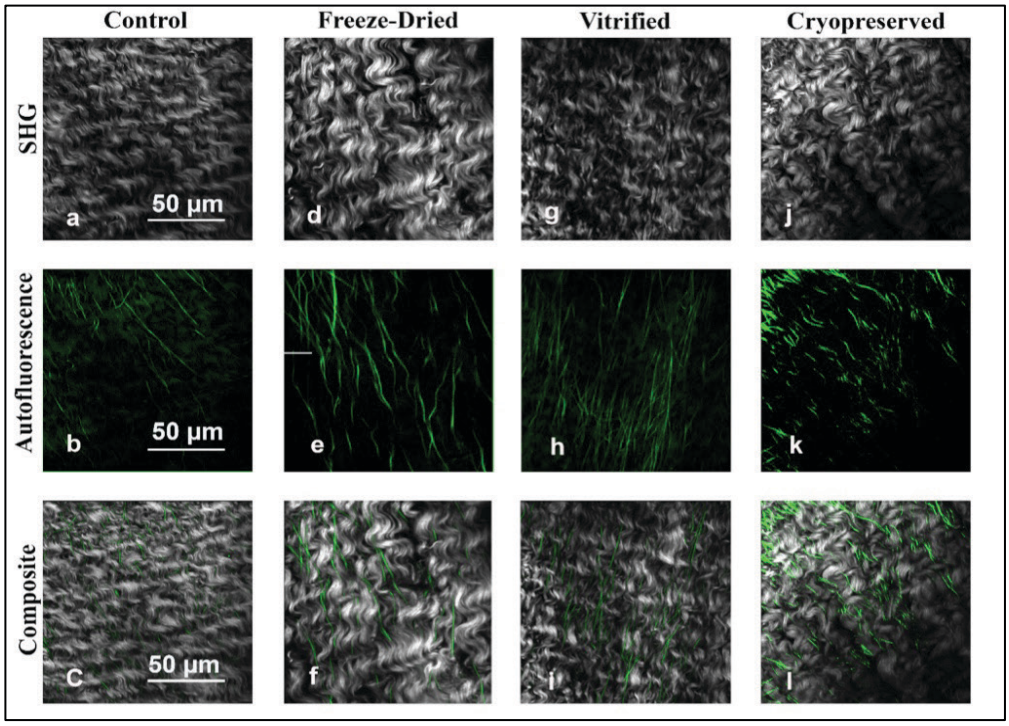

Figure 3-15: *Second harmonic generation (SHG) microscopy and Multiphoton-induced autofluorescence imaging of the control (a-c), FD (d-f), vitrified (g-i), cryopreserved (j-l) DBP patches. Scale bars represent 50 µm.*

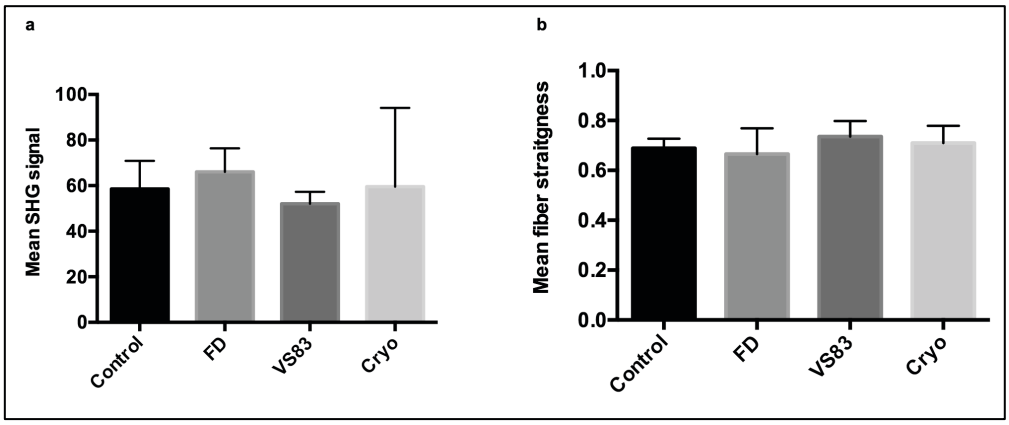

Figure 3-16: *Quantification of SHG signal intensities of collagenous structures (a). (n=4-5). (B) Quantification of straightness parameter of collagen fibers. Data are presented as mean ± SD. No significant differences were found between the groups after preservation and reconstitution.*

3.2.2 Evaluation of protein stability and secondary structure

3.2.2.1 Analysis of denaturation profiles of ECM proteins using DSC

The denaturation profile of DBP patches treated with the different preservation methods was studied using DSC, which provided thermal fingerprints of the scaffolds which were used to detect possible negative effects of preservation processing on ECM proteins. GA-treated scaffold samples were also tested and used as controls. The DSC thermograms of the different treatment groups are shown in Fig. 4-5a and b. Protein denaturation was visible as an endothermic peak, which was determined by the protein composition of the scaffolds (Fig. 4-5a). The shape of the denaturation profile did not show distinct differences among the groups. The T_{onset} of protein denaturation of the control occurred around 67°C and the midpoint around 70°C. The peak area reflecting denaturation enthalpy was approximately 2.4 J/g. The T_{onset} was compared among the treatment groups, and the results showed that the protein denaturation temperature was not significantly affected by any of the preservation protocols (Fig. 4-5b). The T_{onset} of the control and preserved groups ranged between 65-67°C, whereas

GA-fixation significantly increased the denaturation temperature to 83 °C ($p<0.05$)

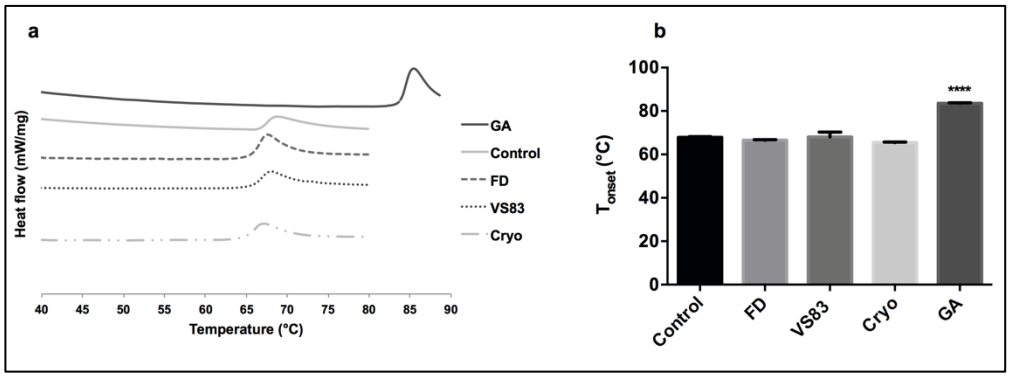

***Figure 3-17**: Investigations of denaturation profile using DSC. Panel A shows DSC thermograms of the tissues after preservation and GA-fixation. B: Bars show the onset temperature of protein denaturation (T_{onset}). GA-treated group demonstrated a significant increase in T_{onset}. No significant differences were found between the groups after storage. Data are presented as mean ± SD. ***P<0.001.*

3.2.2.2 Evaluation of the overall protein secondary structure with FTIR

FTIR was used to study the effect of preservation processing on the overall protein secondary structure of DBP patches. The amide-I region of the spectra was selected, and second derivative spectra were calculated to reveal the different composite bands reflecting distinctive types of protein secondary structure. A typical second derivative spectra of the amide-I region is shown in Fig. 4-6a. The shape of the amide-I band was similar in all spectra. Bands at 1650 and 1630 cm^{-1} have been reported as depicting α-helical and β-sheet structures, respectively. The ratio of the bands at 1650 and 1630 cm^{-1} was used as a parameter to compare the treatment groups [237]. This ratio varied between 0.95 and 0.99 (Fig. 4-6b), but no significant differences were detected between any of the treatment groups and the control. This indicated that the applied preservation methods did not alter the overall protein secondary structure of the DBP scaffolds.

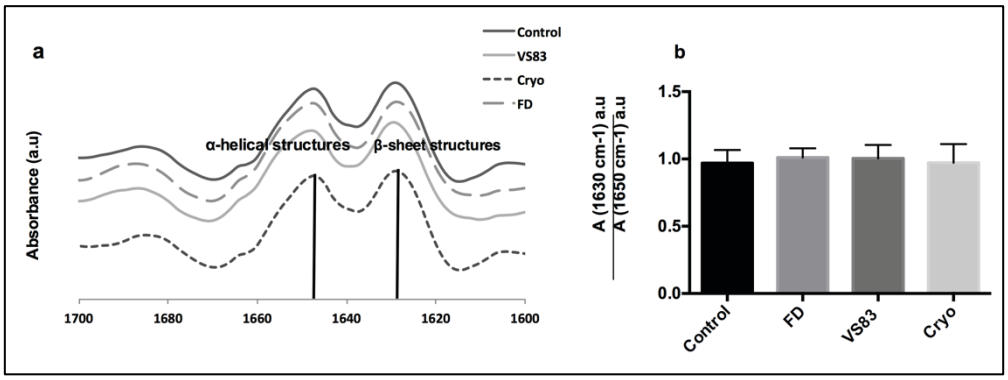

Figure 3-18: *Infrared spectra of DBP scaffolds after preservation and reconstitution. a shows the second derivatives of the recorded spectra between 1600 and 1700 cm^{-1}. Different peaks in the amide-I band (1700–1600 cm^{-1}) represent different types of secondary structure: α-helical structures at 1650 cm^{-1}, and β-sheet structures at 1630 cm^{-1}. Panel b shows the calculated ratio ß/α from the different spectra of the preserved groups. Data are presented as mean ± SD.*

3.2.3 Assessment of the biochemical properties of preserved DBP patches

3.2.3.1 Denatured HYP and sGaGs

Given the important role of GAGs and collagen in the functional properties of the scaffolds, quantification of these compounds was carried out after the various preservation treatments. Quantification of sulfated GAGs in the preserved samples did not show any significant differences compared to the control group. The sGAG contents of control, FD, vitrified and cryopreserved DPB samples were found to be 2.01±0.55, 1.57±0.53, 1.99±0.62 and 2.29±0.56 µg/mg dry weight, respectively (Fig. 4-7a). The dHYP contents of FD, vitrified and cryopreserved patches were estimated to be 18.21±7.61, 22±6.46 and 20.18 ± 8.10 µg/mg dry weight, respectively, without any significant differences between the treatment groups (Fig. 4-7b). Similar dHYP contents were also detected in non-treated DBP (17.89±3.73 µg/mg dry weight), as well as in native BP (12.93±2.19 µg mg-1 dry weight). Autoclaved scaffold patches (control) were found to have a significantly increased dHYP content of 101.89±25.58 µg/mg dry weight. Overall, these results suggested that none of the applied

preservation methods induced collagen denaturation, thus confirming the DSC and FTIR studies.

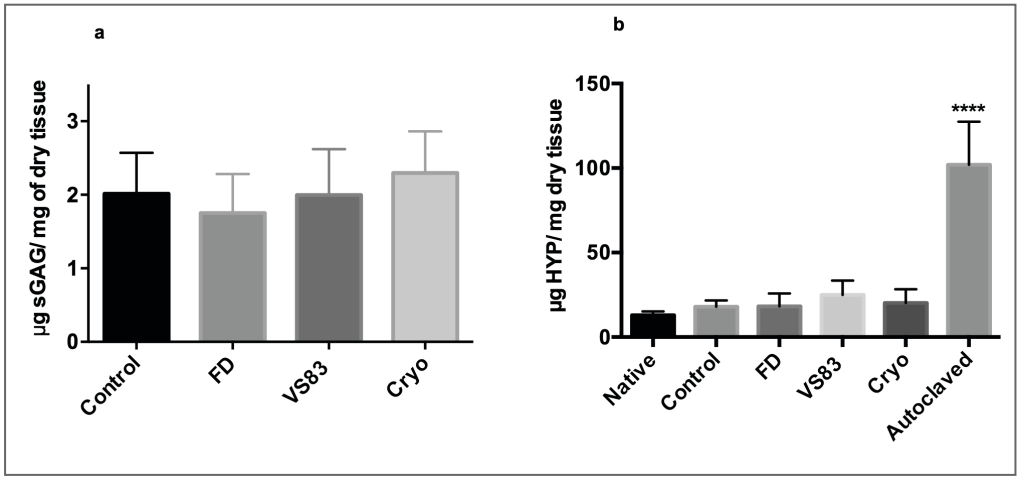

Figure 3-19: *Biochemical results: Quantification of sulfate glycosaminoglycans (a) and denatured hydroxyproline content (b) after preservation and reconstitution. Mean denatured hydroxyproline (dHYP) and sulfated glycosaminoglycans (sGAGs) content per dry weight of tissue (n = 6). No significant differences were observed in sGaGs or in dHYP content after the treatments. Data are presented as mean ± SD. ***P<0.001.*

3.2.4 Evaluation of the biomechanical behavior after preservation

3.2.4.1 Uniaxial tensile testing

Biomechanical assessment was carried out to investigate the mechanical characteristics and behavior of the scaffolds following the different preservation methods. Treated DBP specimens were subjected to low-strain rate uniaxial tensile loading to failure, together with GA- treated scaffolds, which served as control. The acquired force and elongation of each specimen tested were converted to engineering stress and strain, respectively. The stress-strain profiles of each specimen were averaged over the number of specimens in each group and are presented in Fig. 6A. All groups showed the typical stress-strain behavior of soft tissues, which consisted of an initial linear region (elastic phase), followed by a secondary prolonged linear region (collagen phase), prior to failure [238]. The FD and vitrified scaffolds demonstrated similar biomechanical behavior, whereas the

cryopreserved and GA-treated patches showed significant changes compared to the control group (non-preserved decellularized scaffolds). The mean of the calculated biomechanical parameters, derived from the stress-strain curves of the specimens in the different groups, are shown in Fig. 4-8a. The elastic phase modulus of the cryopreserved and GA-treated groups tended to be higher compared to the control, FD, and vitrified ones, suggesting a decrease in compliance for the cryopreserved and GA-treated groups (Fig. 4-9a). However, the differences were not statistically significant. Differences were observed in the collagen-phase modulus of the cryopreserved and GA-treated groups, compared to the non-treated control (57.7±8.9 MPa, $p<0.001$, 57.8 ±11.1 MPa, $p<0.001$, respectively) (Fig. 4-9b), indicating decreased compliance. A significant increase in the collagen-phase modulus was also found in the FD group compared to the control one (42.3±11.7 MPa, $p<0.05$), but the significance of this increase was lower compared to that observed in the case of cryopreserved and GA-treated groups ($p<0.05$) (Fig. 4-9b).

No statistically significant differences in failure strain (Fig. 4-9c) and ultimate tensile strength (Fig. 4-9d) were detected between the groups. An increase in thickness was found in all groups compared to the control, but the differences were statistically significant only in the case of FD and GA-treated groups (Fig. 4-8b).

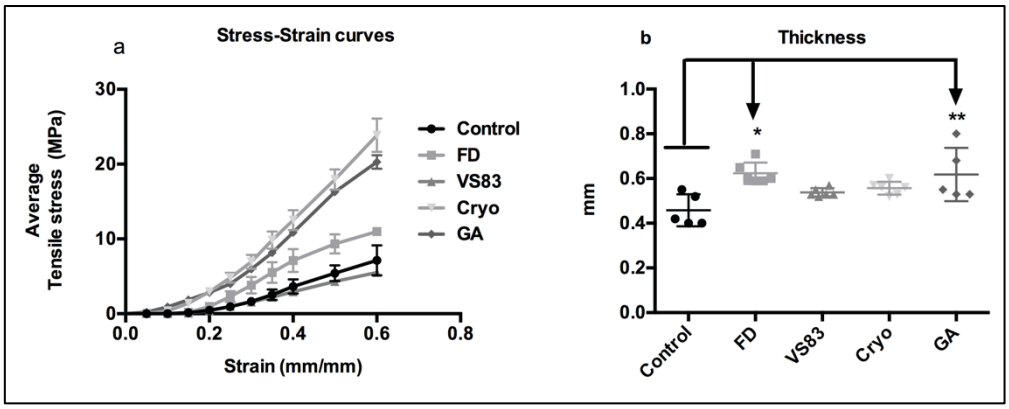

Figure 3-20: *Mean of strain-strain curves and thickness parameter of preserved and GA-Fixed DBP patches. Data are presented as mean ± SE for (a) and SD for (b); asterisks indicate a significant difference between the treated groups compared to the control. *P<0.05, **P<0.01, ***P<0.001*

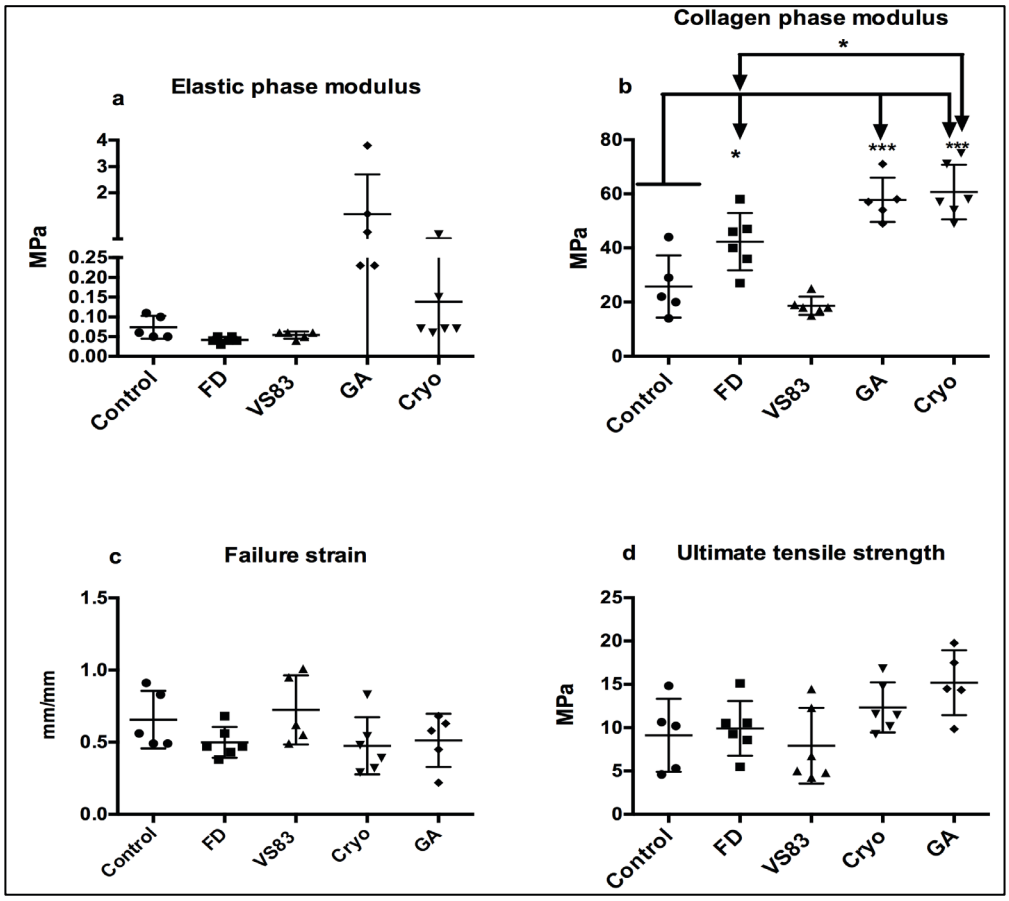

Figure 3-21:*Mean of biomechanical parameters for the preserved pericardial patches compared to non-preserved control and GA-treated tissues. (a) Elastic-phase modulus, (a) Collagen-phase modulus, (c) Failure strain and (d) Ultimate tensile strength. Data are presented as mean ± SD; asterisks indicate a significant difference between the treated groups compared to the control. *P<0.05, **P<0.01, ***P<0.001.*

3.2.5 Evaluation of cytotoxicity of preserved DBP patches

3.2.5.1 Contact cytotoxicity assay and Proliferation assay (MTS)

Scaffold cytocompatibility following preservation was assessed under a contact cytotoxicity assay for 24 and 72 h. There were no cytotoxic effects observed by any of the preservation treatments. HUVECs and hBM-MSCs grew towards and in contact with all scaffold samples, with no evidence of contact inhibition or changes in cell morphology (Fig. 4-10e-j), similar to the case of the control (non-

preserved DBP) (Fig. 4-10c and d). The cyanoacrylate (positive control was obviously toxic (Fig. 4-10k-l). Cells that were seeded on culture plastic, without any scaffolds, proliferated and reached confluency faster (Fig. 4-10a and b). Additionally, cytotoxicity analysis performed using MTS proliferation assay did not reveal any statistically significant decrease in cell viability among the treated samples after 24 h. A notable increase in proliferation was recorded after 72 h, confirming that no cytotoxic effect was induced from the preserved samples (Fig. 4-11a and b). By contrast, statistically significant differences were observed 24 h and 72h after cell incubation with the positive control (cyanoacrylate) in comparison with all preserved groups. Cyanoacrylate appears to be highly toxic to the cells, leading to complete cell death after 72 h (Fig. 4-11a and b).

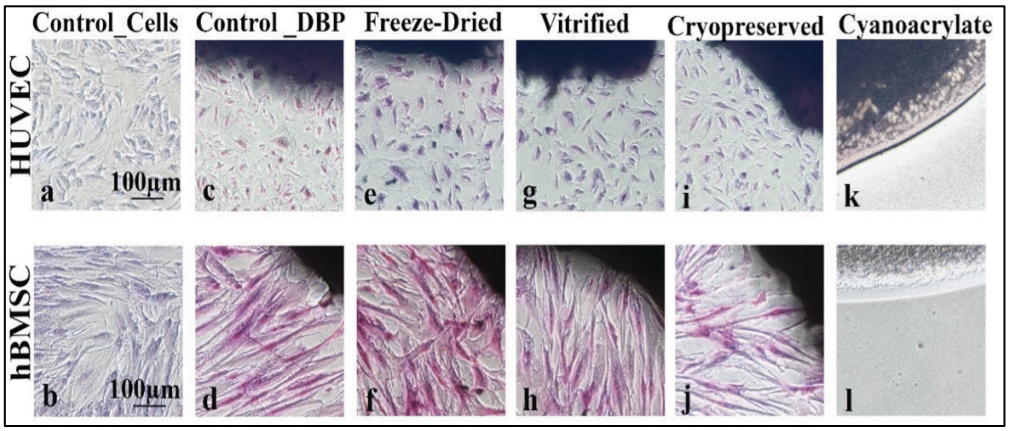

Figure 3-22: *Giemsa-stained contact cytotoxicity using two different types of human cells, hBM-MSC (b, d, f, h, j, l) and HUVEC (a, c, e, g, i, k). Positive control (Cyoanoacrylate) and negative controls (Cells and DBP). Scale bars represent 100 µm.*

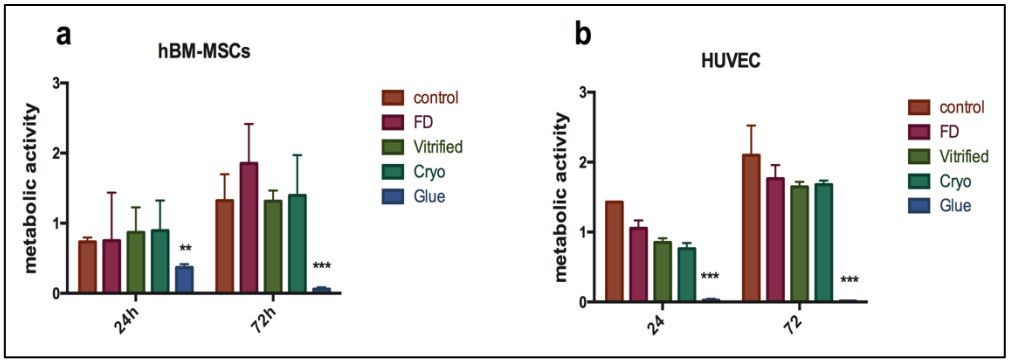

Figure 3-23: *MTS proliferation assay after 24 h and 72 h. Data are presented as mean ± SD; asterisks indicate a significant difference between the treated groups compared to the positive control **P<0.01, ***P<0.001.*

3.3 Evaluation of the preservation methods on porcine pericardial scaffolds

3.3.1 ECM evaluation of preserved DPP patches

3.3.1.1 Histological analysis

Histological staining was used to analyze the ECM architecture. The maintenance of the overall ECM architecture and its components in the preserved samples was confirmed by histological staining with H&E, MT and AB. Collagen-type I was arranged in fibers, highlighting its wavy and crimped appearance in red (H&E) and blue (MT) in the control (Fig. 4-1a and b), as well in the FD (Fig. 4-1d and e), vitrified (Fig. 4-1iand j) and cryopreserved (Fig. 4-1l and m) samples. A similar trend was observed for sGAGs; their distribution pattern did not vary between the groups (Fig4-1c, control; f; FD; k: vitrified; n; cryopreserved), indicating that none of the applied preservation procedures impaired the ECM architecture.

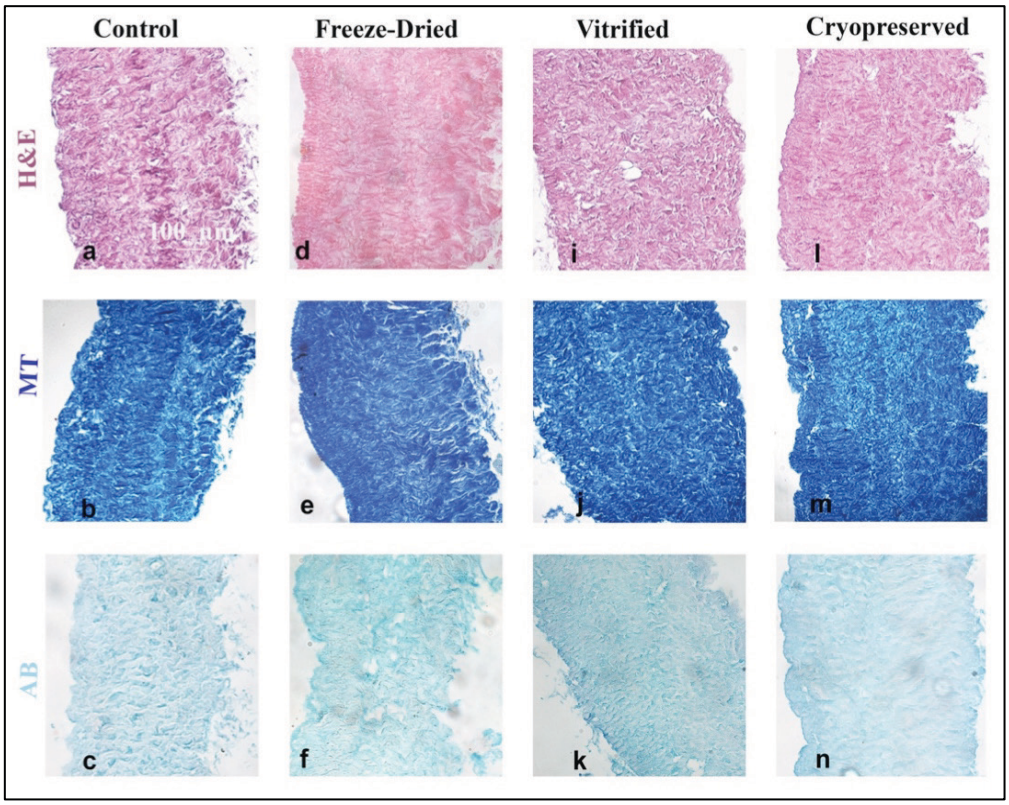

Figure 3-24: *Histological staining of preserved DPP patches. Representative light-micrographs of Hematoxylin/Eosin, Mallory Trichrome and Alcian blue revealed well-preserved collagen structure in control (a-c), FD (d-f), vitrified (i-k) and cryopreserved (l-m). Scale bar represents 100 µm.*

3.3.1.2 Analysis of basal lamina elements using TPM

To evaluate the impact of the preservation methods, indirect immunofluorescence for the major components of basal lamina of preserved DPP patches was performed on cryosections in combination with MPM. No modifications of the basal membrane distribution could be observed among the groups, as displayed by collagen IV, laminin and heparin sulfate respectively for control, FD, vitrified and cryopreserved (Fig. 5-2), which can be detected on the submesothelial basal lamina of the *serosa* and the basal lamina of small-caliber vessels in the *fibrosa*. MPM allows simultaneous visualization of the SHG of collagen and the autofluorescence of elastin in cryosections of all the groups, confirming the previous histological results.

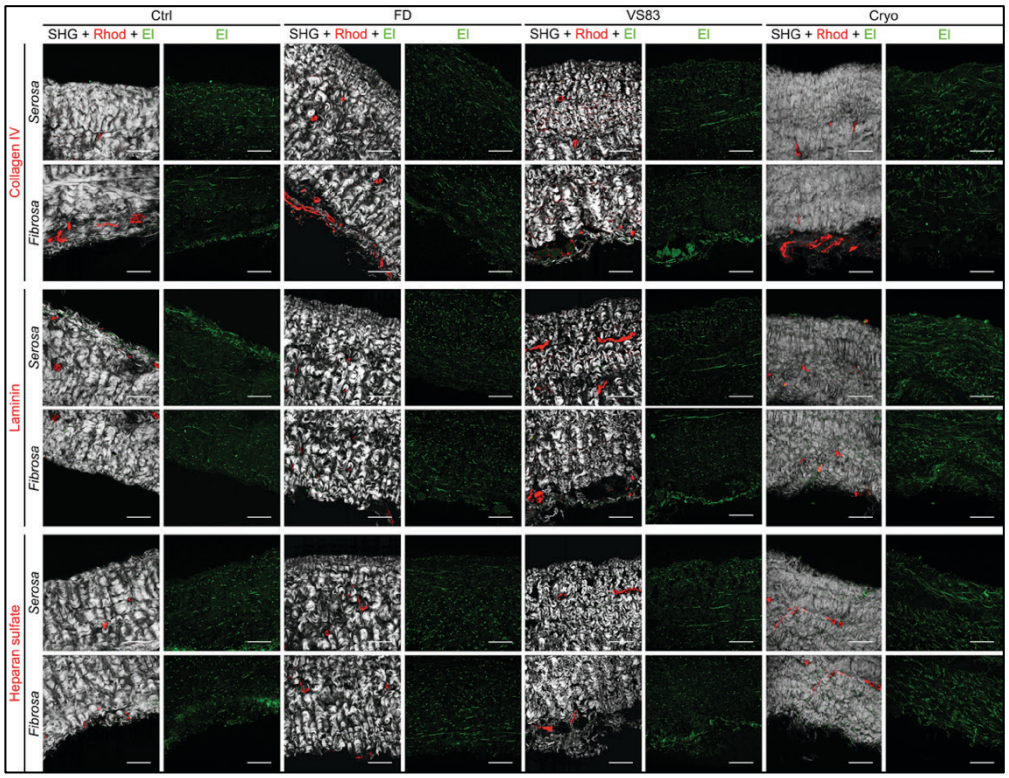

Figure 3-25: *The visualization and investigation of the major components of the basal lamina combining indirect immunofluorescence and MPM. The images revealed similar protein distribution within the preserved groups with respect to the control (DPP). Scale bars indicate 100 µm.*

3.3.1.3 Multiphoton imaging

Multiphoton-excited autofluorescence and SHG microscopy were applied to the preserved patches without the need for prior labeling or fixing of the tissues. The SHG signal and autofluorescence were inducible within all groups. Qualitatively, both collagen (400 nm) and elastic fibers (525 nm) appeared clearly structured in the control (Fig. 5.3a and b), FD (Fig. 5.3d and e), vitrified (Fig. 5.3g and h) and cryopreserved (Fig. 5.3i and k) scaffolds. The composite images showed elastic fibers running parallel to the collagen fibers in all groups (Fig. 5-3c, f, i, l). The analysis with MPM imaging suggests that the ECM components were not impacted by preservation methods. This was confirmed by the quantification of the SHG signal, which did not reveal any statistically significant differences between the groups (Fig. 5-4).

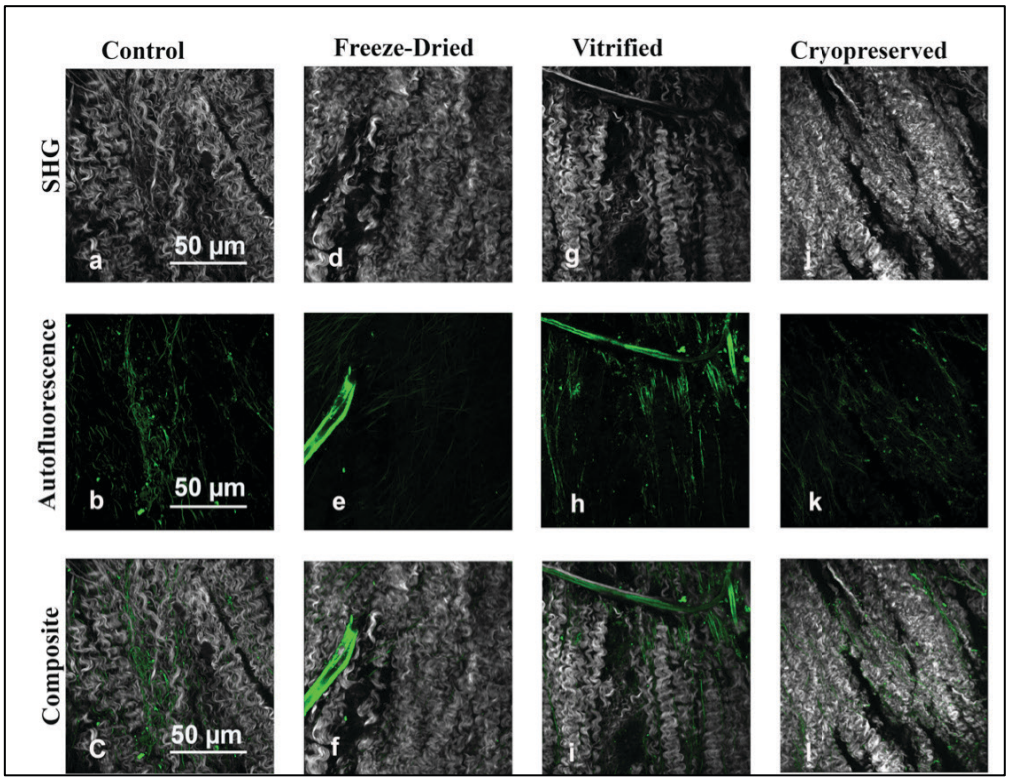

***Figure 3-26**: Second harmonic generation (SHG) microscopy and Multiphoton-induced autofluorescence imaging of the control (a-c), FD (d-f), vitrified (g-i), cryopreserved (j-l) DPP patches. Scale bars represent 50 µm.*

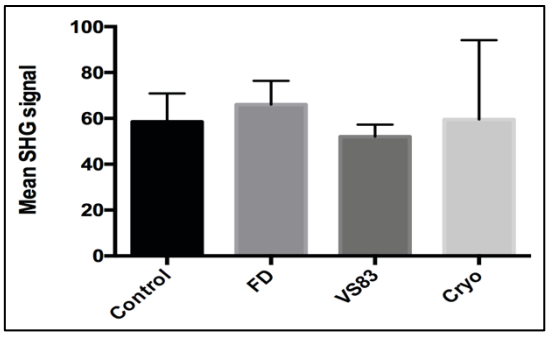

***Figure 3-27:** Quantification of SHG signal intensities of collagenous structures (a) (n=9). Data are presented as mean ± SD. No significant differences were found between the groups after preservation and reconstitution.*

3.3.2 Evaluation of protein stability and secondary structure

3.3.2.1 Analysis of denaturation profiles of ECM proteins using DSC

The denaturation profile of DPP patches after preservation and reconstitution were studied using DSC. GA-treated and thermally denatured samples were also tested and used as controls. The test provided thermal fingerprints of the scaffolds, which were used to detect possible protein damage such as crosslinking or denaturation. Figure 5-5a illustrates DSC thermograms of the treated groups, where protein denaturation is visible as an endothermic peak. The shape of the denaturation profile did not show distinct differences between the preserved and control groups. The T_{onset} of protein denaturation of both the control and the preserved groups occurred at around 65°C, whereas GA-fixation and thermal treatment significantly increased the denaturation temperature, to 83°C and 80°C respectively ($p<0.001$) (Fig. 5-5b). The thermally treated sample showed a lack of denaturation peak. Only a very small negligible peak in the DSC trace was visible, indicating a mostly denatured sample.

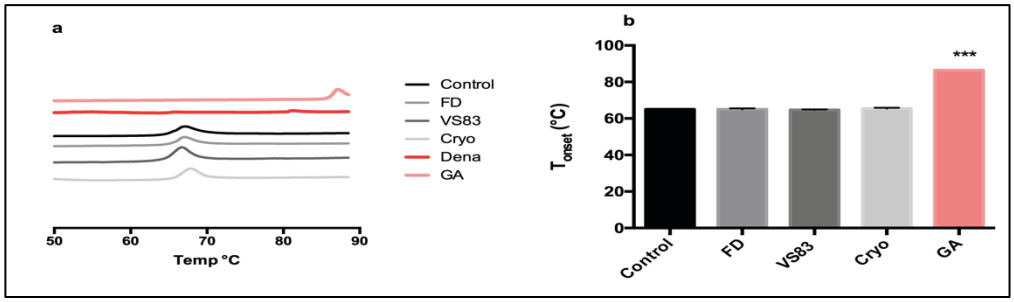

Figure 3-28: *Investigations of denaturation profile using DSC. Panel a shows DSC thermograms of the tissues after preservation and GA-fixation. b: Bars show the onset temperature of protein denaturation (T_{onset}). GA and thermal treated groups demonstrated a significant increase in T_{onset}. No significant differences were found between the groups after storage. Data are presented as mean ± SD. ***P<0.001.*

3.3.2.2 Evaluation of the fingerprint region of the proteins with FTIR

FTIR was used to study the effect of preservation methods on the overall protein secondary structure of DPP patches. Second derivative spectra were calculated from the original spectra of the amide-I region revealing two main distinctive types of protein secondary structure: α-helics and β-sheets. Fig. 5-6 illustrates typical second derivative spectra of the amide-I. The shapes of the bands at 1650 and 1630 cm^{-1}, which are assigned to α-helical and β-sheet structures respectively, were similar in all spectra with the exception of the spectra of denatured scaffolds. The relative content of α-helical structures appears to be altered by thermal treatment. The ratio of the bands at 1650 and 1630 cm^{-1} was calculated as a parameter to compare the treatment groups [237]. This revealed no significant differences between any of the preserved groups and the control. This ratio ranged between 1 and 1.2 (Fig. 5-6b), while the ratio of the denatured sample was twice as high, at around 2 ($P< 0.001$). This indicated that the applied preservation methods did not alter the overall protein secondary structure of the DBP scaffolds

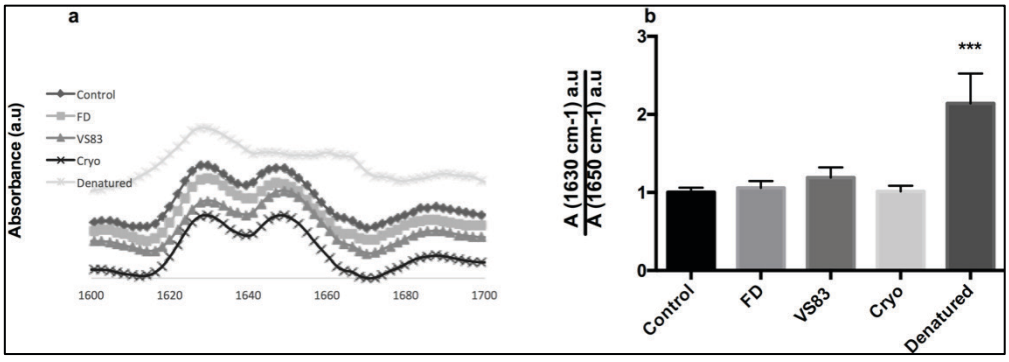

Figure 3-29: *Infrared spectra of DPP scaffolds after preservation and reconstitution. a shows the second derivatives of the recorded spectra between 1600 and 1700 cm^{-1}. Different peaks in the amide-I band (1700–1600 cm^{-1}) represent different types of secondary structure: α-helical structures at 1650 cm-1, and β-sheet structures at 1630 cm^{-1}. b shows the calculated ratio ß/α from the different spectra of the preserved groups. Data are presented as mean ± SD.*

3.3.3 Assessment of the biochemical properties of preserved DPP patches

3.3.3.1 HYP content and sGaGs and Elastin

Biochemical analyses confirmed the maintenance of ECM after preservation as observed with the ultrastructural analysis, FTIR and DSC. Quantification of HYP content did not show any significant difference after preservation compared to the control group. The HYP content of control, FD, vitrified and cryopreserved DPP samples was found to be 111.36±32,02, 125.12 ± 50.02, 106.49±18.86, 100.87 ± 46,09 µg/mg dry weight, respectively (Fig. 5-7a). The sGaGs content of FD, vitrified and cryopreserved patches was estimated to be, 4.53±0.14 and 4.89±0,77 and 5.15 ±0.85 µg/mg dry weight, respectively, without any significant differences between the treatment groups with respect to the control (5.03 ±0.43 µg/mg dry weight) (Fig. 5-7b). The same applies to the elastin content. There was no statistically significant difference between the elastin content values in the control (32.57±3.13 µg/mg dry weight) and the FD, vitrified and cryopreserved patches (40.43±11.17, 42.66±11.7, 44.20±20.25 µg/mg dry weight respectively) (Figure 5-7c). Overall, these results suggested that none of the applied preservation methods impacted the ECM components.

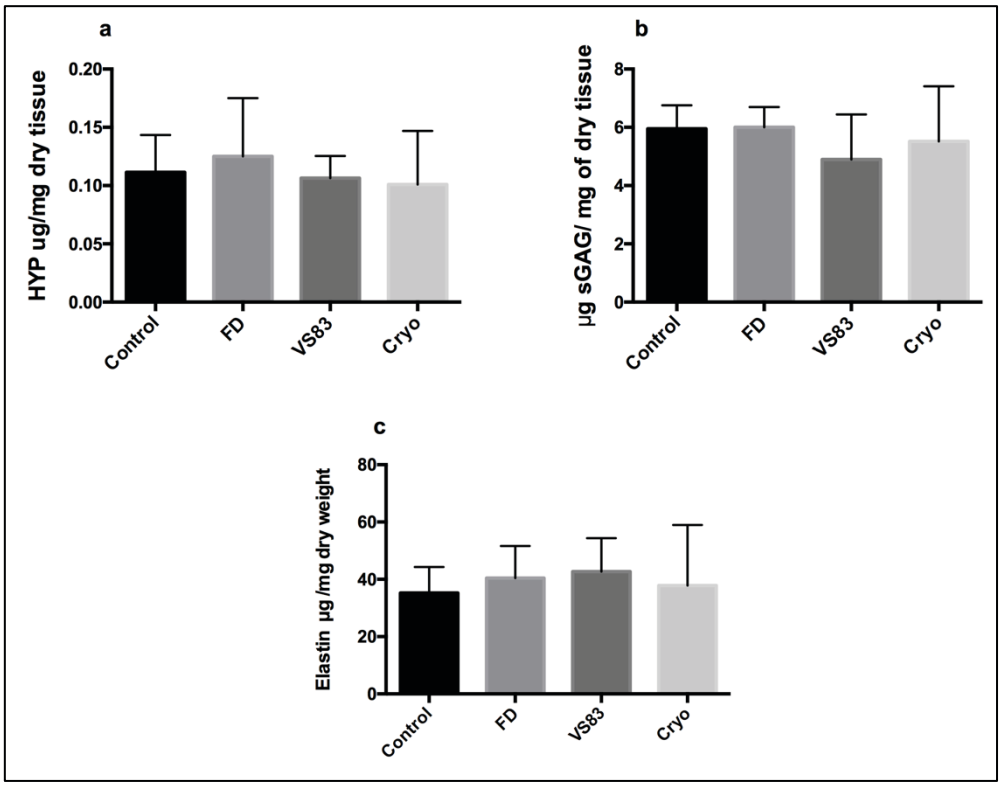

Figure 3-30: *Biochemical results: Quantification of HYP content (a) sGAGs (b) and Elastin (c) after preservation and reconstitution. HYP and sGAGs content per dry weight of tissue (n = 4-5) are presented as mean ± SD. No significant differences were observed in HYP, sGaGs, and elastin contents.*

3.3.4 Evaluation of the biomechanical behavior of DPP after preservation

3.3.4.1 Uniaxial tensile testing

Biomechanical assessment was performed to analyze the mechanical properties of the porcine scaffolds following the different preservation methods, as previously described in paragraph 4.41. Native porcine tissues treated with GA served as control. The calculated parameters are illustrated in figure 5-8. In general, no significant differences were found in any of the biomechanical parameters studied ($p > 0.05$) among the treated groups, except in the case of GA-fixed tissues, where a statistically significant increase in the failure strain was observed compared to that in the decellularized and preserved groups ($p<0.01$) (Fig. 5-8c). However, the elastic-phase

modulus of the cryopreserved and GA-treated groups tended to be higher compared to the control, FD, and vitrified ones, suggesting a decrease in compliance for the cryopreserved and GA-treated groups (Fig. 5-8a). Additionally, the results demonstrated that preservation methods have an effect on thickness; a statistically significant decrease was observed in all groups compared to the control ($p < 0.001$), (Fig. 5-8e). However, a significant difference in thickness between porcine decellularized scaffolds and GA-treated native tissue was also observed.

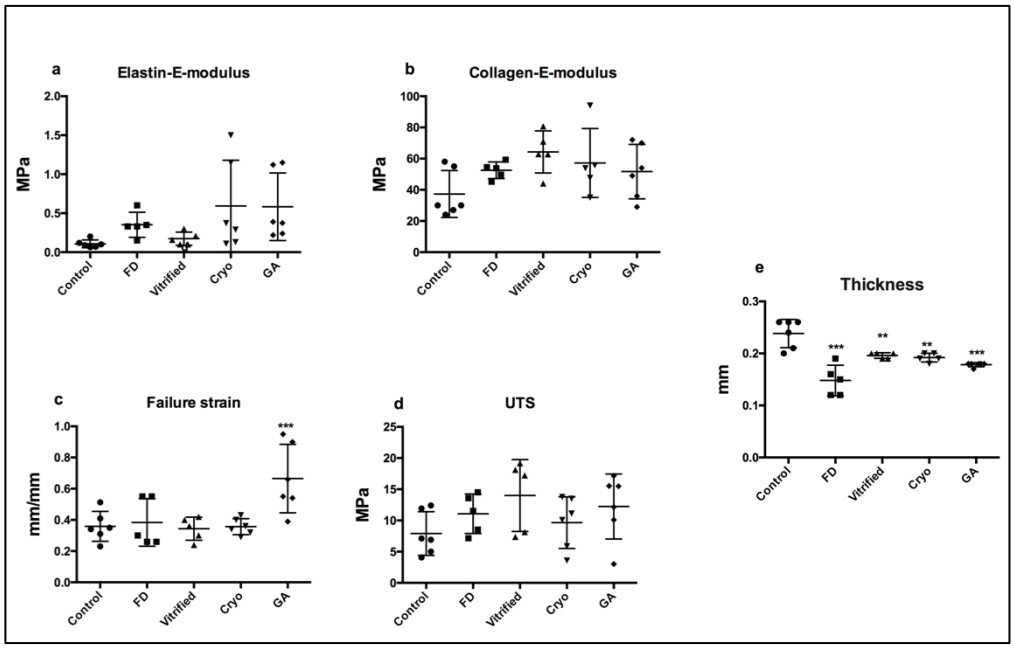

Figure 3-31: *Mean of biomechanical parameters for the preserved pericardial patches compared to non-preserved control and GA-treated tissues. (a) Elastic-phase modulus, (a) Collagen-phase modulus, (c) Failure strain and (d) Ultimate tensile strength. Data are presented as mean ± SD; asterisks indicate a significant difference between the treated groups compared to the control. ***P<0.001.*

3.3.5 Evaluation of cytotoxicity of preserved DPP patches

3.3.5.1 Extract and Direct Contact Cytotoxicity Assays

3.3.5.1.1 Contact Assay

Qualitative macroscopic imaging of contact cytotoxicity demonstrated that both HUVEC and hBM-MSCs attached and grew well into contact with the preserved pericardial scaffolds, with no evidence of contact obstruction (Fig. 5-9e-j). Additionally, cell morphology in close proximity to the preserved punches was similar to that of the negative controls (DPP and Steri-strips). Cell appearance was healthy and confluent, whereas the positive control (cyanoacrylate) was clearly cytotoxic in turn resulting in inhibition of cell adhesion and destruction. This finding was confirmed by the MTS proliferation assay. The test did not reveal any statistically significant decrease in cell viability of either cell line among the treated samples after 24 h and 72 h. An increase in proliferation was observed after 72 hours, confirming that preservation methods were not cytotoxic to the cells (Fig. 5-11a and b). HUVEC were completely dead after incubation with cyanoacrylate and hBM-MSC showed very low cell viability. This was statically significant in all groups ($p<0.001$) (Fig. 5-10 a and b).

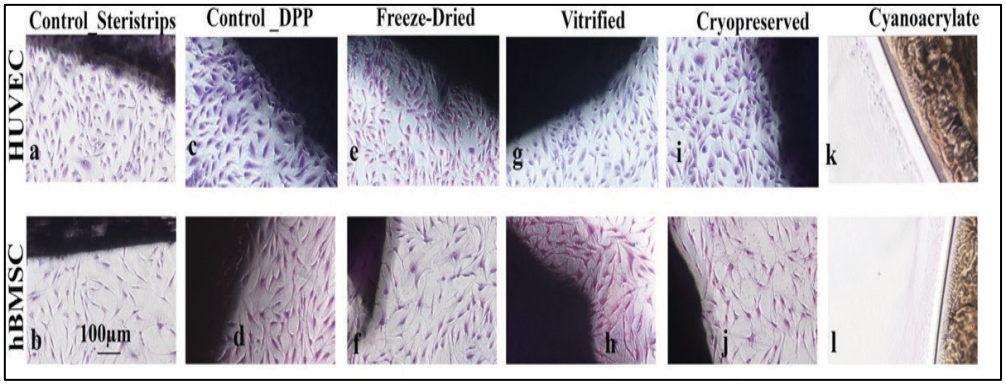

Figure 3-32: *Giemsa stained contact cytotoxicity using two different types of human cells, hBM-MSC (a b, d, f, h, j, l) and HUVEC (a, c, e, g, i, k). Positive control (cyoanoacrylate) and negative controls (steristrips and DPP). Scale bars represent 100 µm.*

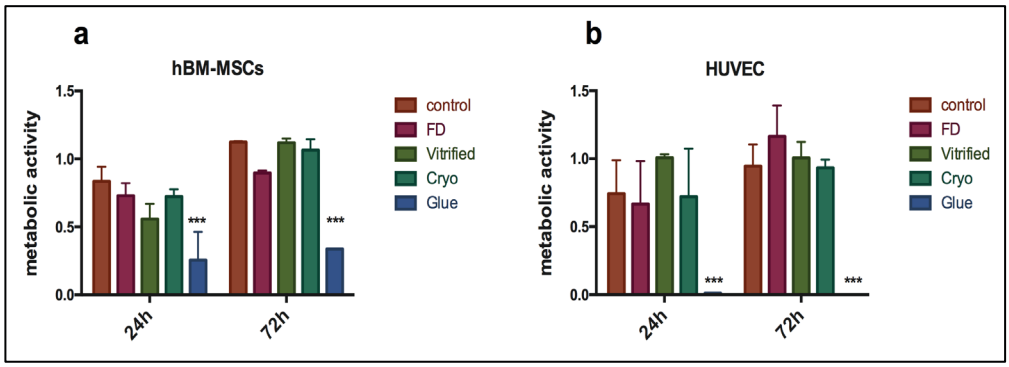

Figure 3-33: *MTS proliferation assay after 24 and 72 h of HUVEC (a) and hBM-MSCs (b). Data are presented as mean ± SD; asterisks indicate a significant difference between the treated groups compared to the positive control **P<0.01, ***P<0.001.*

3.3.5.1.2 Extract Assay

In order to investigate whether the residual CPAs after preservation procedures could be cytotoxic, HUVEC and hBM-MSC have been used to perform extract cytotoxicity assays. For this purpose, both cell lines were cultured in the medium conditioned by differently preserved tissues. The cells cultured with the extract medium of differently preserved groups were studied at the contrast microscopy phase. The analysis did not reveal any impairment of cell expansion compared to the negative controls (cells, and DPP). They showed the typical morphological shapes of both cell lines - cobblestone for HUVECs and spindle-fibroblast-like for hBM-MSCs (Fig 5-11e-l) - whereas the positive control (80% DMSO) results in complete cell death induced by cell lysis and destruction (Fig 5-11m, n). This has been confirmed by MTS and LDH assays. For HUVEC, the proliferation potential did not differ to a statistically significant extent between 24 and 72 h, but on the contrary proliferation increases within the incubation time (Fig. 5-12a2, b2). The same trend was observed for hBM-MSCs. However, significant differences were found between DPP-control, cryopreserved and control cells after 24h ($p<0.01$), though this was no longer seen after 72 h. Moreover, the value of cytotoxicity assessed using LDH tests in both cell lines remained below zero during the incubation period (Fig. 5-12a2, b2). As expected, the positive control (80%DMSO) induced 100% of

cytotoxicity in both cell lines (Fig. 5-12a2, b2). This finding suggests that the preservation methods did not induce cytotoxicity *in vitro*.

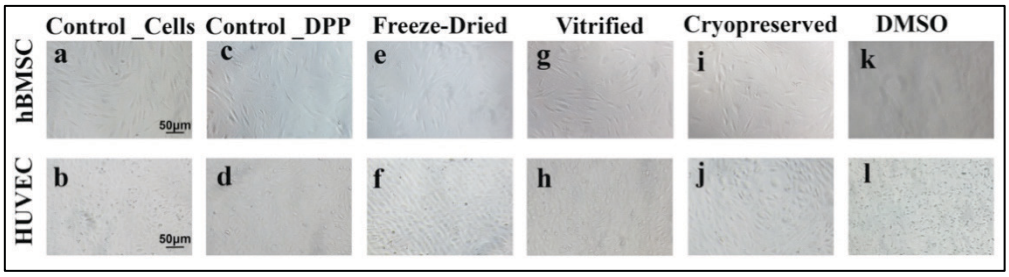

Figure 3-34: *Investigation of Residual of CPAs in preserved scaffolds using HUVEC and hBM-MSC. HUVEC (d, d, f, g, j, l)) and hBM-MSC (a, c, e, g, i. k) cultured in the medium conditioned by differently preserved tissue after 72 hours. Positive control (DMSO) and negative controls (cells, DPP). Scale bars represent 50 µm.*

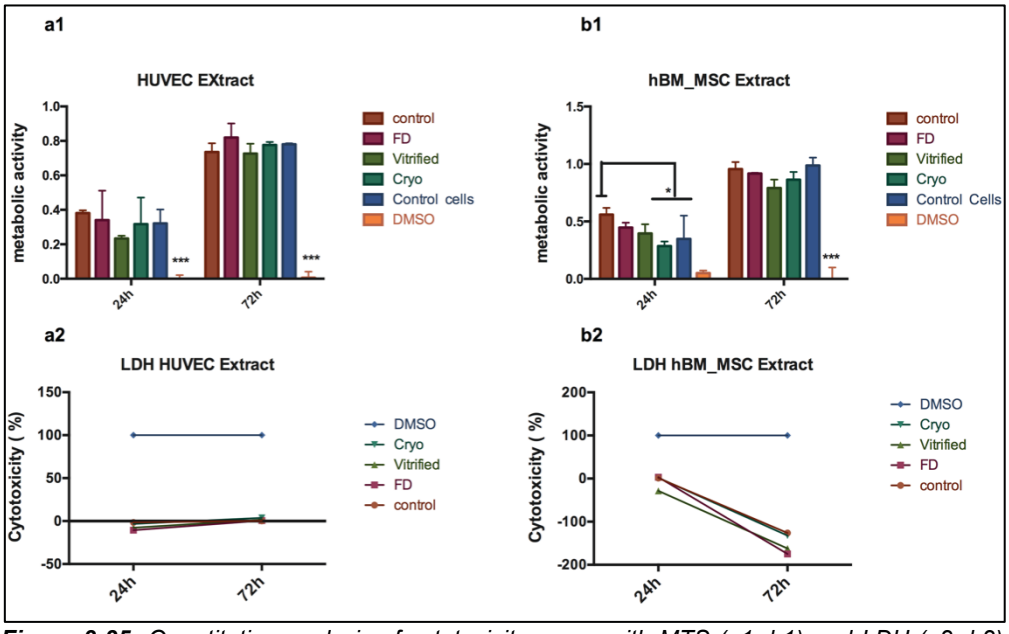

Figure 3-35: *Quantitative analysis of cytotoxicity assay with MTS (a1, b1) and LDH (a2, b2) using HUVEC and hBM-MSC after 24 and 72 h. Data are presented as mean ± SD; asterisks indicate a significant difference between the treated groups compared to the positive control *P<0.05.*

3.3.5.2 Live-dead staining using hBM-MSCs

The viability and attachment of the cell-seeded hBM-MSCs on preserved DPP patches has been investigated using Live-Dead staining under MPM after 72 h. The test allows simultaneous monitoring of viable and dead cells together with detection of the SHG signal of collagen and the autofluorescence of elastin. Viable cells emit

strong green fluorescence while dead cells emit red light. Figure 5-13 showed the results obtained after 72 h of cell culture. hBM-MSCs were able to grow on and adhere to the collagenous scaffolds, showing the typical spindle-shape fibroblast-like phenotype. A count of viable cells revealed that 100% of cells were alive on FD, cryopreserved and control DPP and 93% on vitrified scaffolds (Fig. 5-13a-d).

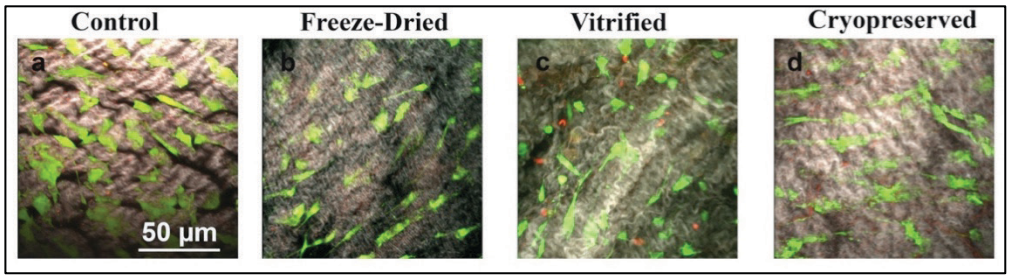

Figure 3-36: *The visualization of live-dead stained hBM-MSCs seeded on differently preserved pericardial scaffolds in combination with MPM. Live cells (green), dead cells (red) and SHG collagen (grey). Scale bars represent 50 µm.*

4 Discussion and future outlook

Decellularization of human biological scaffolds in the cardiovascular field has been introduced to meet the high clinical demand for substitutes for cardiac surgery patients. In spite of the important progress made in this field, widespread use of biological scaffolds such as heart valves remains restricted due to a lack of donor tissues and their limited storage stability in buffer solutions, which represent a major barrier to their routine clinical application [122,129]. Currently, conventional cryopreservation is the gold standard method, which has been used for many years for long-term storage in tissue banks. Following recent advances in decellularized human valves and due to the urgent need for frozen storage/shipment, it is not clear whether this method is able to fulfil the necessary requirement of preserving the original properties of the scaffolds without compromising the positive outcome of decellularization.

Therefore, in this project three different preservation methods were systematically compared for DBP and DPP scaffolds prepared under the premise of the effectiveness of TRICOL technology to achieve acellular scaffolds. The outcomes include histological structure and ultrastructure, matrix components and quality, protein stability, biomechanics, and cytocompatibility.

The pericardium is a tissue which is abundantly available, can be easily acquired, and above all, fulfills the clinical requirements of cardiac surgeons. In order to address the shortage of donor tissues, decellularization of xenogeneic pericardial scaffolds has been introduced to overcome the drawbacks of the bioprosthetic heart valves and patches currently in use, which must undergo glutaraldehyde fixation to avoid immune rejection due to the presence

of xenoantigens [84,148]. Decellularization aims to eliminate all endogenous cell elements and epitopes whilst ideally preserving the native ECM structure, components, biomechanical properties and biocompatibility for cell colonization and repopulation *in vivo*.

Before applying different preservation methods, bovine and porcine pericardia were decellularized with the TRICOL protocol, which is known to be successful for decellularization of pulmonary and aortic heart valves for allograft implantation[17,128] Recently, TRICOL decellularized heart valves have been approved for testing in patients within the framework of clinical trials. Combining an efficient decellularization method, such as TRICOL, with an adequate preservation technology could provide off-the-shelf, functional, durable and self-regenerating scaffolds for use in cardiovascular surgery.

As was shown by the results in the first chapter, TRICOL was found to be equally successful for the decellularization of both porcine and bovine pericardia. Indeed, after TRICOL, cell nuclei and constituents were removed without ultrastructural evidence of damage to the ECM and its components. Histological evaluation and microscopic imaging (SEM and MPM) demonstrated the maintenance of the elastin, sGAGs and collagenous structure and organization in both bovine and porcine tissues.

This finding was confirmed by evaluation of the protein stability using DSC and FTIR and by the biochemical assessments for HYP and sGAGs. Pericardial tissues consist of 90% of collagen, therefore the denaturation profile of the fibrous tissues is largely dominated by this component. The results demonstrated that the overall protein secondary structure and protein denaturation temperature were not affected by decellularization. TRICOL did not induce any changes in the overall protein secondary structure in either tissue. DSC studies were in agreement with FTIR studies depicting only minor differences in porcine pericardium, whilst collagen denaturation temperatures remained unaltered for bovine. The decrease in T_{onset} in DPP could be

associated with the loss of native cells, slightly affecting/shielding its denaturation profile.

Although a tendency toward increased HYP content was observed in both tissues upon decellularization, no significant differences were appreciated. This is likely due to the loss of cells and soluble proteins, which in turn results in a reduction in weight, resulting in a net increase in the collagen content of the decellularized tissues.

This is in agreement with the theory of collagen conservation proposed by Courtman et al. [144]. In contrast to HYP, sGAG content appeared to be reduced after decellularization with a statistically significant difference only for bovine pericardium.

The sGAG reduction was also observed in terms of discoloration of alcian blue staining as an indication of the structural changes introduced in the pericardium by TRICOL, as already reported by our group [239]. The loss of GAGs is, in fact, a common consequence of decellularization of xenogeneic pericardium and heart valves, as observed before by several research groups [135,136,240–242].

sGAG depletion is most probably due to their weak binding to the ECM in comparison to collagen or elastin. Thus, the decellularization process induces them to be washed away more easily than the other ECM components. Other groups also experienced a loss of GAGs during decellularization of bovine pericardium by means of Triton X-10 and alkaline treatments [144,164]. Mendoza. et al. showed that the removal of GAGs varied as a function of the protocol applied for cell extraction, and subsequently suggested the use of non-ionic detergents for decellularization processes. In addition, they argued that their loss is favorable for the diffusion of decellularization reagents into the tissues, as it increases the interstitial space, porosity and surface area. Generally, pericardial tissues possess relatively fewer GAGs but higher amounts of sulfated ones. However, their loss may cause alterations to the biomechanical behavior and structural organization of collagen and impact the tissues remolding cell repopulation, migration and differentiation [239]. They also play many

other important roles within the ECM. GAGs have been identified as interacting with both the protein and cell components of tissues including the assembly of collagen and maintenance of its crimping [243]. In particular, negatively-charged GAG molecules were linked with the prevention of calcification by chelating calcium ions, therefore decellularized scaffolds lacking sufficient GAG content might calcify more rapidly, resulting in scaffold dysfunction *in vivo*. However, replenishment of the GAGs could potentially occur by cell-tissue repopulation with the patient's own cells *in vivo* or through the application of surface coating with different types of GAGs upon decellularization. On the other hand, some works claimed that removing GAGs in xenogeneic scaffolds might be favorable for reducing the risk of immune reaction upon implantation. In the first steps of decellularization, some GAG fragments might be entrapped in the ECM if it is not washed thoroughly enough. Thus, residual GAGs could act as triggers for acute immune rejection [244–246]. Further investigation is necessary to identify and characterize remaining GAG fragments and their drawbacks for scaffold properties both *in vitro* and *vivo*.

In addition to the characterizations described above, biomechanical tests revealed some significant differences between native bovine and porcine tissues and their decellularized counterparts. In particular decellularized scaffolds showed a tendency toward increased extensibility, which was demonstrated through lower collagen and elastic phase slopes and higher failure strain. This was particularly evident and significant in the case of DPP.

This was in line with the histological, MPM imaging, biochemical and protein stability assessment that confirmed the preservation of the original native ECM structure and especially the quality of collagen as the primary load-bearing component. The increase in the scaffolds' compliance upon decellularization was also reported in studies using other detergents such as SDS for cell extraction for human pericardium [166] and heart valves [162,231,247].

Additionally, TRICOL results in a statistically significant gain in thickness in DPP scaffolds but not in bovine ones. Similar findings were reported by Korossis et al[231,248]. for decellularized porcine aortic valves (reduction in GAG content, increase in extensibility and thickness) suggesting that cell removal leads to higher collagen crimping, which in turns results in increased scaffold compliance.

The quantification of the waviness parameter in porcine tissues and bovine tissues confirmed the above-mentioned observation by Korossis et al. [231] . The analysis demonstrated a tendency toward a rise in collagen crimping in porcine scaffolds and a fall in bovine scaffolds following decellularization, which eventually correlated with the significant loss of sGAGs observed in bovine pericardium after decellularization (unpublished internal data). It is known that the GAGs play an important role in the maintenance of collagen crimping [243].

Currently, there is no consensus in the literature about the impact of decellularization on scaffold biomechanics. The studies mentioned above affirm that decellularization increases the scaffolds' compliance, whereas others protocols reported decreasing it [135,249]. In contrast, the literature concurs that GA-fixation causes a decrease in extensibility. GA-treated bovine and porcine were found to be stiffer than their decellularized counterparts [250–252], which was also confirmed by our work.

In conclusion, decellularization protocols produce different degrees of ECM alterations in diverse types of tissue. In the current work, bovine and porcine tissues were successfully decellularized, with TRICOL exerting a more conservative effect on ECM components and biomechanical properties in comparison to previously-described protocols for the decellularization of pericardium.

Additionally, TRICOL technology has been identified as being efficient in the removal of α-gal xenoantigen [253], making decellularized xenografts potentially biocompatible for human implantation. However, alpha-gal is not the only occurring xenoantigen in tissues of animal origin. Non-gal epitopes such as N-

glycolylneuraminic acid are reported to pose an additional problem for xenotransplantation, causing organ damage [254,255]. No clinical information is yet available regarding their impact on the longevity of bioprostheses.

At present, the development of suitable long-term preservation strategies is urgently needed for clinical application of decellularized grafts. The storage of decellularized scaffolds in tissue banks could enable off-the-shelf availability of cardiovascular substitutes, simplifying their distribution in cardiac surgery units.

The main part of this project deals with the suitability of cryopreservation approaches and freeze-drying techniques for the appropriate storage and maintenance of ECM structure, biomechanics and ECM components of decellularized scaffolds, which are currently the subject of much debate. Moreover, the residuals of CPAs such as DMSO, formamide, and propylene glycol, may induce cytotoxic effects for engrafting cells. Therefore, it is pivotal to evaluate the impact of preservation technologies on the *in vitro* properties of decellularized scaffolds in detail.

With regards to allografts, human pericardium and heart valves have been routinely stored by tissue banks using slow-freezing-rate cryopreservation, which is nowadays considered to be the gold standard [174]. Vitrification studies have been performed on native porcine heart valves [207], TE constructs [198,256], cartilage [200] and blood vessels [257] indicating superior preservation of ECM and excellent tissue performance *in vivo* in respect to standard cryopreservation. Additionally *in vivo* and *in vitro* studies with porcine aortic conduits indicated that ice-free cryopreservation results in superior ECM preservation, reduced inflammatory processes, and superior hemodynamics [204,205] when compared to conventional cryopreservation [258].

Because of its great advantages for storage and shipment, freeze-drying (in combination with harsh sterilization treatments) was tested as a preservation method for homograft heart valves in the early

1960s and 1970s [75,77,213]. Due to drawbacks such as tissue deterioration and valve failure, this preservation method was abandoned. In fact, drastic structural and mechanical alterations were observed when it was applied to the preservation of native bovine pericardium [214–216] or decellularized arteries [217]. However, freeze-drying in these studies seems to have been carried out without using any type of lyoprotective agent.

The freeze-drying protocol applied in the present study was a modified version of the protocol described by Wang et al., which was developed for decellularized porcine pulmonary valve scaffolds [218,259]. We utilized a modified version of this previously reported protocol. A high concentration of lyoprotectant (80% (w/v) sucrose) was necessary in order to diminish pore formation in freeze-dried scaffolds and confirmed the lack of pores in the FD, DBP and DPP scaffolds and the preservation of the overall scaffold architecture.

In general, vitrification and freeze-drying have only rarely been used for decellularized scaffolds, whereas the application of cryopreservation for decellularized valvular and pericardial scaffolds *in vitro* [122,260] and *in vivo* [19,146] shows uncertain results.

In this work, qualitative ECM evaluation by histology and SEM revealed unaffected scaffold structure following preservation and reconstitution for both tissue types. Histological analyses showed preservation of collagen type-I network for both preserved bovine and porcine groups and maintenance of GAGs for porcine. Moreover, investigation of the basal lamina did not show any modifications to the original distribution of the proteins (Collagen IV, laminin and heperan sulfate) within the preserved DPP with respect to the control.

Additionally, quantitative scaffold analysis (biochemistry, DSC and FTIR) confirmed the maintenance of ECM integrity and its major components (collagen, sGAGs, elastin) after applying different preservation procedures for bovine and porcine scaffolds with no apparent signs of collagen denaturation, decrease in sGAGs content or alterations in protein secondary structures. This is of great

significance, since the preservation of these ECM components might guarantee the regeneration of the scaffold after implantation. These results confirm previously published studies on heart valves and pericardium [146,204,218,234,239]. These findings are also supported by the results obtained with MPM imaging. The analysis did not reveal disruption or fragmentation of collagen and elastic fibers networks in either the cryopreserved, vitrified or FD patches of bovine or porcine scaffolds. Additionally, the SHG signal intensity did not indicate any changes in the quality of collagen in either species. Previous studies based on the same imaging technology reported adequate maintenance of the whole ECM structure of SynerGraft heart valves (human aortic and pulmonary) following cryopreservation. Quantitative analysis of the collagen and elastin signal intensity did not reveal a significant decrease following cryopreservation [261]. Conversely, Schenke-Layland et al. [189,206] reported serious alterations and significant deterioration in the collagen and elastic fibers in conventionally cryopreserved porcine conduits. These conflicting results for cryopreserved scaffolds have been attributed to residual DMSO, which was used as a CPA. DMSO is a common CPA; in particular, it has been identified as an optical clearing agent, thus disturbing the inter-fiber interaction of collagen, and consequently reducing the SHG signal [188,262]. Indeed, Zimmerly et al. observed a 40% reduction in the SHG of dermal collagen in cryopreserved skin [263].

Preserved DPP and DBP patches will be implanted in a high-pressure area inside the heart. Preservation methods may affect their ability to withstand a high load. Therefore, evaluating their biomechanical properties in order to show whether they meet this requirement is of major importance. The uniaxial tensile testing that was performed for DBP demonstrated significant differences between the decellularized non-preserved control and cryopreserved samples. In particular, the cryopreserved group demonstrated significantly increased collagen and elastic-phase moduli indicating reduced extensibility. The FD scaffolds showed a slightly higher collagen-phase

modulus compared to the control. However, the collagen-phase modulus of the FD group was found to be significantly different from the cryopreserved one. Overall, the biomechanical characteristics of vitrified scaffolds resembled those of the control. In the case of preserved DPP patches, none of the parameters describing the biomechanical properties showed any significant differences compared to the non-preserved control. However, a tendency toward a higher slope in the elastic-phase modulus of the cryopreserved scaffolds was observed, indicating a decrease in extensibility. The most likely explanation for the change in the mechanical properties of the cryopreserved DBP scaffolds is that interstitial ice formation caused by cryopreservation alters the ECM histoarchitecture, as previously described for cryopreserved allografts [197]. The damage caused by ice formation might have affected the crimping and/or have increased collagen fiber mobility, which has been associated with increased stiffness (decrease in compliance) in tissues [249]. There is no agreement in the literature regarding the effect of cryopreservation on decellularized scaffold biomechanics. Some groups have demonstrated significant adverse effects on the mechanical properties and a decrease in the compliance of decellularized and cryopreserved aortic and pulmonary heart valves [260,264], whereas others reported no adverse changes in the biomechanical behavior of decellularized and cryopreserved human pericardium [146]. It seems that the degree of impact of cryopreservation on scaffold biomechanics may depend on the tissue's species. Bovine and porcine scaffolds vary in their mechanical behavior and thickness. Bovine pericardial tissues have approximately double the thickness of porcine ones. These features probably enable bovine pericardium to possess significantly higher mechanical strength when compared to porcine ones [265]. These results suggest that the tissue's origin, as well as its structure, may affect the mechanical behavior of the treated pericardial scaffolds.

The biomechanical investigation of the preservation of fresh bovine pericardium applying vitrification (VS55) and cryopreservation revealed similar results regarding the impact of cryopreservation on

the collagen-phase modulus, indicating a decrease in compliance (Fig. 6-1b). This outcome confirms and supports the idea formulated above. The impact of cryopreservation on scaffold biomechanics was more evident in bovine than porcine pericardia.

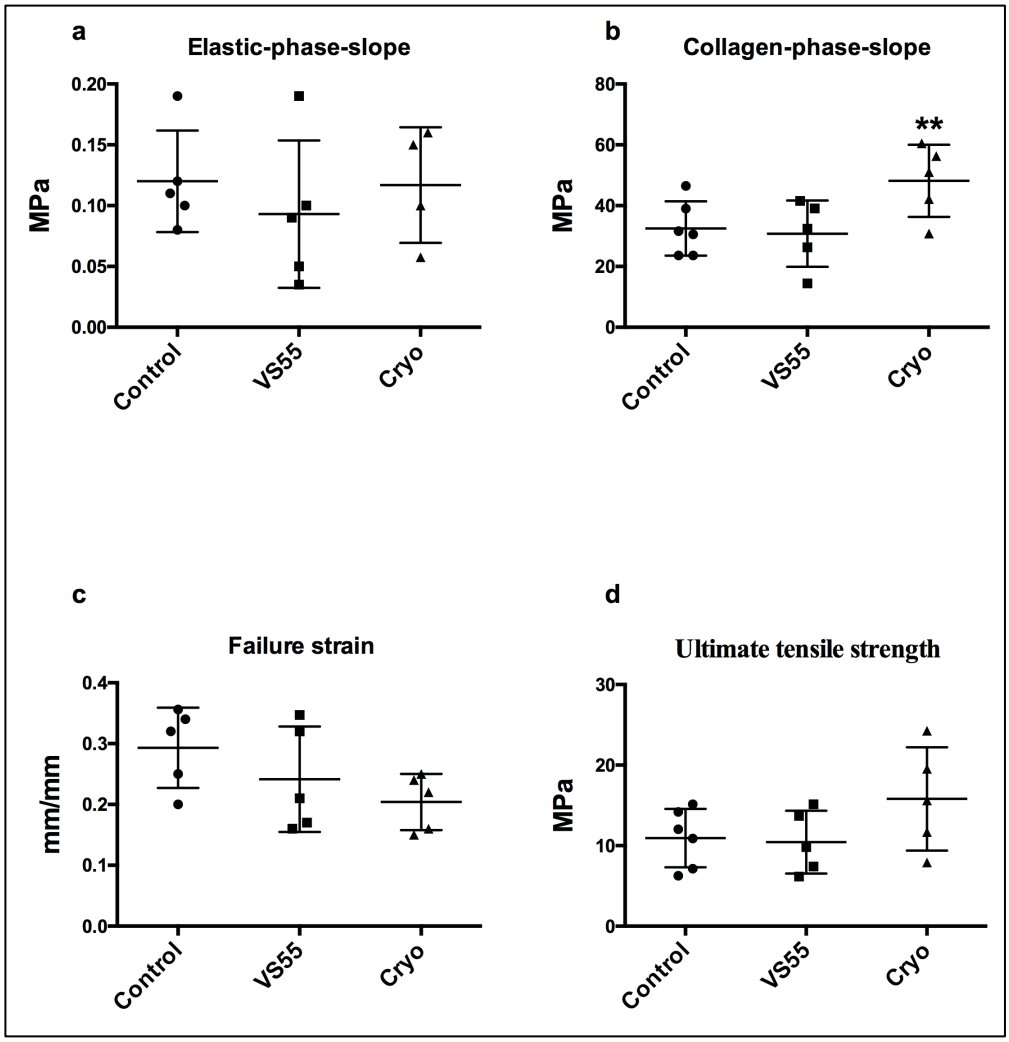

Figure 4-1: *Mean of biomechanical parameters for the fresh preserved bovine pericardial patches compared to the native. (a) Elastic-phase modulus, (a) Collagen-phase modulus, (c) Failure strain and (d) Ultimate tensile strength. Data are presented as mean ± SD; asterisks indicate a significant difference between the treated groups compared to the control. **P<0.01.*

Cytocompatibility assays were performed to verify whether the possibility of toxic CPAs remaining in preserved DBP and DPP scaffolds could compromise cell repopulation and scaffold regeneration *in vivo*. Contact cytotoxicity assay demonstrated that hBM-MSC and HUVEC were able to attach, line the surface and

proliferate equally well onto the control, FD, vitrified and cryopreserved scaffold patches for both species. These results were confirmed by the MTS assay showing cell proliferation after 72 h.

These outcomes indicated that the differently preserved scaffolds possess excellent cytocompatibility *in vitro,* suggesting the proper removal of cytotoxic CPAs during the reconstitution of the preserved scaffolds and likely retention of their original potential for cell repopulation by host cells *in vivo* for both types of tissues scaffolds. Indeed, decellularized heart valves cryopreserved or FD with similar modalities demonstrated cell colonization and migration when implanted into large animal models [19,221].

Altogether, this work showed the application of different preservation methods on porcine and bovine scaffolds revealing retained ECM integrity; maintenance of the major elements of the matrix such as collagen, elastin and sGAGs; and excellent cytocompatibility *in vitro.*

Some limitations of this research could prevent these conclusions from being completely definitive and further attention will be paid to these in future studies. It is worth pointing out that conventional cryopreservation leads to detrimental changes in the biomechanical behavior of DBP. No evidence was found that this alteration in biomechanical properties might also interest DPP. These observations might be particularly important for the clinical use of these biomaterials. Indications in cardiovascular surgery might depend on the specific structural and biomechanical properties of these scaffolds. For example, this should be taken into consideration in the selection and fabrication of pericardial vascular and valvular patches. In order to fully evaluate the effect of different preservation approaches on DBP and DPP scaffolds biomechanics, a biaxial loading test, mimicking an *in vivo* situation, would be appropriate to conclude whether the detected alterations induced by cryopreservation are able to influence or compromise their *in vivo* functional performance.

Although cytocompatibility tests are very informative, they might have a limited ability to determine whether potentially toxic CPA residues have an impact on the remodeling of the scaffolds by host cells *in vivo*. CPA residue analysis can be performed using HPLC/MS for further evaluation of cytotoxicity on treated tissues for greater accuracy in the detection level [122].

Certainly, *in vivo* studies in large animal models are required not only to study the biocompatibility of the preserved scaffolds but also to predict their functionality and durability and to verify whether the observed decrease in scaffold extensibility following cryopreservation of DBP might negatively impact scaffold performance, colonization, remodeling and regeneration. ISO regulations do not specify the optimal animal species of the testing model. The Vietnamese pig might represent an ideal model for testing heart valve substitutes because of its strong similarity with human beings regarding blood coagulation and the growth rate of pediatric patients, as previously demonstrated by our group for the investigation of the outcome of cryopreservation on decellularized porcine heart valves [19]. On the other hand, an ovine model is preferred for studying the pattern of the calcification process in accelerated manner.

A clear asset of the preservation technologies evaluated in this work is their possible clinical translation for the long-term preservation of acellular human scaffolds. Currently, due to the clinical setting and in order to avoid any eventual compromising effect of storage, decellularized grafts are often implanted directly after completing the decellularization procedure. In the future, xenogeneic pericardial scaffolds are expected to be clinically applied after overcoming the immunological barrier. It is shown here that freeze-drying and vitrification can be used as alternative methods to conventional cryopreservation, showing excellent preservation of the ECM structure and components of both tissue scaffolds, whilst vitrification exerts a more preservative effect on the biomechanical characteristics of DBP. Additionally, both methodologies offer a great advantage over

standard cryopreservation in terms of simplification of storage and transport, eliminating the need for liquid nitrogen. Vitrification permits storage at -80°C above the glass transition temperature, whereas freeze-drying allows room temperature storage reducing infrastructural costs for storage and shipment. Cryopreservation and vitrification are considered relatively complicated procedures and require the use of potentially toxic CPAs. Freeze-drying can be done using sugars as lyoprotectants, which do not necessarily need to be completely removed before implantation. Because of these advantages, freeze-drying is the preferred method for storing acellular scaffolds for direct use in clinical settings.

5 References

[1] J.A. Spertus, K.A. Eagle, H.M. Krumholz, K.R. Mitchell, S.L.T. Normand, American College of Cardiology and American Heart Association methodology for the selection and creation of performance measures for quantifying the quality of cardiovascular care, Circulation. 111 (2005) 1703–1712. doi:10.1161/01.CIR.0000157096.95223.D7.

[2] Yacoub, J.J.M. Takkenberg, Will heart valve tissue engineering change the world?, Nat. Clin. Pract. Cardiovasc. Med. 2 (2005) 60–61. doi:10.1038/ncpcardio0112.

[3] A.G. Mikos, S.W. Herring, P. Ochareon, J. Elisseeff, H.H. Lu, R. Kandel, F.J. Schoen, M. Toner, D. Mooney, A. Atala, M.E. Van Dyke, D. Kaplan, G. Vunjak-Novakovic, Engineering Complex Tissues, Tissue Eng. 12 (2006) 3307–3339. doi:10.1089/ten.2006.12.3307.

[4] A. Kheradvar, E.M. Groves, C.J. Goergen, S.H. Alavi, R. Tranquillo, C.A. Simmons, L.P. Dasi, K.J. Grande-Allen, M.R.K. Mofrad, A. Falahatpisheh, B. Griffith, F. Baaijens, S.H. Little, S. Canic, Emerging Trends in Heart Valve Engineering: Part II. Novel and Standard Technologies for Aortic Valve Replacement, Ann. Biomed. Eng. 43 (2015) 844–857. doi:10.1007/s10439-014-1191-5.

[5] E.L. Chaikof, The Development of Prosthetic Heart Valves — Lessons in Form and Function, N. Engl. J. Med. 357 (2007) 1368–1371. doi:10.1056/NEJMp078175.

[6] A. Carpentier, G. Lemaigre, L. Robert, S. Carpentier, C. Dubost, Biological factors affecting long-term results of valvular heterografts, J. Thorac. Cardiovasc. Surg. 58 (1969) 467–483. http://www.ncbi.nlm.nih.gov/pubmed/5344189 (accessed June 26, 2018).

[7] A. Carpentier, A. Deloche, J. Relland, J.N. Fabiani, J. Forman, J.P. Camilleri, R. Soyer, C. Dubost, Six-year follow-up of glutaraldehyde-preserved heterografts. With particular reference to the treatment of congenital valve malformations, J Thorac Cardiovasc Surg. 68 (1974) 771–782. http://www.ncbi.nlm.nih.gov/pubmed/4214526 (accessed June 26, 2018).

[8] N.C. Poirier, L.C. Pelletier, M. Pellerin, M. Carrier, 15-Year experience with the Carpentier-Edwards pericardial bioprosthesis, in: Ann. Thorac. Surg., 1998. doi:10.1016/S0003-4975(98)01110-2.

[9] M.I. Ionescu, A.P. Tandon, D.A.S. Mary, A. Abid, Heart valve replacement with the Ionescu-Shiley pericardial xenograft, J. Thorac. Cardiovasc. Surg. 73 (1977) 31–42. http://www.ncbi.nlm.nih.gov/pubmed/831009 (accessed June 26, 2018).

[10] X. Li, Y. Guo, K.R. Ziegler, L.S. Model, S.D.D. Eghbalieh, R.A. Brenes, S.T. Kim, C. Shu, A. Dardik, Current usage and future directions for the bovine pericardial patch, Ann. Vasc. Surg. 25 (2011) 561–568. doi:10.1016/j.avsg.2010.11.007.Current.

[11] D. Ross, HOMOGRAFT REPLACEMENT OF THE AORTIC VALVE, Lancet. 280 (1962) 487. doi:10.1016/S0140-6736(62)90345-8.

[12] B.G. Barratt-Boyes, Homograft valve replacement for aortic valve disease, Mod. Concepts Cardiovasc. Dis. 36 (1965) 1–6. http://www.ncbi.nlm.nih.gov/pubmed/6036611 (accessed June 26, 2018).

[13] F.J. Schoen, Evolving concepts of cardiac valve dynamics: The continuum of development, functional structure, pathobiology, and tissue engineering, Circulation. 118 (2008) 1864–1880. doi:10.1161/CIRCULATIONAHA.108.805911.

[14] K. Bando, G.K. Danielson, H. V. Schaff, D.D. Mair, P.R. Julsrud, F.J. Puga, Outcome of pulmonary and aortic homografts for right ventricular outflow tract reconstruction, J. Thorac. Cardiovasc. Surg. 109 (1995) 509–518. doi:10.1016/S0022-5223(95)70282-2.

[15] D.R. Clarke, D.N. Campbell, A.R. Hayward, D.A. Bishop, Degeneration of aortic valve allografts in young recipients., J. Thorac. Cardiovasc. Surg. 105 (1993) 934-941; discussion 941-942. http://www.ncbi.nlm.nih.gov/pubmed/8487572 (accessed June 26, 2018).

[16] S. Sarikouch, A. Horke, I. Tudorache, P. Beerbaum, M. Westhoff-Bleck, D. Boethig, O. Repin, L. Maniuc, A. Ciubotaru, A. Haverich, S. Cebotari, Decellularized fresh homografts for pulmonary valve replacement: A decade of clinical experience, Eur. J. Cardio-Thoracic Surg. 50 (2016) 281–290. doi:10.1093/ejcts/ezw050.

[17] L. Iop, A. Bonetti, F. Naso, S. Rizzo, S. Cagnin, R. Bianco, C. Dal Lin, P. Martini, H. Poser, P. Franci, G. Lanfranchi, R. Busetto, M. Spina, C. Basso, M. Marchini, A. Gandaglia, F. Ortolani, G. Gerosa, Decellularized allogeneic heart valves demonstrate self-regeneration potential after a long-term preclinical evaluation, PLoS One. 9 (2014). doi:10.1371/journal.pone.0099593.

[18] K. Brockbank, F.G. Lightfoot, Y.C. Song, M.J. Taylor, Interstitial ice formation in cryopreserved homografts: A possible cause of tissue deterioration and calcification in vivo, J. Heart Valve Dis. 9 (2000) 200–206.

[19] M. Gallo, A. Bonetti, H. Poser, F. Naso, T. Bottio, R. Bianco, A. Paolin, P. Franci, R. Busetto, A.C. Frigo, E. Buratto, M. Spina, M. Marchini, F. Ortolani, L. Iop, G. Gerosa, Decellularized aortic conduits: could their cryopreservation affect post-implantation outcomes? A morpho-functional study on porcine homografts, Heart Vessels. 31 (2016) 1862–1873. doi:10.1007/s00380-016-0839-5.

[20] J.F.M. Bechtel, J. Gellissen, A.W. Erasmi, M. Petersen, A. Hiob, U. Stierle, H.H. Sievers, Mid-term findings on echocardiography and computed tomography after RVOT-reconstruction: Comparison of decellularized (SynerGraft) and conventional allograft, in: Eur. J. Cardio-Thoracic Surg., 2005: pp. 410–415. doi:10.1016/j.ejcts.2004.12.017.

[21] K.D. Keele, Leonardo Da Vinci's Elements of the Science of Man, 1983. doi:10.1016/B978-0-12-403980-3.50010-3.

[22] The history of the heart, (n.d.). https://web.stanford.edu/class/history13/earlysciencelab/body/heartpages/heart.html (accessed June 27, 2018).

[23] S. Unguru, *Leonardo da Vinci's Elements of the Science of Man* . Kenneth D. Keele, Isis. 76 (1985) 635–636. doi:10.1086/354020.

[24] M.M. Shoja, P.S. Agutter, M. Loukas, B. Benninger, G. Shokouhi, H. Namdar, K. Ghabili, M. Khalili, R.S. Tubbs, Leonardo da Vinci's studies of the heart, Int. J. Cardiol. 167 (2013) 1126–1133. doi:10.1016/j.ijcard.2012.09.078.

[25] D.A. Lerman, S. Prasad, N. Alotti, Calcific aortic valve disease: Molecular mechanisms and therapeutic approaches, Eur. Cardiol. Rev. 10 (2015) 108–112. doi:10.15420/ecr.2015.10.2.108.

[26] K. Saladin, Anatomy & Phisiology: The Unity of Form and Function, McGraw-Hill, 2014.

[27] Mitral Valve Regurgitation: Treating a Leaky Valve, (2014). http://www.secondscount.org/treatments/treatments-detail-2/mitral-valve-regurgitation-treating-leaky-2#.W0nP3X4yUWo (accessed July 14, 2018).

[28] F.M. Filipoiu, Atlas of Heart Anatomy and Development, 2014. doi:10.1007/978-1-4471-5382-5.

[29] F.H. Netter, Atlas of Human Anatomy, 2014.

[30] P.A. Iaizzo, Handbook of cardiac anatomy, physiology, and devices, 2005. doi:10.1007/978-1-59259-835-9.

[31] E.R. Rodriguez, C.D. Tan, Structure and Anatomy of the Human Pericardium, Prog. Cardiovasc. Dis. 59 (2017) 327–340. doi:10.1016/j.pcad.2016.12.010.

[32] J.P. Holt, The normal pericardium., Am. J. Cardiol. 26 (1970) 455–65. doi:10.1016/0002-9149(70)90702-2.

[33] R. Shabetai, L. Mangiardi, V. Bhargava, J. Ross, C.B. Higgins, The pericardium and cardiac function, Prog. Cardiovasc. Dis. 22 (1979) 107–134. doi:10.1016/0033-0620(79)90017-3.

[34] T. Ishihara, V.J. Ferrans, M. Jones, S.W. Boyce, O. Kawanami, W.C. Roberts, Histologic and ultrastructural features of normal human parietal pericardium, Am. J. Cardiol. 46 (1980) 744–753. doi:10.1016/0002-9149(80)90424-5.

[35] M. Jaworska-Wilczynska, P. Trzaskoma, A.A. Szczepankiewicz, T. Hryniewiecki, Pericardium: Structure and function in health and disease, Folia Histochem. Cytobiol. 54 (2016) 121–125. doi:10.5603/FHC.a2016.0014.

[36] NIH, How the Heart Works | National Heart, Lung, and Blood Institute, (n.d.). https://www.nhlbi.nih.gov/health-topics/how-heart-works (accessed June 27, 2018).

[37] P.A. Iaizzo, R.W. Bianco, A.J. Hill, J.D. St. Louis, Heart valves: From design to clinical implantation, 2013. doi:10.1007/978-1-4614-6144-9.

[38] M. Misfeld, H.H. Sievers, Heart valve macro- and microstructure, Philos. Trans. R. Soc. B Biol. Sci. 362 (2007) 1421–1436. doi:10.1098/rstb.2007.2125.

[39] R. B.Hilton, K. E.Yutzey, Heart valve structure and function in development and disease, Annu. Rev. Physiol. (2011) 29–46.

doi:10.1146/annurev-physiol-012110-142145.Heart.

[40] S. Yen Ho, Anatomy of the Mitral Valve, Heart. 88 (2002) 5–10. doi:Doi 10.1002/Ca.20692.

[41] C. Millington-Sanders, A. Meir, L. Lawrence, C. Stolinski, Structure of chordae tendineae in the left ventricle of the human heart., J. Anat. 192 (Pt 4 (1998) 573–81. http://www.ncbi.nlm.nih.gov/pubmed/9723984 (accessed July 3, 2018).

[42] M.E. Bowdish, S.R. Kumar, V.A. Starnes, The Ross procedure: an excellent option in the right hands, Ann. Transl. Med. 4 (2016) 471–471. doi:10.21037/atm.2016.11.32.

[43] N. Latif, P. Sarathchandra, P.M. Taylor, J. Antoniw, M.H. Yacoub, Localization and pattern of expression of extracellular matrix components in human heart valves., J. Heart Valve Dis. 14 (2005) 218–27. http://www.ncbi.nlm.nih.gov/pubmed/15792183 (accessed July 4, 2018).

[44] C.H. Ku, P.H. Johnson, P. Batten, P. Sarathchandra, R.C. Chambers, P.M. Taylor, M.H. Yacoub, A.H. Chester, Collagen synthesis by mesenchymal stem cells and aortic valve interstitial cells in response to mechanical stretch, Cardiovasc. Res. 71 (2006) 548–556. doi:10.1016/j.cardiores.2006.03.022.

[45] K.S. Kunzelman, R.P. Cochran, S.S. Murphree, W.S. Ring, E.D. Verrier, R.C. Eberhart, Differential collagen distribution in the mitral valve and its influence on biomechanical behaviour., J. Heart Valve Dis. 2 (1993) 236–44. http://www.ncbi.nlm.nih.gov/pubmed/8261162 (accessed July 4, 2018).

[46] M.S. Sacks, A.P. Yoganathan, Heart valve function: a biomechanical perspective., Philos. Trans. R. Soc. Lond. B. Biol. Sci. 362 (2007) 1369–91. doi:10.1098/rstb.2007.2122.

[47] M. Scott, I. Vesely, Aortic valve cusp microstructure: the role of elastin., Ann. Thorac. Surg. 60 (1995) S391-4. http://www.ncbi.nlm.nih.gov/pubmed/7646194 (accessed July 4, 2018).

[48] T.C. Flanagan, A. Pandit, Living artificial heart valve alternatives: a review., Eur. Cell. Mater. 6 (2003) 28–45; discussion 45. http://www.ncbi.nlm.nih.gov/pubmed/14639553 (accessed July 4, 2018).

[49] A.M. Christov, L. Liu, S. Lowe, C. Icton, J. Dunmore-Buyze, D.R.

Boughner, E. Dai, A. Lucas, Laser-induced fluorescence (LIF) recognition of the structural composition of porcine heart valves., Photochem. Photobiol. 69 (1999) 382–9. http://www.ncbi.nlm.nih.gov/pubmed/10089832 (accessed July 4, 2018).

[50] E.M. Culav, C.H. Clark, M.J. Merrilees, Connective tissues: matrix composition and its relevance to physical therapy., Phys. Ther. 79 (1999) 308–319. doi:papers3://publication/uuid/B84613AE-EB80-4E94-874E-6C572C2896BD.

[51] T. Cary, J. Pearce, Aortic stenosis: Pathophysiology, diagnosis, and medical management of nonsurgical patients, Crit. Care Nurse. 33 (2013) 58–72. doi:10.4037/ccn2013820.

[52] B.A. Carabello, W.J. Paulus, Aortic stenosis, Lancet. 373 (2009) 956–966. doi:10.1016/S0140-6736(09)60211-7.

[53] K. Akat, M. Borggrefe, J.J. Kaden, Aortic valve calcification: basic science to clinical practice, Heart. 95 (2009) 616–623. doi:10.1136/hrt.2007.134783.

[54] L. Cripe, G. Andelfinger, L.J. Martin, K. Shooner, D.W. Benson, Bicuspid aortic valve is heritable, J. Am. Coll. Cardiol. 44 (2004) 138–143. doi:10.1016/j.jacc.2004.03.050.

[55] C.M. Otto, B. Prendergast, Aortic-Valve Stenosis — From Patients at Risk to Severe Valve Obstruction, N. Engl. J. Med. 371 (2014) 744–756. doi:10.1056/NEJMra1313875.

[56] N.M. Rajamannan, Myxomatous mitral valve disease bench to bedside: LDL-density-pressure regulates Lrp5, Expert Rev. Cardiovasc. Ther. 12 (2014) 383–392. doi:10.1586/14779072.2014.893191.

[57] Mitral valve prolapse - Symptoms and causes - Mayo Clinic, (n.d.). https://www.mayoclinic.org/diseases-conditions/mitral-valve-prolapse/symptoms-causes/syc-20355446 (accessed July 14, 2018).

[58] R.A. Levine, A.A. Hagége, D.P. Judge, M. Padala, J.P. Dal-Bianco, E. Aikawa, J. Beaudoin, J. Bischoff, N. Bouatia-Naji, P. Bruneval, J.T. Butcher, A. Carpentier, M. Chaput, A.H. Chester, C. Clusel, F.N. Delling, H.C. Dietz, C. Dina, R. Durst, L. Fernandez-Friera, M.D. Handschumacher, M.O. Jensen, X.P. Jeunemaitre, H. Le Marec, T. Le Tourneau, R.R. Markwald, J. Mérot, E. Messas, D.P. Milan, T. Neri, R.A. Norris, D. Peal, M. Perrocheau, V. Probst, M. Pucéat, N. Rosenthal, J. Solis, J.-J.

Schott, E. Schwammenthal, S.A. Slaugenhaupt, J.-K. Song, M.H. Yacoub, Mitral valve disease—morphology and mechanisms, Nat. Rev. Cardiol. 12 (2015) 689–710. doi:10.1038/nrcardio.2015.161.

[59] B. Iung, A. Vahanian, Epidemiology of valvular heart disease in the adult, Nat. Rev. Cardiol. 8 (2011) 162–172. doi:10.1038/nrcardio.2010.202.

[60] P. Pibarot, J.G. Dumesnil, Prosthetic heart valves: Selection of the optimal prosthesis and long-term management, Circulation. 119 (2009) 1034–1048. doi:10.1161/CIRCULATIONAHA.108.778886.

[61] G.D. Dangas, J.I. Weitz, G. Giustino, R. Makkar, R. Mehran, Prosthetic Heart Valve Thrombosis, J. Am. Coll. Cardiol. 68 (2016) 2670–2689. doi:10.1016/j.jacc.2016.09.958.

[62] S.L. Hilbert, F.J. Schöen, V.J. Ferrans, Overview: Allograft heart valves, Card. Reconstr. with Allograft Tissues. (2005) 193–199. doi:10.1007/0-387-26515-5_21.

[63] W. Vongpatanasin, L.D. Hillis, R.A. Lange, Prosthetic Heart Valves, N. Engl. J. Med. 335 (1996) 407–416. doi:10.1056/NEJM199608083350607.

[64] Mechanical Prosthesis, (n.d.). https://www.cthsurgery.com/mechanical-prosthesis.html (accessed July 11, 2018).

[65] A. Kheradvar, E.M. Groves, C.J. Goergen, S.H. Alavi, R. Tranquillo, C.A. Simmons, L.P. Dasi, K.J. Grande-Allen, M.R.K. Mofrad, A. Falahatpisheh, B. Griffith, F. Baaijens, S.H. Little, S. Canic, Emerging Trends in Heart Valve Engineering: Part II. Novel and Standard Technologies for Aortic Valve Replacement, Ann. Biomed. Eng. 43 (2015) 844–857. doi:10.1007/s10439-014-1191-5.

[66] M. Legg, E. Mathews, R. Pelzer, The design and development of a stented tissue mitral and aortic heart valve replacement for human implantation., Cardiovasc. J. Afr. 23 (2012) 126–30. doi:10.5830/CVJ-21.059.

[67] J. Ennker, A. Albert, I.C. Ennker, Stentless aortic valves. Current aspects., HSR Proc. Intensive Care Cardiovasc. Anesth. 4 (2012) 77–82. http://www.ncbi.nlm.nih.gov/pubmed/23439732 (accessed July 12, 2018).

[68] I. El-Hamamsy, L. Clark, L.M. Stevens, Z. Sarang, G. Melina, J.J.M. Takkenberg, M.H. Yacoub, Late Outcomes Following

Freestyle Versus Homograft Aortic Root Replacement: Results From a Prospective Randomized Trial, J. Am. Coll. Cardiol. 55 (2010) 368–376. doi:10.1016/J.JACC.2009.09.030.

[69] T.A. Folliguet, F. Laborde, K. Zannis, G. Ghorayeb, A. Haverich, M. Shrestha, Sutureless perceval aortic valve replacement: Results of two European centers, Ann. Thorac. Surg. 93 (2012) 1483–1488. doi:10.1016/j.athoracsur.2012.01.071.

[70] D. Mazilu, M. Li, O. Kocaturk, K.A. Horvath, Self-Expanding Stent and Delivery System for Aortic Valve Replacement, J. Med. Device. 6 (2012) 041006. doi:10.1115/1.4007750.

[71] J.A. Terré, I. George, C.R. Smith, Pros and cons of transcatheter aortic valve implantation (TAVI) Keynote Lecture Series, Ann Cardiothorac Surg. 6 (2017) 444–452. doi:10.21037/acs.2017.09.15.

[72] B.Y.T. Modine, D. Mylotte, N. Piazza, Aortic Valves : What ' s Coming ?, Card. Interv. Today. 11 (2017) 59–67.

[73] C.R. Lam, H.H. Aram, E.R. Munnell, An experimental study of aortic valve homografts., Surg. Gynecol. Obstet. 94 (1952) 129–135. http://www.ncbi.nlm.nih.gov/pubmed/14901246 (accessed July 14, 2018).

[74] G. Murray, W. Roschlau, W. Lougheed, Homologous aortic-valve-segment transplants as surgical treatment for aortic and mitral insufficiency, Angiology. 7 (1956) 466–471. doi:10.1177/000331975600700509.

[75] D. Ross, M.H. Yacoub, Homograft replacement of the aortic valve. A critical review, Prog. Cardiovasc. Dis. 11 (1969) 275–293. doi:10.1016/0033-0620(69)90054-1.

[76] Barratt-Boyes, HOMOGRAFT AORTIC VALVE REPLACEMENT IN AORTIC INCOMPETENCE AND STENOSIS., Thorax. 19 (1964) 131–150. doi:10.1136/thx.19.2.131.

[77] R.A. Hopkins, Historical Development of the Use of Homograft Valves, in: Card. Reconstr. with Allograft Valves, Springer New York, New York, NY, 1989: pp. 3–13. doi:10.1007/978-1-4612-3568-2_1.

[78] A. Ciubotaru, S. Cebotari, I. Tudorache, E. Beckmann, A. Hilfiker, A. Haverich, Biological heart valves, Biomed. Tech. 58 (2013) 389–397. doi:10.1515/bmt-2012-0148.

[79] K. Niwaya, C.J. Knott-Craig, K. Santangelo, M.M. Lane, K. Chandrasekaran, R.C. Elkins, Advantage of autograft and

homograft valve replacement for complex aortic valve endocarditis, Ann. Thorac. Surg. 67 (1999) 1603–1608. doi:10.1016/S0003-4975(99)00402-6.

[80] P.B. Herdson, B.G. Barratt-Boyes, The pathology of chemically-sterilized human heart valve allografts, Pathology. 4 (1972) 175–183. doi:10.3109/00313027209068939.

[81] R.O. Heimbecker, Whither the Homograft Valve?, Ann. Thorac. Surg. 9 (1970) 487–488. doi:10.1016/S0003-4975(10)65543-9.

[82] S. Solari, S. Mastrobuoni, L. De Kerchove, E. Navarra, P. Astarci, P. Noirhomme, A. Poncelet, R. Jashari, J. Rubay, G. El Khoury, Over 20 years experience with aortic homograft in aortic valve replacement during acute infective endocarditis, Eur. J. Cardio-Thoracic Surg. 50 (2016) 1158–1164. doi:10.1093/ejcts/ezw175.

[83] M. Yacoub, N.R.H. Rasmi, T.M. Sundt, O. Lund, E. Boyland, R. Radley-Smith, A. Khaghani, A. Mitchell, Fourteen-year experience with homovital homografts for aortic valve replacement, J. Thorac. Cardiovasc. Surg. 110 (1995) 186–194. doi:10.1016/S0022-5223(05)80025-X.

[84] F.J. Schoen, R.J. Levy, Calcification of tissue heart valve substitutes: Progress toward understanding and prevention, Ann. Thorac. Surg. 79 (2005) 1072–1080. doi:10.1016/j.athoracsur.2004.06.033.

[85] R. Henaine, F. Roubertie, M. Vergnat, J. Ninet, Valve replacement in children: A challenge for a whole life, Arch. Cardiovasc. Dis. 105 (2012) 517–528. doi:10.1016/j.acvd.2012.02.013.

[86] R. Bagur, P. Pibarot, C.M. Otto, Importance of the valve durability-life expectancy ratio in selection of a prosthetic aortic valve, Heart. 103 (2017) 1756–1759. doi:10.1136/heartjnl-2017-312348.

[87] R.N. Mitchell, R.A. Jonas, F.J. Schoen, Pathology of explanted cryopreserved allograft heart valves: Comparison with aortic valves from orthotopic heart transplants, J. Thorac. Cardiovasc. Surg. 115 (1998) 118–127. doi:10.1016/S0022-5223(98)70450-7.

[88] F.J. Schoen, R.J. Levy, Calcification of tissue heart valve substitutes: Progress toward understanding and prevention, Ann. Thorac. Surg. 79 (2005) 1072–1080. doi:10.1016/j.athoracsur.2004.06.033.

[89] N. Piazza, S. Bleiziffer, G. Brockmann, R. Hendrick, M.A. Deutsch, A. Opitz, D. Mazzitelli, P. Tassani-Prell, C. Schreiber, R. Lange, Transcatheter Aortic Valve Implantation for Failing Surgical Aortic Bioprosthetic Valve: From Concept to Clinical Application and Evaluation (Part 1), JACC Cardiovasc. Interv. 4 (2011) 721–732. doi:10.1016/j.jcin.2011.03.016.

[90] R.J. Levy, F.J. Schoen, H.C. Anderson, H. Harasaki, T.H. Koch, W. Brown, J.B. Lian, R. Cumming, J.B. Gavin, Cardiovascular implant calcification: a survey and update, Biomaterials. 12 (1991) 707–714. doi:10.1016/0142-9612(91)90017-5.

[91] N. Vyavahare, M. Ogle, F.J. Schoen, R.J. Levy, Elastin calcification and its prevention with aluminum chloride pretreatment, Am. J. Pathol. 155 (1999) 973–982. doi:10.1016/S0002-9440(10)65197-8.

[92] M.T. Bailey, S. Pillarisetti, H. Xiao, N.R. Vyavahare, Role of elastin in pathologic calcification of xenograft heart valves, J. Biomed. Mater. Res. - Part A. 66 (2003) 93–102. doi:10.1002/jbm.a.10543.

[93] McGregor, A. Carpentier, N. Lila, J.S. Logan, G.W. Byrne, Cardiac xenotransplantation technology provides materials for improved bioprosthetic heart valves, J. Thorac. Cardiovasc. Surg. 141 (2011) 269–275. doi:10.1016/j.jtcvs.2010.08.064.

[94] N. Lila, C.G.A. McGregor, S. Carpentier, J. Rancic, G.W. Byrne, A. Carpentier, Gal knockout pig pericardium: New source of material for heart valve bioprostheses, J. Hear. Lung Transplant. 29 (2010) 538–543. doi:10.1016/j.healun.2009.10.007.

[95] H. Shang, S.M. Claessens, B. Tian, G.A. Wright, Aldehyde reduction in a novel pericardial tissue reduces calcification using rabbit intramuscular model, J. Mater. Sci. Mater. Med. 28 (2017) 16. doi:10.1007/s10856-016-5829-8.

[96] C. Kneib, C.Q.C. von Glehn, F.D.A. Costa, M.T.B.A. Costa, M.F. Susin, Evaluation of humoral immune response to donor HLA after implantation of cellularized versus decellularized human heart valve allografts, Tissue Antigens. 80 (2012) 165–174. doi:10.1111/j.1399-0039.2012.01885.x.

[97] F.J. Schoen, R.J. Levy, Pathology of Substitute Heart Valves: New Concepts and Developments, J. Card. Surg. 9 (1994) 222–227. doi:10.1111/j.1540-8191.1994.tb00932.x.

[98] R. Dignan, M. O'Brien, P. Hogan, J. Passage, F. Stephens, A. Thornton, S. Harrocks, Influence of HLA matching and

associated factors on aortic valve homograft function, J. Heart Valve Dis. 9 (2000) 504–511. http://www.ncbi.nlm.nih.gov/pubmed/10947042 (accessed July 23, 2018).

[99] J.A. Hawkins, J.P. Breinholt, L.M. Lambert, T.C. Fuller, T. Profaizer, E.C. McGough, R.E. Shaddy, Class I and class II anti-hla antibodies after implantation of cryopreserved allograft material in pediatric patients, J. Thorac. Cardiovasc. Surg. 119 (2000) 324–330. doi:10.1016/S0022-5223(00)70188-7.

[100] S. Jana, B.J. Tefft, D.B. Spoon, R.D. Simari, Scaffolds for tissue engineering of cardiac valves, Acta Biomater. 10 (2014) 2877–2893. doi:10.1016/j.actbio.2014.03.014.

[101] B.P. Chan, K.W. Leong, Scaffolding in tissue engineering: General approaches and tissue-specific considerations, Eur. Spine J. 17 (2008). doi:10.1007/s00586-008-0745-3.

[102] N.J. Kaiser, K.L.K. Coulombe, Physiologically inspired cardiac scaffolds for tailored in vivo function and heart regeneration, Biomed. Mater. 10 (2015) 034003. doi:10.1088/1748-6041/10/3/034003.

[103] T. Shinoka, C.K. Breuer, R.E. Tanel, G. Zund, T. Miura, P.X. Ma, R. Langer, J.P. Vacanti, J.E. Mayer, Tissue engineering heart valves: valve leaflet replacement study in a lamb model., Ann. Thorac. Surg. 60 (1995) S513-6. http://www.ncbi.nlm.nih.gov/pubmed/8604922 (accessed July 19, 2018).

[104] C.K. Breuer, T. Shin'oka, R.E. Tanel, G. Zund, D.J. Mooney, P.X. Ma, T. Miura, S. Colan, R. Langer, J.E. Mayer, J.P. Vacanti, Tissue engineering lamb heart valve leaflets, Biotechnol. Bioeng. 50 (1996) 562–567. doi:10.1002/(SICI)1097-0290(19960605)50:5<562::AID-BIT11>3.0.CO;2-L.

[105] S. Stratton, N.B. Shelke, K. Hoshino, S. Rudraiah, S.G. Kumbar, Bioactive polymeric scaffolds for tissue engineering, Bioact. Mater. 1 (2016) 93–108. doi:10.1016/j.bioactmat.2016.11.001.

[106] S.P. Hoerstrup, R. Sodian, S. Daebritz, J. Wang, E.A. Bacha, D.P. Martin, A.M. Moran, K.J. Guleserian, J.S. Sperling, S. Kaushal, J.P. Vacanti, F.J. Schoen, J.E. Mayer, Functional Living Trileaflet Heart Valves Grown In Vitro, Circulation. 102 (2000) III-44-III-49. doi:10.1161/01.CIR.102.suppl_3.III-44.

[107] S. Zhong, W.E. Teo, X. Zhu, R.W. Beuerman, S. Ramakrishna, L.Y.L. Yung, An aligned nanofibrous collagen scaffold by

electrospinning and its effects onin vitro fibroblast culture, J. Biomed. Mater. Res. Part A. 79A (2006) 456–463. doi:10.1002/jbm.a.30870.

[108] F.J. O'Brien, Biomaterials and scaffolds for tissue engineering, Mater. Today. 14 (2011) 88–95. doi:10.1016/S1369-7021(11)70058-X.

[109] K. Ragaert, S. Van de Velde, L. Cardon, F. De Somer, G. Van Nooten, P. Somers, Rapid manufacturing of collagen scaffolds for cardiac tissue engineering, in: High Value Manuf. Adv. Res. Virtual Rapid Prototyp., CRC Press, 2013: pp. 137–142. doi:10.1201/b15961-26.

[110] L. Bauman, CosmoDerm/CosmoPlast (human bioengineered collagen) for the aging face, Facial Plast. Surg. 20 (2004) 125–128. doi:10.1055/s-2004-861752.

[111] A.P. Sclafani, T. Romo, A.A. Jacono, Rejuvenation of the aging lip with an injectable acellular dermal graft (Cymetra)., Arch. Facial Plast. Surg. 4 (2002) 252–257. doi:10.1001/archfaci.4.4.252.

[112] K. Toda, M. Yoshitatsu, H. Izutani, K. Ihara, Surgical management of penetrating cardiac injuries using a fibrin glue sheet, Interact. Cardiovasc. Thorac. Surg. 6 (2007) 577–578. doi:10.1510/icvts.2007.156372.

[113] R. Patel, R.P. Caruso, S. Taneja, M. Stifelman, Use of Fibrin Glue and Gelfoam to Repair Collecting System Injuries in a Porcine Model: Implications for the Technique of Laparoscopic Partial Nephrectomy, J. Endourol. 17 (2003) 799–804. doi:10.1089/089277903770802416.

[114] Q. Ye, G. Zünd, P. Benedikt, S. Jockenhoevel, S.P. Hoerstrup, S. Sakyama, J.A. Hubbell, M. Turina, Fibrin gel as a three dimensional matrix in cardiovascular tissue engineering, Eur. J. Cardio-Thoracic Surg. 17 (2000) 587–591. doi:10.1016/S1010-7940(00)00373-0.

[115] S. Jockenhoevel, K. Chalabi, J.S. Sachweh, H. V. Groesdonk, L. Demircan, M. Grossmann, G. Zund, B.J. Messmer, Tissue Engineering: Complete Autologous Valve Conduit - A New Moulding Technique*, Thorac. Cardiovasc. Surg. 49 (2001) 287–290. doi:10.1055/s-2001-17807.

[116] B. Tschoeke, T.C. Flanagan, S. Koch, M.S. Harwoko, T. Deichmann, V. Ella, J.S. Sachweh, M. Kellomaki, T. Gries, T. Schmitz-Rode, S. Jockenhoevel, Tissue-Engineered Small-

Caliber Vascular Graft Based on a Novel Biodegradable Composite Fibrin-Polylactide Scaffold, Tissue Eng. Part A. 15 (2009) 1909–1918. doi:10.1089/ten.tea.2008.0499.

[117] D.D. Swartz, J.A. Russell, S.T. Andreadis, Engineering of fibrin-based functional and implantable small-diameter blood vessels, Am. J. Physiol. Circ. Physiol. 288 (2005) H1451–H1460. doi:10.1152/ajpheart.00479.2004.

[118] G.T. Finosh, M. Jayabalan, Regenerative therapy and tissue engineering for the treatment of end-stage cardiac failure: new developments and challenges., Biomatter. 2 (2012) 1–14. doi:10.4161/biom.19429.

[119] A. Liberski, N. Latif, C. Raynaud, C. Bollensdorff, M. Yacoub, Alginate for cardiac regeneration: From seaweed to clinical trials., Glob. Cardiol. Sci. Pract. 2016 (2016) e201604. doi:10.21542/gcsp.2016.4.

[120] R. Moreira, C. Neusser, M. Kruse, S. Mulderrig, F. Wolf, J. Spillner, T. Schmitz-Rode, S. Jockenhoevel, P. Mela, Tissue-Engineered Fibrin-Based Heart Valve with Bio-Inspired Textile Reinforcement, Adv. Healthc. Mater. 5 (2016) 2113–2121. doi:10.1002/adhm.201600300.

[121] A. Neumann, S. Sarikouch, T. Breymann, S. Cebotari, D. Boethig, A. Horke, P. Beerbaum, M. Westhoff-Bleck, H. Bertram, M. Ono, I. Tudorache, A. Haverich, G. Beutel, Early systemic cellular immune response in children and young adults receiving decellularized fresh allografts for pulmonary valve replacement., Tissue Eng. Part A. 20 (2014) 1003–11. doi:10.1089/ten.TEA.2013.0316.

[122] L. Iop, A. Paolin, P. Aguiari, D. Trojan, E. Cogliati, G. Gerosa, Decellularized Cryopreserved Allografts as Off-the-Shelf Allogeneic Alternative for Heart Valve Replacement: In Vitro Assessment Before Clinical Translation, J. Cardiovasc. Transl. Res. (2017) 1–11. doi:10.1007/s12265-017-9738-0.

[123] W. Lee, C. Long, J. Ramsoondar, D. Ayares, D.K.C. Cooper, R.A. Manji, H. Hara, Human antibody recognition of xenogeneic antigens (NeuGc and Gal) on porcine heart valves: could genetically modified pig heart valves reduce structural valve deterioration?, Xenotransplantation. 23 (2016) 370–380. doi:10.1111/xen.12254.

[124] T.B. Wissing, V. Bonito, C.V.C. Bouten, A.I.P.M. Smits, Biomaterial-driven in situ cardiovascular tissue engineering—a multi-disciplinary perspective, Npj Regen. Med. 2 (2017) 18.

doi:10.1038/s41536-017-0023-2.

[125] C.R.H. Wildevuur, B. van der Lei, J.M. Schakenraad, Basic aspects of the regeneration of small-calibre neoarteries in biodegradable vascular grafts in rats, Biomaterials. 8 (1987) 418–422. doi:10.1016/0142-9612(87)90076-7.

[126] L.A. Bockeria, O. Svanidze, A. Kim, K. Shatalov, V. Makarenko, M. Cox, T. Carrel, Total cavopulmonary connection with a new bioabsorbable vascular graft: First clinical experience, J. Thorac. Cardiovasc. Surg. 153 (2017) 1542–1550. doi:10.1016/j.jtcvs.2016.11.071.

[127] N. Nagiah, R. Johnson, R. Anderson, W. Elliott, W. Tan, Highly Compliant Vascular Grafts with Gelatin-Sheathed Coaxially Structured Nanofibers., Langmuir. 31 (2015) 12993–3002. doi:10.1021/acs.langmuir.5b03177.

[128] M. Gallo, F. Naso, H. Poser, A. Rossi, P. Franci, R. Bianco, M. Micciolo, F. Zanella, U. Cucchini, L. Aresu, E. Buratto, R. Busetto, M. Spina, A. Gandaglia, G. Gerosa, Physiological Performance of a Detergent Decellularized Heart Valve Implanted for 15 Months in Vietnamese Pigs: Surgical Procedure, Follow-up, and Explant Inspection, Artif. Organs. 36 (2012). doi:10.1111/j.1525-1594.2012.01447.x.

[129] S. Cebotari, I. Tudorache, A. Ciubotaru, D. Boethig, S. Sarikouch, A. Goerler, A. Lichtenberg, E. Cheptanaru, S. Barnaciuc, A. Cazacu, O. Maliga, O. Repin, L. Maniuc, T. Breymann, A. Haverich, Use of fresh decellularized allografts for pulmonary valve replacement may reduce the reoperation rate in children and young adults: Early report, Circulation. (2011). doi:10.1161/CIRCULATIONAHA.110.012161.

[130] F.D.A. Da Costa, P.M. Dohmen, S.V. Lopes, G. Lacerda, F. Pohl, R. Vilani, M.B.A. Da Costa, E.D. Vieira, S. Yoschi, W. Konertz, I.A. Da Costa, Comparison of cryopreserved homografts and decellularized porcine heterografts implanted in sheep, Artif. Organs. 28 (2004) 366–370. doi:10.1111/j.1525-1594.2004.47357.x.

[131] A. Neumann, S. Sarikouch, T. Breymann, S. Cebotari, D. Boethig, A. Horke, P. Beerbaum, M. Westhoff-Bleck, H. Bertram, M. Ono, I. Tudorache, A. Haverich, G. Beutel, Early Systemic Cellular Immune Response in Children and Young Adults Receiving Decellularized Fresh Allografts for Pulmonary Valve Replacement, Tissue Eng. Part A. 20 (2014) 1003–1011. doi:10.1089/ten.tea.2013.0316.

[132] F. Sayk, I. Bos, U. Schubert, T. Wedel, H.-H. Sievers, Histopathologic Findings in a Novel Decellularized Pulmonary Homograft: An Autopsy Study, Ann. Thorac. Surg. 79 (2005) 1755–1758. doi:10.1016/j.athoracsur.2003.11.049.

[133] J.W. Brown, R.C. Elkins, D.R. Clarke, J.S. Tweddell, C.B. Huddleston, J.R. Doty, J.W. Fehrenbacher, J.J.M. Takkenberg, Performance of the CryoValve SG human decellularized pulmonary valve in 342 patients relative to the conventional CryoValve at a mean follow-up of four years, J. Thorac. Cardiovasc. Surg. 139 (2010) 339–348. doi:10.1016/j.jtcvs.2009.04.065.

[134] R. Ramm, H. Niemann, B. Petersen, A. Haverich, A. Hilfiker, Decellularized GGTA1-KO pig heart valves do not bind preformed human xenoantibodies, Basic Res. Cardiol. 111 (2016) 39. doi:10.1007/s00395-016-0560-7.

[135] M. Granados, L. Morticelli, S. Andriopoulou, P. Kalozoumis, M. Pflaum, P. Iablonskii, B. Glasmacher, M. Harder, J. Hegermann, C. Wrede, I. Tudorache, S. Cebotari, A. Hilfiker, A. Haverich, S. Korossis, Development and Characterization of a Porcine Mitral Valve Scaffold for Tissue Engineering, J. Cardiovasc. Transl. Res. 10 (2017) 374–390. doi:10.1007/s12265-017-9747-z.

[136] L. Morticelli, D. Thomas, E. Ingham, S. Korossis, Investigation of the Suitability of Decellularised Porcine Pericardium for Mitral Valve Reconstruction, QScience Proc. 2012 (2012) 39. doi:10.5339/qproc.2012.heartvalve.4.39.

[137] P. Aguiari, L. Iop, F. Favaretto, C.M.L. Fidalgo, F. Naso, G. Milan, V. Vindigni, M. Spina, F. Bassetto, A. Bagno, R. Vettor, G. Gerosa, In vitro comparative assessment of decellularized bovine pericardial patches and commercial bioprosthetic heart valves, Biomed. Mater. 12 (2017) 015021. doi:10.1088/1748-605X/aa5644.

[138] F. Zafar, R.B. Hinton, R.A. Moore, R.S. Baker, R. Bryant, D.A. Narmoneva, M.D. Taylor, D.L. Morales, Physiological Growth, Remodeling Potential, and Preserved Function of a Novel Bioprosthetic Tricuspid Valve: Tubular Bioprosthesis Made of Small Intestinal Submucosa-Derived Extracellular Matrix, J. Am. Coll. Cardiol. 66 (2015) 877–888. doi:10.1016/j.jacc.2015.06.1091.

[139] O'Brien, S. Goldstein, S. Walsh, K.S. Black, R. Elkins, D. Clarke, The SynerGraft valve: a new acellular (nonglutaraldehyde-fixed) tissue heart valve for autologous recellularization first

experimental studies before clinical implantation., Semin. Thorac. Cardiovasc. Surg. 11 (1999) 194–200. doi:S1043067999000787 [pii].

[140] P. Simon, M.T. Kasimir, G. Seebacher, G. Weigel, R. Ullrich, U. Salzer-Muhar, E. Rieder, E. Wolner, Early failure of the tissue engineered porcine heart valve SYNERGRAFT^{TM} in pediatric patients, in: Eur. J. Cardio-Thoracic Surg., 2003: pp. 1002–1006. doi:10.1016/S1010-7940(03)00094-0.

[141] W. Konertz, P.M. Dohmen, J. Liu, S. Beholz, S. Dushe, S. Posner, A. Lembcke, W. Erdbrügger, Hemodynamic characteristics of the Matrix P decellularized xenograft for pulmonary valve replacement during the Ross operation., J. Heart Valve Dis. 14 (2005) 78–81. http://www.ncbi.nlm.nih.gov/pubmed/15700440 (accessed July 23, 2018).

[142] A. Rüffer, A. Purbojo, I. Cicha, M. Glöckler, S. Potapov, S. Dittrich, R.A. Cesnjevar, Early failure of xenogenous de-cellularised pulmonary valve conduits - a word of caution!, Eur. J. Cardio-Thoracic Surg. 38 (2010) 78–85. doi:10.1016/j.ejcts.2010.01.044.

[143] S. Park, W.H. Kim, S.Y. Choi, Y.J. Kim, Removal of alpha-gal epitopes from porcine aortic valve and pericardium using recombinant human alpha galactosidase A, J. Korean Med. Sci. 24 (2009) 1126–1131. doi:10.3346/jkms.2009.24.6.1126.

[144] D.W. Courtman, C.A. Pereira, V. Kashef, D. McComb, J.M. Lee, G.J. Wilson, Development of a pericardial acellular matrix biomaterial: Biochemical and mechanical effects of cell extraction, J. Biomed. Mater. Res. 28 (1994) 655–666. doi:10.1002/jbm.820280602.

[145] Y. Chang, H. Liang, H. Wei, C. Chu, H. Sung, Tissue regeneration patterns in acellular bovine pericardia implanted in a canine model as a vascular patch., J. Biomed. Mater. Res. A. 69 (2004) 323–333. doi:10.1002/jbm.a.30003.

[146] M.C. Vinci, G. Tessitore, L. Castiglioni, F. Prandi, M. Soncini, R. Santoro, F. Consolo, F. Colazzo, B. Micheli, L. Sironi, G. Polvani, M. Pesce, Mechanical Compliance and Immunological Compatibility of Fixative-Free Decellularized/Cryopreserved Human Pericardium, PLoS One. 8 (2013). doi:10.1371/journal.pone.0064769.

[147] Products - CryoLife, Inc., (n.d.). https://www.cryolife.com/products/ (accessed July 26, 2018).

[148] F. Nappi, C. Spadaccio, M. Chello, M. Lusini, C. Acar, Long-Term Structural Valve Degeneration in Cryopreserved Mitral and Aortic Homograft : Is Pregnancy a Factor ?, (2014) 277–286.

[149] P.M. Crapo, T.W. Gilbert, S.F. Badylak, An overview of tissue and whole organ decellularization processes, Biomaterials. 32 (2011) 3233–3243. doi:10.1016/j.biomaterials.2011.01.057.

[150] K. Burkewitz, K. Choe, K. Strange, Hypertonic stress induces rapid and widespread protein damage in C. elegans, Am. J. Physiol. Physiol. 301 (2011) C566–C576. doi:10.1152/ajpcell.00030.2011.

[151] R.W. Grauss, M.G. Hazekamp, F. Oppenhuizen, C.J. Van Munsteren, A.C. Gittenberger-De Groot, M.C. DeRuiter, Histological evaluation of decellularised porcine aortic valves: Matrix changes due to different decellularisation methods, in: Eur. J. Cardio-Thoracic Surg., 2005: pp. 566–571. doi:10.1016/j.ejcts.2004.12.052.

[152] S.L.M. Dahl, J. Koh, V. Prabhakar, L.E. Niklason, Decellularized native and engineered arterial scaffolds for transplantation., Cell Transplant. 12 (2003) 659–66. http://www.ncbi.nlm.nih.gov/pubmed/14579934 (accessed July 23, 2018).

[153] M. Spina, F. Ortolani, A. El Messlemani, A. Gandaglia, J. Bujan, N. Garcia-Honduvilla, I. Vesely, G. Gerosa, D. Casarotto, L. Petrelli, M. Marchini, Isolation of intact aortic valve scaffolds for heart-valve bioprostheses: Extracellular matrix structure, prevention from calcification, and cell repopulation features, J. Biomed. Mater. Res. 67A (2003) 1338–1350. doi:10.1002/jbm.a.20025.

[154] Patel, E. Solanki, R. Picciani, V. Cavett, J.A. Caldwell-Busby, S.K. Bhattacharya, Strategies to recover proteins from ocular tissues for proteomics, Proteomics. 8 (2008) 1055–1070. doi:10.1002/pmic.200700856.

[155] R.A. Guyton, L.M. Dorsey, M.S. Silberman, H.K. Hawkins, W.H. Williams, C.R. Hatcher, The broadly based pericardial flap. A tissue for atrial wall replacement that grows., J. Thorac. Cardiovasc. Surg. 87 (1984) 619–25. http://www.ncbi.nlm.nih.gov/pubmed/6708582 (accessed July 24, 2018).

[156] C. Duran, Autologous Pericardium Revisited, in: Card. Surg., Springer US, Boston, MA, 1995: pp. 93–102. doi:10.1007/978-1-4615-1925-6_9.

[157] E. Remi, N. Khelil, I. Di, C. Roques, M. Ba, F. Medjahed-Hamidi, F. Chaubet, D. Letourneur, E. Lansac, A. Meddahi-Pelle, Pericardial Processing: Challenges, Outcomes and Future Prospects, in: Biomater. Sci. Eng., InTech, 2011. doi:10.5772/24949.

[158] M. Dahm, D. Prüfer, E. Mayer, E. Groh, Y.H. Choi, H. Oelert, Early failure of an autologous pericardium aortic heart valve (ATCV) prosthesis., J. Heart Valve Dis. 7 (1998) 30–3. http://www.ncbi.nlm.nih.gov/pubmed/9502136.

[159] C. Duran, R. Gallo, N. Kumar, Aortic Valve Replacement with Autologous Pericardium: Surgical Technique, J. Card. Surg. 10 (1995) 1–9. doi:10.1111/j.1540-8191.1995.tb00582.x.

[160] C. Gross, P. Simon, M. Grabenwöger, R. Mair, K. Sihorsch, A. Kypta, M. Grimm, P. Brücke, Midterm results after aortic valve replacement with the autologous tissue cardiac valve, Eur. J. Cardio-Thoracic Surg. 16 (1999) 533–539. doi:10.1016/S1010-7940(99)00309-7.

[161] M. Grabenwoger, J. Sider, F. Fitzal, C. Zelenka, U. Windberger, M. Grimm, A. Moritz, P. Bock, E. Wolner, Impact of glutaraldehyde on calcification of pericardial bioprosthetic heart valve material., Ann. Thorac. Surg. 62 (1996) 772–777.

[162] D.W. Courtman, C.A. Pereira, V. Kashef, D. McComb, J.M. Lee, G.J. Wilson, Development of a pericardial acellular matrix biomaterial: Biochemical and mechanical effects of cell extraction, J. Biomed. Mater. Res. 28 (1994) 655–666. doi:10.1002/jbm.820280602.

[163] M. Yang, C.Z. Chen, X.N. Wang, Y. Bin Zhu, Y.J. Gu, Favorable effects of the detergent and enzyme extraction method for preparing decellularized bovine pericardium scaffold for tissue engineered heart valves, J. Biomed. Mater. Res. - Part B Appl. Biomater. 91 (2009) 354–361. doi:10.1002/jbm.b.31409.

[164] B. Mendoza-Novelo, E.E. Avila, J. V. Cauich-Rodr??guez, E. Jorge-Herrero, F.J. Rojo, G. V. Guinea, J.L. Mata-Mata, Decellularization of pericardial tissue and its impact on tensile viscoelasticity and glycosaminoglycan content, Acta Biomater. (2011). doi:10.1016/j.actbio.2010.11.017.

[165] S. Sajith, Comparative Study of Two Decellularization Protocols on a Biomaterial for Tissue Engineering, J. Clin. Exp. Cardiolog. 08 (2017). doi:10.4172/2155-9880.1000523.

[166] S. Mirsadraee, H.E. Wilcox, S.A. Korossis, J.N. Kearney, K.G.

Watterson, J. Fisher, E. Ingham, Development and Characterization of an Acellular Human Pericardial Matrix for Tissue Engineering, Tissue Eng. 12 (2006) 763–773. doi:10.1089/ten.2006.12.763.

[167] J.M. García Páez, E.J. Herrero, A.C. San Martín, J. V García Sestafe, G. Téllez, I. Millán, J. Salvador, A. Cordón, J.L. Castillo-Olivares, The influence of chemical treatment and suture on the elastic behavior of calf pericardium utilized in the construction of cardiac bioprostheses, J. Mater. Sci. Mater. Med. 11 (2000) 273–277. doi:10.1023/A:1008901128613.

[168] H. Aubin, C. Mas-Moruno, M. Iijima, N. Schütterle, M. Steinbrink, A. Assmann, J. Gil, A. Lichtenberg, M. Pegueroles, P. Akhyari, Customized interface biofunctionalization of decellularized extracellular matrix: towards enhanced endothelialization, Mary Ann Liebert, Inc., 2016. doi:10.1089/ten.TEC.2015.0556.

[169] X. Dong, X. Wei, W. Yi, C. Gu, X. Kang, Y. Liu, Q. Li, D. Yi, RGD-modified acellular bovine pericardium as a bioprosthetic scaffold for tissue engineering, J. Mater. Sci. Mater. Med. 20 (2009) 2327–2336. doi:10.1007/s10856-009-3791-4.

[170] A. Assmann, C. Delfs, H. Munakata, F. Schiffer, K. Horstkötter, K. Huynh, M. Barth, V.R. Stoldt, H. Kamiya, U. Boeken, A. Lichtenberg, P. Akhyari, Acceleration of autologous invivo recellularization of decellularized aortic conduits by fibronectin surface coating, Biomaterials. 34 (2013) 6015–6026. doi:10.1016/j.biomaterials.2013.04.037.

[171] T. Shimada, T. Nishibe, H. Miura, K. Hazama, H. Kato, F. Kudo, T. Murashita, Y. Okuda, Improved Healing of Small-Caliber, Long-Fibril Expanded Polytetrafluoroethylene Vascular Grafts by Covalent Bonding of Fibronectin, Surg. Today. 34 (2004) 1025–1030. doi:10.1007/s00595-004-2862-x.

[172] J.M. Bastijanic, R.E. Marchant, F. Kligman, M.T. Allemang, R.O. Lakin, D. Kendrick, V.S. Kashyap, K. Kottke-Marchant, In vivo evaluation of biomimetic fluorosurfactant polymer-coated expanded polytetrafluoroethylene vascular grafts in a porcine carotid artery bypass model, J. Vasc. Surg. 63 (2016) 1620–1630e4. doi:10.1016/j.jvs.2015.01.060.

[173] R. Jashari, Y. Goffin, A. Vanderkelen, B. Van Hoeck, A. du Verger, Y. Fan, V. Holovska, O. Brahy, European Homograft Bank: Twenty Years of Cardiovascular Tissue Banking and Collaboration With Transplant Coordination in Europe, Transplant. Proc. 42 (2010) 183–189.

doi:10.1016/j.transproceed.2009.11.022.

[174] T.M.M.H. de By, R. Parker, E.M. Delmo Walter, R. Hetzer, Cardiovascular tissue banking in Europe., HSR Proc. Intensive Care Cardiovasc. Anesth. 4 (2012) 251–60. http://www.pubmedcentral.nih.gov/articlerender.fcgi?artid=3563559&tool=pmcentrez&rendertype=abstract.

[175] Objectives / Aims - ESPOIR, (n.d.). http://www.espoir-clinicaltrial.eu/about-espoir/objectives.html (accessed July 29, 2018).

[176] About ARISE - ARISE, (n.d.). http://arise-clinicaltrial.eu/about-espoir0.html (accessed July 29, 2018).

[177] K. Brockbank, J.C. Covault, M. Taylor, A Guide to Cryopreservation Techniques, Thermo Electron Corp. (2004) 1–24.

[178] K.G. Brockbank, K.M. Smith, Synergistic interaction of low-molecular-weight polyvinylpyrrolidones with dimethylsulfoxide during cell cryopreservation., Transplant. Proc. 25 (1993) 3185–7. http://www.ncbi.nlm.nih.gov/pubmed/8266509 (accessed July 29, 2018).

[179] L. Wolfinbarger, K.G.M. Brockbank, R.A. Hopkins, Application of cryopreservation to heart valves, 2005. doi:10.1007/0-387-26515-5_16.

[180] D.E. Pegg, Principles of Cryopreservation Chapter 1, in: Wolkers W., Oldenhof H. Cryopreserv. Free. Protoc. Methods Mol. Biol. (Methods Protoc. Vol 1257. Springer, New York, NY, 2015: pp. 21–82. doi:10.1007/978-1-4939-2193-5.

[181] Brockbank, M.M.J. Taylor, 8 Tissue Preservation, Adv. Biopreservation. (2006) 157–196. http://www.andrew.cmu.edu/user/yr25/TaylorPublications/MJTaylor108.pdf.

[182] Brockbank, J.F. Carpenter, P.E. Dawson, Effects of storage temperature on viable bioprosthetic heart valves, Cryobiology. 29 (1992) 537–542. doi:10.1016/0011-2240(92)90058-A.

[183] N. Manuchehrabadi, Z. Gao, J. Zhang, H.L. Ring, Q. Shao, F. Liu, M. McDermott, A. Fok, Y. Rabin, K.G.M. Brockbank, M. Garwood, C.L. Haynes, J.C. Bischof, Improved tissue cryopreservation using inductive heating of magnetic nanoparticles, Sci. Transl. Med. 9 (2017). doi:10.1126/scitranslmed.aah4586.

[184] B.C. Elford, C.A. Walter, Preservation of Structure and Function of Smooth Muscle cooled to -79°C in Unfrozen Aqueous Media, Nat. New Biol. 236 (1972) 58–60. doi:10.1038/239137a0.

[185] M.J. Taylor, C.A. Walter, B.C. Elford, The pH-dependent recovery of smooth muscle from storage at −13 °C in unfrozen media, Cryobiology. 15 (1978) 452–460. doi:10.1016/0011-2240(78)90065-2.

[186] D. Aidulis, D.E. Pegg, C.J. Hunt, Y.A. Goffin, A. Vanderkelen, B. van Hoeck, T. Santiago, T. Ramos, E. Gruys, W. Voorhout, Processing of ovine cardiac valve allografts: 1. Effects of preservation method on structure and mechanical properties, Cell Tissue Bank. 3 (2002) 79–89. doi:10.1023/A:1022873513040.

[187] D.E. Pegg, The preservation of tissues for transplantation, Cell Tissue Bank. 7 (2006) 349–358. doi:10.1007/s10561-006-9013-0.

[188] C.J. Gerson, S. Goldstein, A.E. Heacox, Retained structural integrity of collagen and elastin within cryopreserved human heart valve tissue as detected by two-photon laser scanning confocal microscopy, Cryobiology. 59 (2009) 171–179. doi:10.1016/j.cryobiol.2009.06.012.

[189] K. Schenke-Layland, J. Xie, S. Heydarkhan-Hagvall, S.F. Hamm-Alvarez, U.A. Stock, K.G.M. Brockbank, W.R. MacLellan, Optimized Preservation of Extracellular Matrix in Cardiac Tissues: Implications for Long-Term Graft Durability, Ann. Thorac. Surg. 83 (2007) 1641–1650. doi:10.1016/j.athoracsur.2006.12.005.

[190] Brockbank, Y.C. Song, Morphological analyses of ice-free and frozen cryopreserved heart valve explants., J. Heart Valve Dis. 13 (2004) 297–301. http://europepmc.org/abstract/med/15086270.

[191] C.J. Hunt, M.J. Taylor, D.E. Pegg, Freeze-substitution and isothermal freeze-fixation studies to elucidate the pattern of ice formation in smooth muscle at 252 K (-21°C), J. Microsc. 125 (1982) 177–186. doi:10.1111/j.1365-2818.1982.tb00335.x.

[192] M.J. Taylor, D.E. Pegg, The effect of ice formation on the function of smooth muscle tissue stored at −21 or −60 °C, Cryobiology. 20 (1983) 36–40. doi:10.1016/0011-2240(83)90057-3.

[193] R. Cuevas-Uribe, E. Hu, H. Daniels, A.O. Gill, T.R. Tiersch,

Vitrification as an Alternative Approach for Sperm Cryopreservation in Marine Fishes., N. Am. J. Aquac. 79 (2017) 187–196. doi:10.1080/15222055.2017.1281855.

[194] J. Aizpurua, L. Medrano, M. Enciso, J. Sarasa, A. Romero, M.A. Fernández, M.J. Gómez-Torres, New permeable cryoprotectant-free vitrification method for native human sperm, Hum. Reprod. 32 (2017) 2007–2015. doi:10.1093/humrep/dex281.

[195] L. Rienzi, C. Gracia, R. Maggiulli, A.R. LaBarbera, D.J. Kaser, F.M. Ubaldi, S. Vanderpoel, C. Racowsky, Oocyte, embryo and blastocyst cryopreservation in ART: systematic review and meta-analysis comparing slow-freezing versus vitrification to produce evidence for the development of global guidance, Hum. Reprod. Update. 23 (2016) 139–155. doi:10.1093/humupd/dmw038.

[196] S. Silber, Chapter 13 Human Ovarian Tissue Vitrification, in: Methods Mol. Biol., 2017: pp. 177–194. doi:10.1007/978-1-4939-6828-2_13.

[197] K. Brockbank, Z. Chen, E.D. Greene, L.H. Campbell, Vitrification of Heart Valve Tissues, in: W.F. Wolkers, H. Oldenhof (Eds.), Cryopreserv. Free. Protoc., Springer New York, New York, NY, 2015: pp. 399–421. doi:10.1007/978-1-4939-2193-5_20.

[198] G.M. Fahy, B. Wowk, Principles of cryopreservation by vitrification, Methods Mol. Biol. 1257 (2015) 21–82. doi:10.1007/978-1-4939-2193-5_2.

[199] W.F. Wolkers, H. Oldenhof, Cryopreservation and freeze-drying protocols, n.d.

[200] K. Brockbank, Z.Z. Chen, Y.C. Song, Vitrification of porcine articular cartilage, Cryobiology. 60 (2010) 217–221. doi:10.1016/j.cryobiol.2009.12.003.

[201] Y.C. Song, B.S. Khirabadi, F. Lightfoot, K.G.M. Brockbank, M.J. Taylor, Vitreous cryopreservation maintains the function of vascular grafts, Nat. Biotechnol. 18 (2000) 296–299. doi:10.1038/73737.

[202] W.F. Rall, G.M. Fahy, Ice-free cryopreservation of mouse embryos at -196°C by vitrification, Nature. 313 (1985) 573–575. doi:10.1038/313573a0.

[203] P.M. Mehl, Nucleation and Crystal Growth in a Vitrification Solution Tested for Organ Cryopreservation by Vitrification, Cryobiology. 30 (1993) 509–518. doi:10.1006/cryo.1993.1051.

[204] K. Brockbank, K. Schenke-Layland, E.D. Greene, Z. Chen, O. Fritze, M. Schleicher, R. Kaulitz, I. Riemann, F. Fend, J.M. Albes, U.A. Stock, M. Lisy, Ice-free cryopreservation of heart valve allografts: Better extracellular matrix preservation in vivo and preclinical results, Cell Tissue Bank. (2012). doi:10.1007/s10561-011-9288-7.

[205] A.J.T. Huber, T. Aberle, M. Schleicher, H.P. Wendel, K.G.M. Brockbank, Characterization of a simplified ice-free cryopreservation method for heart valves, Cell Tissue Bank. 14 (2013) 195–203. doi:10.1007/s10561-012-9319-z.

[206] K. Schenke-Layland, N. Madershahian, I. Riemann, B. Starcher, K.J. Halbhuber, K. König, U.A. Stock, Impact of cryopreservation on extracellular matrix structures of heart valve leaflets, Ann. Thorac. Surg. 81 (2006) 918–926. doi:10.1016/j.athoracsur.2005.09.016.

[207] K. Brockbank, G.J. Wright, H. Yao, E.D. Greene, Z.Z. Chen, K. Schenke-Layland, Allogeneic heart valve storage above the glass transition at -80°C, Ann. Thorac. Surg. 91 (2011) 1829–1835. doi:10.1016/j.athoracsur.2011.02.043.

[208] Y. Song, P.O. Hagen, F.G. Lightfoot, M.J. Taylor, A.C. Smith, K.G. Brockbank, In vivo evaluation of the effects of a new ice-free cryopreservation process on autologous vascular grafts., J. Invest. Surg. 13 (2000) 279–88. http://www.ncbi.nlm.nih.gov/pubmed/11071564.

[209] G.D.J. Adams, I. Cook, K.R. Ward, The principles of freeze-drying, Methods Mol. Biol. 1257 (2015) 121–143. doi:10.1007/978-1-4939-2193-5_4.

[210] J.F. Carpenter, J.H. Crowe, An infrared spectroscopic study of the interactions of carbohydrates with dried proteins, Biochemistry. 28 (1989) 3916–3922. doi:10.1021/bi00435a044.

[211] J.A. Searles, Freezing and Annealing Phenomena in Lyophilization, in: L. Rey, J.C. May (Eds.), Free. Drying/Lyophilization Pharm. Biol. Prod., third, Informa healthcare, New York, London, 2004: pp. 52–81. doi:10.3109/9781439825761.003.

[212] L. Keskintepe, A. Eroglu, Freeze-drying of mammalian sperm, Methods Mol. Biol. 1257 (2015) 489–497. doi:10.1007/978-1-4939-2193-5_25.

[213] R.E. Hudson, Pathology of the human aortic valve homograft., Br. Heart J. 28 (1966) 291–301.

[214] C.F. Borgognoni, V.T. Junior, A.M.I.B. Ayrosa, B. Polakiewicz, A.A. Leirner, M.J.S. Maizato, O.Z. Higa, M.M. Beppu, R.N. de M. Pitombo, The influence of freezing rates on bovine pericardium tissue freeze-drying, Brazilian Arch. Biol. Technol. 52 (2009) 1493–1504. doi:10.1590/S1516-89132009000600021.

[215] R. Polak, R.N.M. Pitombo, Care during freeze-drying of bovine pericardium tissue to be used as a biomaterial: A comparative study, Cryobiology. 63 (2011) 61–66. doi:10.1016/j.cryobiol.2011.05.001.

[216] Y.M. Hafeez, A.B.Z. Zuki, N. Yusof, H. Asnah, M.Y. Loqman, M.M. Noordin, M.Y. Ainul-Yuzairi, Effect of freeze-drying and gamma irradiation on biomechanical properties of bovine pericardium, Cell Tissue Bank. 6 (2005) 85–89. doi:10.1007/s10561-004-1888-z.

[217] W.S. Sheridan, G.P. Duffy, B.P. Murphy, Optimum Parameters for Freeze-Drying Decellularized Arterial Scaffolds, Tissue Eng. Part C Methods. 19 (2013) 981–990. doi:10.1089/ten.tec.2012.0741.

[218] S. Wang, T. Goecke, C. Meixner, A. Haverich, A. Hilfiker, W.F. Wolkers, Freeze-Dried Heart Valve Scaffolds, Tissue Eng. Part C Methods. 18 (2012) 517–525. doi:10.1089/ten.tec.2011.0398.

[219] W.F. Wolkers, Andres Hilfiker, Freeze-drying of decellularized heart valve tissues, Methods Mol. Biol. 1257 (2015) 499–506. doi:10.1007/978-1-4939-2193-5_26.

[220] W.F. Wolkers, H. Oldenhof, Sucrose Diffusion in Decellularized Heart Valves for Freeze-Drying, Tissue Eng. Part C Methods. 21 (2015) 922–931. doi:10.1089/ten.tec.2014.0681.

[221] T. Goecke, K. Theodoridis, I. Tudorache, A. Ciubotaru, S. Cebotari, R. Ramm, K. Höffler, S. Sarikouch, A. Vásquez-Rivera, A. Haverich, W.F. Wolkers, A. Hilfiker, In vivo performance of freeze-dried decellularized pulmonary heart valve allo- and xenografts orthotopically implanted into juvenile sheep, Acta Biomater. 68 (2018) 41–52. doi:10.1016/j.actbio.2017.11.041.

[222] A.J.T. Huber, K.G.M. Brockbank, T. Aberle, M. Schleicher, Z.Z. Chen, E.D. Greene, M. Lisy, U.A. Stock, Development of a Simplified Ice-Free Cryopreservation Method for Heart Valves Employing VS83, an 83% Cryoprotectant Formulation, Biopreserv. Biobank. 10 (2012) 479–484. doi:10.1089/bio.2012.0006.

[223] A. Filippi, E. Dal Sasso, L. Iop, A. Armani, M. Gintoli, M. Sandri, G. Gerosa, F. Romanato, G. Borile, Multimodal label-free ex vivo imaging using a dual-wavelength microscope with axial chromatic aberration compensation, J. Biomed. Opt. 23 (2018) 1. doi:10.1117/1.JBO.23.9.091403.

[224] R. Rezakhaniha, A. Agianniotis, J.T.C. Schrauwen, A. Griffa, D. Sage, C.V.C. Bouten, F.N. Van De Vosse, M. Unser, N. Stergiopulos, Experimental investigation of collagen waviness and orientation in the arterial adventitia using confocal laser scanning microscopy, Biomech. Model. Mechanobiol. 11 (2012) 461–473. doi:10.1007/s10237-011-0325-z.

[225] R.W. Farndale, D.J. Buttle, A.J. Barrett, Improved quantitation and discrimination of sulphated glycosaminoglycans by use of dimethylmethylene blue, BBA - Gen. Subj. 883 (1986) 173–177. doi:10.1016/0304-4165(86)90306-5.

[226] S. Chandrasekhar, M.A. Esterman, H.A. Hoffman, Microdetermination of proteoglycans and glycosaminoglycans in the presence of guanidine hydrochloride, Anal. Biochem. 161 (1987) 103–108. doi:10.1016/0003-2697(87)90658-0.

[227] I. Barbosa, S. Garcia, V. Barbier-Chassefière, J.P. Caruelle, I. Martelly, D. Papy-García, Improved and simple micro assay for sulfated glycosaminoglycans quantification in biological extracts and its use in skin and muscle tissue studies, Glycobiology. 13 (2003) 647–653. doi:10.1093/glycob/cwg082.

[228] C.A. Edwards, W.D. O'Brien, Modified assay for determination of hydroxyproline in a tissue hydrolyzate, Clin. Chim. Acta. 104 (1980) 161–167. doi:10.1016/0009-8981(80)90192-8.

[229] R.A. Bank, M. Krikken, B. Beekman, R. Stoop, A. Maroudas, F.P.J.G. Lafebers, J.M. Te Koppele, A simplified measurement of degraded collagen in tissues: Application in healthy, fibrillated and osteoarthritic cartilage, Matrix Biol. 16 (1997) 233–243. doi:10.1016/S0945-053X(97)90012-3.

[230] Michael S. Sacks; C J Charles Chuong, Collagen Fiber Architecture of Bovine Pericardium, Am. Soc. Artif. Intern. Orga. 40 (1994) 632–637. https://insights.ovid.com/pubmed?pmid=8555591.

[231] S.A. Korossis, C. Booth, H.E. Wilcox, K.G. Watterson, J.N. Kearney, J. Fisher, E. Ingham, Tissue engineering of cardiac valve prostheses II: biomechanical characterization of decellularized porcine aortic heart valves., J. Heart Valve Dis. 11 (2002) 463–471.

[232] Y. Fung, Mechanical Properties of Living Tissues, in: Biomechanics, 2nd Ed I, 1982: p. 568. doi:10.1007/978-1-4757-2257-4.

[233] ISO (International Organization for Standardization), ISO 10993-5:2009: Biological evaluation of medical devices -- Part 5: Tests for in vitro cytotoxicity, Communication. (2009). doi:10.5594/J09750.

[234] C. Fidalgo, L. Iop, M. Sciro, M. Harder, D. Mavrilas, S. Korossis, A. Bagno, G. Palù, P. Aguiari, G. Gerosa, A Sterilization Method for Decellularized Xenogeneic Cardiovascular Scaffolds, Acta Biomater. (2017). doi:10.1016/j.actbio.2017.11.035.

[235] S. Cebotari, I. Tudorache, T. Jaekel, A. Hilfiker, S. Dorfman, W. Ternes, A. Haverich, A. Lichtenberg, Detergent decellularization of heart valves for tissue engineering: Toxicological effects of residual detergents on human endothelial cells, Artif. Organs. 34 (2010) 206–210. doi:10.1111/j.1525-1594.2009.00796.x.

[236] G. a. Holzapfel, Biomechanics of Soft Tissue in Cardiovascular Systems, in: Biomech. Soft Tissue Cardiovasc. Syst., 2003: pp. 109–184.

[237] W. Gallagher, FTIR Analysis of Protein Structure, Biochemistry. (1997) 662–666.

[238] G. Holzapfel, Biomechanics of Soft Tissue, in: J. Lemaitre. (Ed.), Handb. Mater. Behav. Model., Academic Press, 2001: pp. 1057–1071. doi:10.1016/B978-012443341-0/50107-1.

[239] A. Cigliano, A. Gandaglia, A.J. Lepedda, E. Zinellu, F. Naso, A. Gastaldello, P. Aguiari, P. De Muro, G. Gerosa, M. Spina, M. Formato, Fine structure of glycosaminoglycans from fresh and decellularized porcine cardiac valves and pericardium, Biochem. Res. Int. 2012 (2012). doi:10.1155/2012/979351.

[240] K. Schenke-Layland, F. Opitz, M. Gross, C. Döring, K.J. Halbhuber, F. Schirrmeister, T. Wahlers, U.A. Stock, Complete dynamic repopulation of decellularized heart valves by application of defined physical signals - An in vitro study, Cardiovasc. Res. 60 (2003) 497–509. doi:10.1016/j.cardiores.2003.09.002.

[241] G.L. Converse, M. Armstrong, R.W. Quinn, E.E. Buse, M.L. Cromwell, S.J. Moriarty, G.K. Lofland, S.L. Hilbert, R.A. Hopkins, Effects of cryopreservation, decellularization and novel extracellular matrix conditioning on the quasi-static and time-dependent properties of the pulmonary valve leaflet, Acta

Biomater. (2012). doi:10.1016/j.actbio.2012.03.047.

[242] J. Luo, S.A. Korossis, S.-P. Wilshaw, L.M. Jennings, J. Fisher, E. Ingham, Development and Characterization of Acellular Porcine Pulmonary Valve Scaffolds for Tissue Engineering, Tissue Eng. Part A. 20 (2014). doi:10.1089/ten.tea.2013.0573.

[243] M. Rothenburger, W. Völker, P. Vischer, B. Glasmacher, H.H. Scheld, M. Deiwick, Ultrastructure of Proteoglycans in Tissue-Engineered Cardiovascular Structures, Tissue Eng. 8 (2002) 1049–1056. doi:10.1089/107632702320934146.

[244] V. Padler-Karavani, A. Varki, Potential impact of the non-human sialic acid N-glycolylneuraminic acid on transplant rejection risk, Xenotransplantation. 18 (2011) 1–5. doi:10.1111/j.1399-3089.2011.00622.x.

[245] M. Agostino, E. Yuriev, P.A. Ramsland, Antibody Recognition of Cancer-Related Gangliosides and Their Mimics Investigated Using in silico Site Mapping, PLoS One. 7 (2012) e35457. doi:10.1371/journal.pone.0035457.

[246] F. Naso, A. Gandaglia, Different approaches to heart valve decellularization: A comprehensive overview of the past 30 years, Xenotransplantation. 25 (2017) e12354. doi:10.1111/xen.12354.

[247] K. Theodoridis, J. Mueller, R. Ramm, K. Findeisen, B. Andree, S. Korossis, A. Haverich, A. Hilfiker, Effects of combined cryopreservation and decellularization on the biomechanical, structural and biochemical properties of porcine pulmonary heart valves, Acta Biomater. 43 (2016) 71–77. doi:10.1016/j.actbio.2016.07.013.

[248] S.A. Korossis, H.E. Wilcox, K.G. Watterson, J.N. Kearney, E. Ingham, J. Fisher, In-vitro assessment of the functional performance of the decellularized intact porcine aortic root., J. Heart Valve Dis. 14 (2005) 408–21; discussion 422. http://www.ncbi.nlm.nih.gov/pubmed/15974537 (accessed September 29, 2018).

[249] C. Williams, J. Liao, E.M. Joyce, B. Wang, J.B. Leach, M.S. Sacks, J.Y. Wong, Altered structural and mechanical properties in decellularized rabbit carotid arteries, Acta Biomater. 5 (2009) 993–1005. doi:10.1016/j.actbio.2008.11.028.

[250] D. Oswal, S. Korossis, S. Mirsadraee, H. Wilcox, K. Watterson, J. Fisher, E. Ingham, Biomechanical characterization of decellularized and cross-linked bovine pericardium., J. Heart

Valve Dis. (2007).

[251] R. Gauvin, G. Marinov, Y. Mehri, J. Klein, B. Li, D. Larouche, R. Guzman, Z. Zhang, L. Germain, R. Guidoin, A comparative study of bovine and porcine pericardium to highlight their potential advantages to manufacture percutaneous cardiovascular implants, J. Biomater. Appl. 28 (2013) 552–565. doi:10.1177/0885328212465482.

[252] J.A. Choe, S. Jana, B.J. Tefft, R.S. Hennessy, J. Go, D. Morse, A. Lerman, M.D. Young, Biomaterial characterization of off-the-shelf decellularized porcine pericardial tissue for use in prosthetic valvular applications, J. Tissue Eng. Regen. Med. 12 (2018) 1608–1620. doi:10.1002/term.2686.

[253] F. Naso, A. Gandaglia, L. Iop, M. Spina, G. Gerosa, First quantitative assay of alpha-Gal in soft tissues: Presence and distribution of the epitope before and after cell removal from xenogeneic heart valves, Acta Biomater. 7 (2011) 1728–1734. doi:10.1016/j.actbio.2010.11.030.

[254] M.E. Breimer, Gal/non-Gal antigens in pig tissues and human non-Gal antibodies in the GalT-KO era1, Xenotransplantation. 18 (2011) 215–228. doi:10.1111/j.1399-3089.2011.00644.x.

[255] R.E. Taylor, C.J. Gregg, V. Padler-Karavani, D. Ghaderi, H. Yu, S. Huang, R.U. Sorensen, X. Chen, J. Inostroza, V. Nizet, A. Varki, Novel mechanism for the generation of human xeno-autoantibodies against the nonhuman sialic acid *N* -glycolylneuraminic acid, J. Exp. Med. 207 (2010) 1637–1646. doi:10.1084/jem.20100575.

[256] L.L. Kuleshova, S.S. Gouk, D.W. Hutmacher, Vitrification as a prospect for cryopreservation of tissue-engineered constructs, Biomaterials. 28 (2007) 1585–1596. doi:10.1016/j.biomaterials.2006.11.047.

[257] Y.C. Song, B.S. Khirabadi, F. Lightfoot, K.G. Brocklebank, M.J. Taylor, Vitreous cryopreservation Inaintains the function of vascular grafts, Nat. Biotechnol. 18 (2000) 296–299.

[258] M. Lisy, J. Pennecke, K.G.M. Brockbank, O. Fritze, M. Schleicher, K. Schenke-Layland, R. Kaulitz, I. Riemann, C.N. Weber, J. Braun, K.E. Mueller, F. Fend, T. Scheunert, A.D. Gruber, J.M. Albes, A.J. Huber, U.A. Stock, The performance of ice-free cryopreserved heart valve allografts in an orthotopic pulmonary sheep model, Biomaterials. 31 (2010) 5306–5311. doi:10.1016/j.biomaterials.2010.03.038.

[259] S. Wang, H. Oldenhof, T. Goecke, R. Ramm, M. Harder, A. Haverich, A. Hilfiker, W.F. Wolkers, Sucrose Diffusion in Decellularized Heart Valves for Freeze-Drying, Tissue Eng. Part C Methods. 21 (2015) 922–931. doi:10.1089/ten.tec.2014.0681.

[260] K. Theodoridis, J. Mueller, R. Ramm, K. Findeisen, B. Andree, S. Korossis, A. Haverich, A. Hilfiker, Effects of combined cryopreservation and decellularization on the biomechanical, structural and biochemical properties of porcine pulmonary heart valves, Acta Biomater. 43 (2016) 71–77. doi:10.1016/j.actbio.2016.07.013.

[261] C.J. Gerson, R.C. Elkins, S. Goldstein, A.E. Heacox, Structural integrity of collagen and elastin in SynerGraft® decellularized-cryopreserved human heart valves, Cryobiology. 64 (2012) 33–42. doi:10.1016/j.cryobiol.2011.11.001.

[262] A.K. Bui, R.A. McClure, J. Chang, C. Stoianovici, J. Hirshburg, A.T. Yeh, B. Choi, Revisiting optical clearing with dimethyl sulfoxide DMSO, Lasers Surg. Med. 41 (2009) 142–148. doi:10.1002/lsm.20742.

[263] M. Zimmerley, R.A. McClure, B. Choi, E.O. Potma, Following dimethyl sulfoxide skin optical clearing dynamics with quantitative nonlinear multimodal microscopy., Appl. Opt. 48 (2009) D79-87. http://www.ncbi.nlm.nih.gov/pubmed/19340127 (accessed August 28, 2018).

[264] K. Narine, E.C. Ing, M. Cornelissen, F. Desomer, H. Beele, L. Vanlangenhove, S. De Smet, G. Van Nooten, Readily available porcine aortic valve matrices for use in tissue valve engineering. Is cryopreservation an option?, Cryobiology. 53 (2006) 169–181. doi:10.1016/j.cryobiol.2006.05.007.

[265] R. Gauvin, G. Marinov, Y. Mehri, J. Klein, B. Li, D. Larouche, R. Guzman, Z. Zhang, L. Germain, R. Guidoin, A comparative study of bovine and porcine pericardium to highlight their potential advantages to manufacture percutaneous cardiovascular implants, J. Biomater. Appl. 28 (2013) 552–565. doi:10.1177/0885328212465482.

•

List of Figures

List of Tables

Scientific presentations and publications

Scientific presentations

- Vásquez-Rivera A., **Zouhair S.**, Goecke T., Oldenhof H., Hilfiker A., Wolkers W. F., "Dry preservation of heart valve scaffolds", Poster presentation at PhD Program Regenerative Sciences Retreat. April 12 – 13, 2016, Hannover, Germany;
- D'Alessandro C., Badria A**., Zouhair S**., Gerosa G., Korossis S., Koutsoukos P, Mavrilas D. "*In Vitro* Calcification: Advancing through the development of an accurate model", Oral presentation, 2016, Greece;
- **Zouhair S.**, Aguiari P., Iop L., Korossis S., Wolkers W. F., Gerosa G., "Advanced preservation methodologies for decellularized cardiovascular scaffolds", Oral presentation and podium presentation at the Annual VIMM Retreat, February 17– 19, 2017, Preganziol, Veneto, Treviso, Italy;
- **Zouhair S.**, Aguiari P., Iop L., Korossis S., Wolkers W. F., Gerosa G., "Advanced preservation methodologies for decellularized cardiovascular scaffolds", Oral presentation, Annual Meeting of the German Society of Biomechanics, March 29 – 31, 2017, Hannover, Germany;
- **Zouhair S**., Aguiari P., Iop L., Korossis S., Wolkers W. F., Gerosa G., "Advanced preservation methodologies for decellularized cardiovascular scaffolds", Oral presentation, 26th

Annual Congress of the European Association of Tissue Banks (EATB), October 18–20, 2017, Treviso, Italy;

- **Zouhair S**., Aguiari P., Iop L., Korossis S., Wolkers W. F., Gerosa G. “Novel preservation methodologies for decellularized cardiovascular scaffolds”, Oral presentation, 26th Annual Congress of the European Association of Tissue Banks (EATB), October 18–20, 2017, Treviso, Italy;
- **Zouhair S**., Aguiari P., Iop L., Korossis S., Wolkers W. F., Gerosa G., “Advanced preservation methodologies for decellularized cardiovascular scaffolds”, Poster-presentation at the Annual VIMM Retreat, March 2–3, 2018, Preganziol, Veneto, Treviso, Italy;

Scientific publications

- **Sabra Zouhair** Paola Aguiari , Laura Iop , Andrés Vásquez-Rivera , Andrea Filippi,Filippo Romanato , Sotirios Korossis , Willem F. Wolkers , Gino Gerosa : Preservation strategies for decellularized pericardial scaffolds for off-the-shelf availability. Submitted to “Acta biomaterialia”

- **Sabra Zouhair** , Eleonora Dal Sasso , Sugat R. Tuladhar , Paola Aguiari , Catia Fidalgo, Andrea Filippi , Giulia Borile , Andrea Bagno , Sotirios Korossis , Wim Wolkers, Filippo Romanato , Gino Gerosa * and Laura Iop *L: A comprehensive comparison of decellularized bovine and porcine pericardia. In submission.

- **Sabra Zouhair,** Paola Aguiari , Laura Iop , Eleonora Dal Sasso , Sugat R. Tuladhar, Andrés Vásquez-Rivera , Andrea Filippi, Filippo Romanato , Sotirios Korossis, Willem F. Wolkers , Gino Gerosa : Effect of advanced preservation strategies on biomechanical, biochemical and bioactive properties of porcine pericardium. In preparation

Acknowledgements

This research is part of the TECAS ITN Network and was funded by the People Programme (Marie Curie Actions) of the European Union's Seventh Framework Programme FP7/2007-2013/ under REA grant agreement n° 317512.

I would like to thank several people since without their support and dedication this would not be possible

First and foremost, my acknowledgements to my tutor and to my supervisors at the University of Padova. I would like to sincerely thank Prof. Gino Gerosa, Prof. Laura Iop and Dr. Paola Aguiari for their supervision and guidance during the whole period of my PhD studies. I cannot imagine how the project would have gone without your constant support and advice.

There are not enough words to express my gratitude to Dr. Ir. Willem

F. Wolkers for hosting me in his institute, making me feel welcome and treating me as a member of his group. Thank you very much for all your time spent supervising me and guiding me during the last three years. I have been very fortunate to have you as my co-supervisor.

My deepest thanks go to Prof. Korossis. Thank you for your expert advice on performing biomechanical experiments during my secondments at Hannover medical school and in particular for your constant encouragement and guidance during my PhD period.

My thesis would not have been achievable without the extraordinary support and patience of the great supervisors mentioned above!

A general acknowledgement to all TECAS investigators for their scientific input and suggestions during TECAS meetings.

I would like to thank Dr. Furlan for his assistance in the preparation and acquisition of SEM images.

To all my colleagues from the Cardiovascular Regenerative Medicine lab, thank you for your support and your friendship. Special thanks go to Eleonora, Catia, Sugat and Davide for the fruitful discussions and fun we had during my stay in Padova, and for making my life in Italy a happy one.

It is really important for me to express my deepest thanks to Dr. Laura Astolfi and Dr. Edi Simone for their assistance and patience in using microtome and microscopes and to Eleonora and Tea for helping in my last weeks in the lab and taking care of me during the first months of my pregnancy.

Special thanks also go to my colleagues and friends from Hannover Leibniz University, Miao, Bulat, Vitalii, Andrès, and Laura for the amazing time I experienced in this cold city and for their wonderful friendship and help during my stay in Hannover.

I would like to extend my thanks to my amazing friends from Germany and Holland, Marta, Teresa, Amal and Latifa, Khadija for their moral support and motivation.

I wish to thank my parents, who have enabled me to continue my studies abroad, and to my family in Germany. I am really grateful to all of you.

I am thankful to my lovely husband, Karsten, who believed in me and encouraged me to move to Italy. Thank you for your moral and financial support. Thanks for being there by my side every time I was mad and happy, for sharing my tears and my dreams at every moment!

Thanks to all of you for sharing both hard and enjoyable times with me, you made this journey wonderful and possible! Thank you!